Natural Resources Canada | Ressources naturelles Canada

GEOLOGICAL SURVEY OF CANADA
OPEN FILE 8788

Synthesis of organic matter composition and maturation and gas data from selected deep source rock units for some wells in the Fox Creek area

D. Lavoie, O.H. Ardakani, and C. Rivard

2021

Canada

GEOLOGICAL SURVEY OF CANADA
OPEN FILE 8788

Synthesis of organic matter composition and maturation and gas data from selected deep source rock units for some wells in the Fox Creek area

D. Lavoie, O.H. Ardakani, and C. Rivard

2021

© Her Majesty the Queen in Right of Canada, as represented by the Minister of Natural Resources, 2021

Information contained in this publication or product may be reproduced, in part or in whole, and by any means, for personal or public non-commercial purposes, without charge or further permission, unless otherwise specified.
You are asked to:
- exercise due diligence in ensuring the accuracy of the materials reproduced;
- indicate the complete title of the materials reproduced, and the name of the author organization; and
- indicate that the reproduction is a copy of an official work that is published by Natural Resources Canada (NRCan) and that the reproduction has not been produced in affiliation with, or with the endorsement of, NRCan.

Commercial reproduction and distribution is prohibited except with written permission from NRCan. For more information, contact NRCan at nrcan.copyrightdroitdauteur.rncan@canada.ca.

Permanent link: https://doi.org/10.4095/328238

This publication is available for free download through GEOSCAN (https://geoscan.nrcan.gc.ca/).

Recommended citation
Lavoie, D., Ardakani, O.H., and Rivard, C., 2021. Synthesis of organic matter composition and maturation and gas data from selected deep source rock units for some wells in the Fox Creek area; Geological Survey of Canada, Open File 8788, 95 p. https://doi.org/10.4095/328238

Publications in this series have not been edited; they are released as submitted by the author.

Table of Contents

ABSTRACT

An analysis of historical and new organic matter data, as well as gas composition and isotopic ratios for deep hydrocarbon source rocks, is part of a holistic study of the potential environmental impact of unconventional hydrocarbon development in the Fox Creek area in Alberta. The goal of this activity is to use thermal maturation and gas data from deep source rocks to generate a database for the interpretation of source rocks for eventual dissolved hydrocarbons in shallow groundwater.

The organic matter study consists of new petrographic observations on pellets from the Duvernay, Montney, Nordegg, and Mannville organic-rich samples. The petrography indicates that the organic matter is of marine Type II origin with one coal (Type III) sample in the Mannville Group. The organic matter reflectance measurements were taken on bitumen and converted to equivalent vitrinite reflectance values; vitrinite reflectance has been directly measured from the coal sample. The data indicate that all units reached thermal conditions for the production of hydrocarbons. The deep Duvernay Formation has the highest thermal maturity data that suggest the end of the oil window in the eastern end of the study area and the onset of the condensate zone in the western part of the study area.

Rock-Eval data from publicly available wells in the GSC database were evaluated for the Duvernay, Montney, and Nordegg units. The Tmax values indicate that these units are within the hydrocarbon production zones. As with the vitrinite-equivalent data, the Duvernay Formation has reached the highest thermal maturity in the study area with values indicative of the condensate zone, the other units belong to the oil zone.

Gas samples were collected in isotubes at the time of drilling. Samples were collected at various depths with some wells having only a short interval with data, while others have samples from a much longer interval. Data from 7 wells were available for our study, 6 of the wells are located at the eastern end of the study area while the last one is much further north. From gas composition (wetness ratio: C1/(C2+C3)) and $\delta^{13}C$ ratios of methane, the origin of the gas is thermogenic. The vertical trends of $\delta^{13}C$ ratios of ethane versus depth and wetness, as well as butane ratios (iC4/nC4) versus depth and wetness for wells with a longer distribution of samples, suggest partial isotopic roll-over. The roll-over was not fully developed as nowhere do we see $\delta^{13}C$ ratios of ethane being lighter (more negative) than that $\delta^{13}C$ ratio of methane. This suggests, as supported by the organic matter reflectance and Rock-Eval data, that the study area never reached very high thermal conditions. The fact that significant statistical overlap of $\delta^{13}C$ ratios of methane and the inverted trend of $\delta^{13}C$ ratios for ethane challenges the use of these isotopes data for source interpretation of eventual dissolved hydrocarbons in groundwater. However, some limited data for the shallowest sampling intervals (<1500 m) in some wells suggest that more significantly different data might be present in shallower sections in the subsurface. Data from eventual shallow coals intercepted by monitoring wells to be drilled are considered critical for the interpretation of the source for eventual dissolved hydrocarbons in groundwater.

INTRODUCTION

Fox Creek shallow aquifer project

The Environmental Geoscience and Groundwater Geoscience programs have developed a joint 5-year project (2019-2024) for the evaluation and understanding of potential environmental impacts of unconventional hydrocarbon development in the Fox Creek area in west-central Alberta. The Fox Creek area has been one of the most active hydrocarbon development domains in Canada over the last 50 years, with production primarily from the Devonian Duvernay Formation; directional drilling and hydraulic fracturing are fundamental technologies that have allowed economic production of these unconventional hydrocarbons. Within the framework of this project, new groundwater and rock data will be acquired through strategic shallow drilling (< 100 m) in the study area. This study will determine the possible major source(s) of dissolved hydrocarbons potentially present in shallow groundwater.

This report presents a synthesis of available organic matter (composition and maturation) and gas profile data (composition and $\delta^{13}C$ ratios) from available wells in the study (watershed) area. The study focuses on some of the best source rocks in the Fox Creek area, from the deep Duvernay Formation to other shallower units. New organic matter data (composition and Vitrinite-equivalent reflectance) have been acquired and integrated with vintage data. The information presented in this report will provide the fundamental data in order to evaluate the deep source(s) of eventual dissolved hydrocarbons in shallow groundwater in the eventuality of natural connectivity with deep hydrocarbon source rocks. Eventual coal samples from upcoming shallow drilling will be the focus of future detailed organic matter study providing similar information for shallow units hosting the aquifers.

Stratigraphy

The Fox Creek area is in the West-Central Plains domain in Alberta. The succession consists of sediments ranging in age from the Middle Cambrian to the Lower Paleogene. The base of the preserved succession is progressively older westerly with the youngest basal sediments over the Precambrian basement being Lower Devonian in the areas northeast of the Fox Creek area (Corlett et al., 2018; AGS, 2019). The sedimentary package is around 4 to 4.5 km thick and the succession thickens westward. The succession in the Fox Creek area can be divided into two broad lithostratigraphic assemblages (Fig. 1).

Cambrian – Mississippian

The first assemblage (1.5 to 2 km thick) is Middle Cambrian to Mississippian in age and is primarily made up of shallow marine carbonates (limestone and dolostone) with major Devonian reef complexes interbedded and/or laterally equivalent to fine-grained clastic sediments (shale, mudstone, and siltstone) some of which are rich in organic matter. Some thick evaporite (halite, anhydrite) intervals are present in the Devonian section. Dolomitized Devonian reefs and carbonate platforms and Mississippian carbonates are historical major conventional hydrocarbon reservoirs in this area.

Permian – Paleocene

The second assemblage (2.5 to 3 km thick) ranges from the Permian to the Paleocene (Fig. 1); the succession is strongly dominated by clastics with fluvial-deltaic-nearshore coarse-grained units (sandstone and conglomerate) being interbedded with finer-grained intervals (shale, mudstone, and siltstone). Coals are abundant in the Cretaceous and Cenozoic intervals. The fine-grained, deep shelf Jurassic Nordegg Member (Fernie Formation) is the only significant carbonate-rich unit of this assemblage. Cretaceous thick channel sandstones and conglomerates are significant conventional hydrocarbon reservoirs. The shallow aquifers of the Fox Creek area are hosted by the locally coal-rich Lower Paleogene Paskapoo Formation (Fig.1).

Source Rocks

The hydrocarbon prolific Western Canada Sedimentary Basin hosts abundant intervals of Paleozoic-Mesozoic organic-rich shales, as well as Cretaceous and younger coals. The organic-rich shales sourced the hydrocarbons for the numerous conventional reservoirs. Some of them with more favorable thickness, brittleness, and volume of trapped hydrocarbons are currently being developed as unconventional reservoirs.

Organic-rich units (shale and coals) are abundant in west-central Alberta. The Devonian Duvernay Formation is currently intensely developed as a shale reservoir. It is the deepest significant hydrocarbon source rocks in the study area (Fig. 1). Overlying the Duvernay, the most significant organic-matter rich intervals are found in 1) the uppermost Devonian – lowermost Mississippian Exshaw Formation, 2) the Triassic Montney – Doig formations, 3) the Jurassic Nordegg – Gordendale members, 4) the Lower Cretaceous Mannville Group (coals), and 5) the Fish Scale and Second White Speckled Shale of the Upper Cretaceous Colorado Group. Of note thin to thick coal beds are found at numerous intervals in the Paleogene succession.

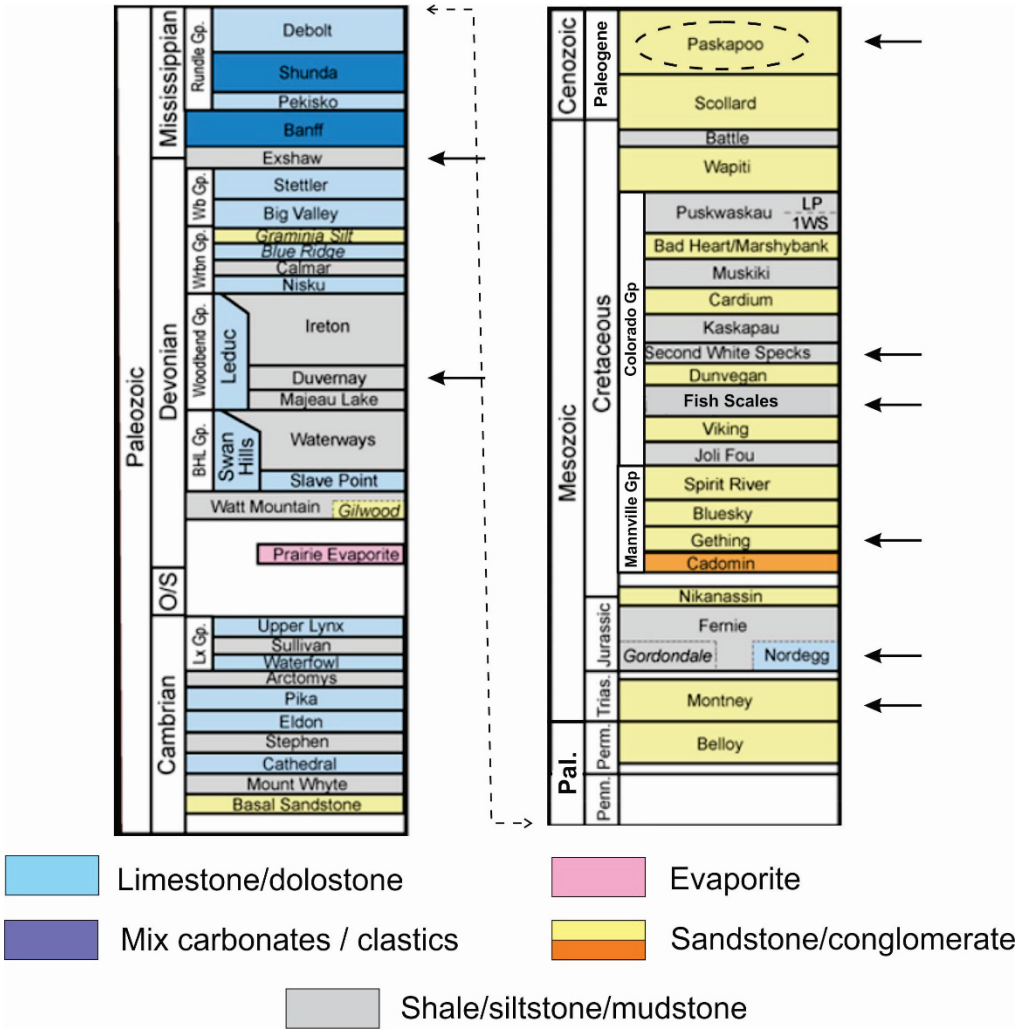

Figure 1. Stratigraphic summary of the Fox Creek area, arrows point to significant shale source rocks and coals. Modified from Corlett et al. (2018) and AGS (2019).

1. Organic matter in the Fox Creek area: petrography and organic matter reflectance

This activity aims at describing the type of organic matter and its stage of thermal maturation for various stratigraphic units in the Fox Creek area. The goal is to characterize and compare the best-known hydrocarbon source rocks of the area that could have generated eventual hydrocarbons dissolved in shallow groundwater. For this initial work, the studied material and data comes from the GSC-Calgary rock collection: 1) new pellets (organic matter petrographic thin sections) were prepared for a detailed description of the composition and organic matter reflectance and 2) vintage data of organic matter reflectance available for the study area.

The stratigraphic units covered in this first study are (1) the Duvernay Formation (Upper Devonian), (2) the Montney Formation (Triassic), (3) the Nordegg / Gordondale members (Jurassic), and (4) the Mannville Group (Cretaceous). A second phase for the petrographic/reflectance study will characterize the eventual coal intervals from the Paskapoo Formation (Paleocene) that could be intercepted by shallow drilling in late 2020.

The new and vintage data are provided in a table that presents a detailed summary of data as a function of specific wells. The data are reported on maps of the study area recognizing eventual patterns of thermal maturation; these allow to evaluate of the nature of hydrocarbons produced in the subsurface as a function of thermal maturation and the nature of organic matter.

Reflectance (%VRo) and hydrocarbon generation

Based on their relative abundance of hydrogen (H), carbon (C), and oxygen (O), three types of organic matter or kerogen are proposed, the differences result in various responses to thermal processes of organic matter degradation and hydrocarbon generation. Type I organic matter is very rich in H, it is usually composed of algal and microbial material of lacustrine origin. Type II organic matter is rich in H but less than Type I; it is made up of various marine microfossils and algae. Finally, Type III organic matter is richer in O and has variable H and C content; this organic matter is primarily composed of lignite (plants) of continental origin. An important sub-class of Type II is rich in sulfur; it is designated Type II-S.

Because of their different elemental chemistry, the diverse types of kerogens have different activation energies for initiating at various temperatures, hydrocarbon generation. For organic matter, the increase in temperature results in a modification of optical properties of the material as the latter reflects more intensely incident light as thermal alteration increases. This increase varies between organoclasts and bitumen and many equations link reflectance values of the studied particles to the recognized standard, vitrinite. In the case of the current study of new material, most of the analyses were made on bitumen and the equation used to convert %BRo (bitumen reflectance) to %VRo (vitrinite reflectance) is: [(%BRo + 0.03)/0.96] (Bertrand, 1990). The various stages of hydrocarbon generation are related to %VRo values. Figure 1.1 presents the hydrocarbon generation stages as a function of %VRo and the type of organic matter. It is important to know that the fields in Figure 1.1 are not exclusive, there is gas produced in the oil window, and oil generation does not stop suddenly at %VRo = 1.3%. As a rule of thumb, a %VRo of 0.6% is considered to correspond to a burial temperature of about 60°C and a %VRo of 1.3%, to about 135°C. The spatial distribution of data on maps of Figures 1.3 to 1.5 is based on the general fields of Figure 1.1.

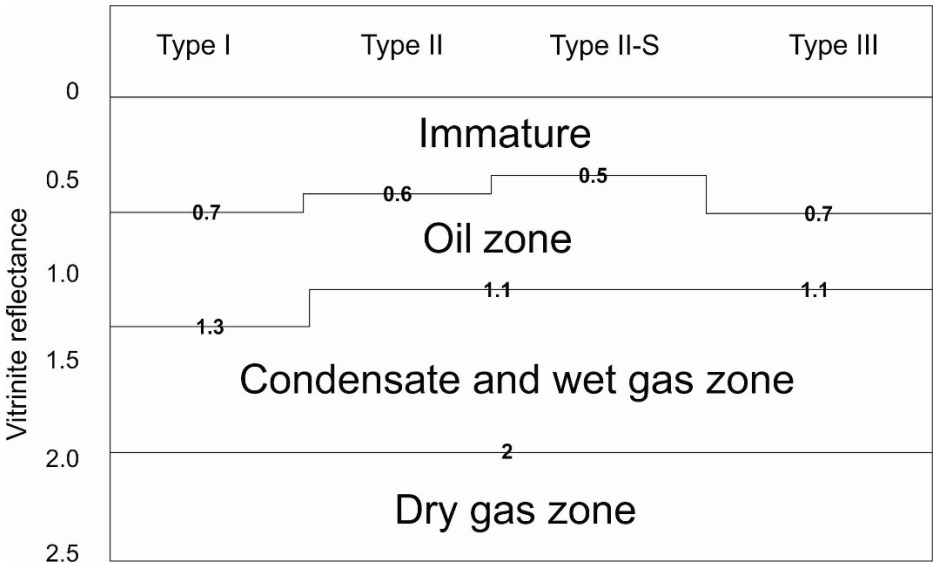

Figure 1.1: Hydrocarbon zones as a function of organic matter types and vitrinite reflectance.

Duvernay Formation (Upper Devonian)

The Duvernay Formation and its stratigraphic equivalent the Muskwa Formation is a well-known source rock for the conventional giant reef reservoirs in western Canada (Leduc, Nisku, and equivalents) (Switzer et al., 1994). The development of hydraulic fracturing and precise geo-steering of horizontal drilling has recently opened up the Duvernay to the development of its unconventional reservoir potential. The Montney and Duvernay formations are top priority targets for hydrocarbon development in Alberta and in particular in the Fox Creek area. In the project study area, the Duvernay Formation is found at depths between 3 to 4 km with an average thickness of around 50 to 70 m (Knapp et al., 2019).

Organic petrology

Organic petrographic analysis and previous studies (Van de Wetering et al., 2016; Knapp et al., 2020) revealed that solid bitumen is the dominant form of organic matter (Fig. 1.2), followed by minor inertinite (Fig. 1.2B, D), and trace zooclasts (i.e. chitinozoan). Solid bitumen occurs as *in situ* bituminized algae (Fig. 1.2A), as well as pore- and fracture-fills (Fig. 1.2A, B, and D), and fine-grained disseminated bitumen/amorphous kerogen (Fig. 1.2). Pore- and fracture-filling solid bitumen have adapted to the shape of the pore or fracture they occupy (e.g., Jacob, 1989), engulf detrital and authigenic minerals (Fig. 1.2), and are the dominant forms of solid bitumen in the studied samples. The pore-filling nature of bitumen classifies it as post-oil solid bitumen, which is the product of liquid petroleum that was generated from a mature source rock, locally migrated within the source rock, and eventually thermally cracked and transformed into solid bitumen (Mastalerz et al., 2018). Bituminized algae are a form of solid bitumen that formed *in situ* from thermal alteration of alginite and have preserved the shape of the precursor algae (Fig. 1.2A). Trace amounts of chitinozoans were observed in some samples. Chitinozoans are small organic-walled microfossils (Grahn and Paris, 2011), and are characteristic of lower Paleozoic marine rocks from Ordovician to Devonian. Chitinozoans and inertinite contribute to total organic carbon (TOC) content but do not have any hydrocarbon generation potential.

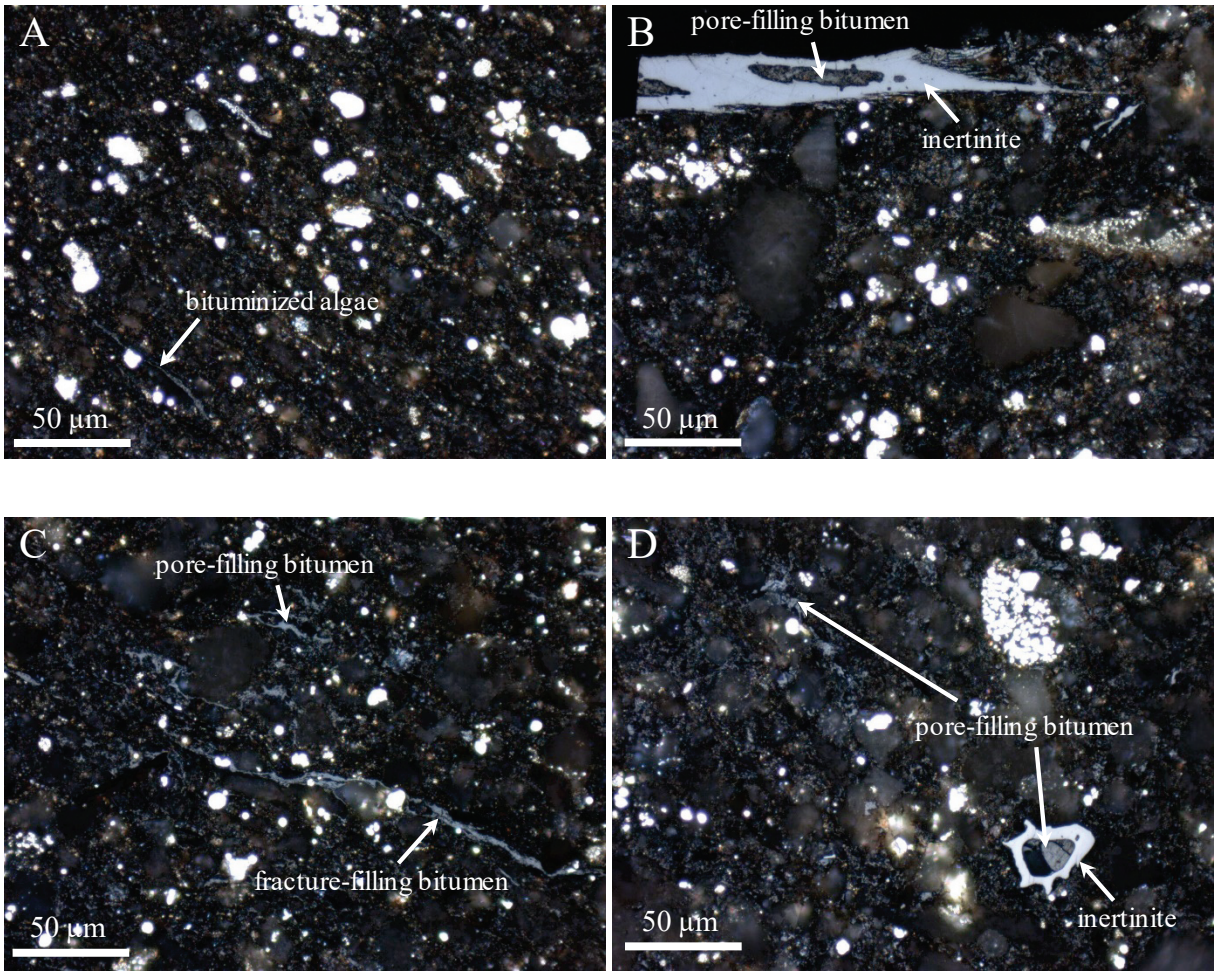

Figure 1.2: Organic petrography photomicrographs of selected samples in the study area. All images were taken with white incident light under oil immersion ×50 objective. The majority of organic matter macerals in the studied samples are solid bitumen as *in situ* or migra-bitumen. Inertinite and chitinozoans are present in minor to trace amounts. (A) *in situ* bituminized algae in a pyritic shale matrix; (B) inertinite particle with pore-filling solid bitumen in its pores; (C and D) combination of pore- and fracture-fill solid bitumen in the studied samples.

Vitrinite reflectance

The results are from 10 new petrographic pellets and 18 vintage data and are presented in Table 1.1 and statistical data are shown in the following pages of the table (attached documents). The 28 results are from 6 oil and gas (O&G) wells drilled in the Fox Creek area and located in Figure 1.3. Measurements were taken on bitumen (%Bro) and the average of reflectance data are presented in vitrinite equivalent data (%VRo).

The average vitrinite reflectance data range from a minimum of 0.95% in the eastern sector of the study area up to a maximum of 1.8% in the western area. The distribution of average values from the six studied wells indicates a westerly increase of reflectance data, thus an increase of thermal conditions in that direction. This thermal increase is associated with a depth increase for the Duvernay top of about 1 km between wells #4 and #6 (Table 1.1, Fig. 1.3).

Sample C-598640 (Table 1.1) has a bimodal distribution of reflectance with a late phase of low reflectance bitumen as a result of a late oil charge. The organic matter of the Duvernay Formation is dominated by Type II kerogen. Therefore, based on the zonation of Figure 1.1, the data indicate the end of the oil window in the eastern domain, then condensates and wet gas zones moving westward.

Table 1.1: summary of %VRo data for the Duvernay Formation.

Well ID	Well# on Map	Latitude	Longitude
1001325059919W500	1	54.134853	-116.72382
100012406123W500	2	54.284094	-117.30146
100051106018W500	3	54.173845	-116.59809
100103305622W500	4	53.884177	-117.20676
100081506218W500	5	54.359822	-116.60413
100051106018W500	6	54.173845	-116.59809

New Duvernay Formation Reflectance Data

Pellet#	C#	Well# on Map	Depth (m)	Depth (m)	mean %BRo	mean $\%VRo_{eqv}$	average well VRo_{eqv}
450/14	C-590329	1	3213.8		1.10	1.18	1.18
002/17	C-590365	2	3706.4		1.14	1.22	
003/17	C-590368	2	3710.7		1.20	1.28	1.34
012/16	C-598640	2	3706.4	3712.8	1.80	1.91	
194/19	C-594262	3	3052.3		.86	0.93	
195/19	C-594276	3	3066.0		1.05	1.13	1.06
196/19	C-594293	3	3083.2		1.04	1.12	
013/17	C-594392	4	4037.7		1.24	1.32	
014/17	C-594410	4	4056.5		2.01	2.12	1.80
013/16	C-598641	4	4055.5	4063.51	1.85	1.96	

Historical Duvernay Formation Reflectance Data

C-590365	2	3706.35	1.19	
C-590368	2	3710.65	1.19	1.30
C-598640	2	3706.35	1.53	
C-579980	5	3016.29	1.35	
C-586314	5	2993.25	1.01	
C-586322	5	2995.75	1.01	
C-586332	5	2998.6	1.03	
C-586342	5	3002.2	0.94	
C-586350	5	3004.8	1	1.03
C-586361	5	3008	0.97	
C-586377	5	3012	1.02	
C-586395	5	3016.8	1.02	
C-586417	5	3022.8	0.99	
C-586429	5	3026.2	1	
C-586439	5	3028.6	1.01	
C-594262	6	3052.26	0.75	
C-594276	6	3066.02	1.06	0.95
C-594293	6	3083.18	1.04	

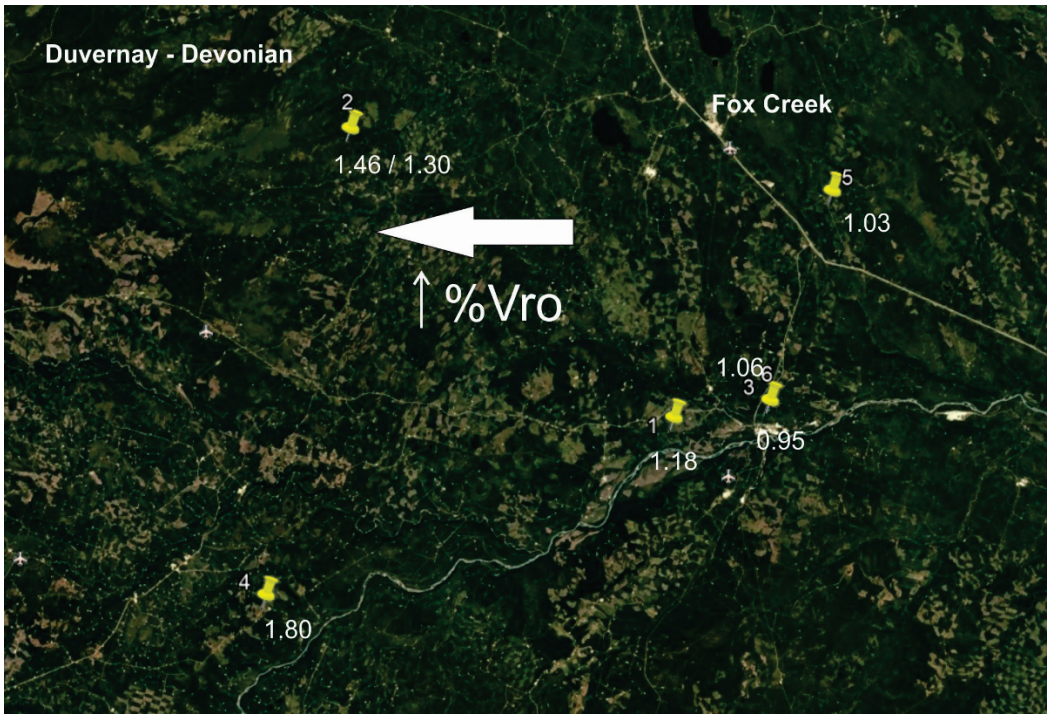

Figure 1.3: Spatial distribution of average %VRo data for the Duvernay Formation in the Fox Creek area. The yellow pins correspond to well locations. For well #2, the first value is the new petrographic data and the second is the vintage data.

Montney Formation (Triassic)

The Triassic Montney Formation is a major liquid-rich gas resource play in North America, which straddles Alberta and British Columbia. The Montney Formation has a complex internal stratigraphy with a sandstone-dominated assemblage at its actual eastern facies belt passing towards the west and southwest to dark grey dolomitic siltstone interbedded with shales. The upper Montney is a light brown, blocky siltstone with interlaminated fine-grained sandstone. The formation reaches its maximum thickness in the Cordillera (Rocky Mountain) foothills and deep basin area (circa 300 m) and thins to an eastern eroded edge near Peace River northwestern Alberta, and south of Fort Nelson, northeastern British Columbia.

The Montney Formation is, with the Duvernay, the most prolific unconventional play in western Canada and is considered as one of the largest gas resources in the world. Its main development area occurs west and southwest of the Duvernay play area. The Montney play is considered a hybrid unconventional play as significant hydrocarbon resources are hosted in the porous and permeable dolomitic siltstone and fine-grained sandstone with the hydrocarbons having migrated from the interbedded shales. Long laterals and multi-stage fracking is necessary for optimal economic production of these unconventional hydrocarbons. Production consists of natural gas, natural gas liquids, condensates, and black oil. In the Fox Creek area, even if Montney strata are present at a depth between 2 – 2.5 km, the unit is not targeted for development, because their hydrocarbon content is not sufficient to be economically extracted.

Organic petrology

The origin of organic matter in the Montney Formation has been a matter of debate in recent years (Crombez et al., 2016; Euzen et al., 2018; Chalmers and Bustin, 2012; Sanei et al., 2015; Wood et al, 2018, 2020). The majority of organic petrographic observations demonstrated that OM in the medium- to coarse-grained siltstones of the

Montney tight-gas and hydrocarbon liquids fairway is composed almost entirely of pore-filling solid bitumen/pyrobitumen. (Sanei et al., 2015a; Wood et al, 2018, 2020). However, limited organic petrographic data showed the presence of marine algae in certain intervals of the Montney Formation in western Alberta (Beaton et al., 2010). The origin of hydrocarbon in Western Canadian Sedimentary Basin (WCSB) Triassic reservoirs has been speculated to source from the basal portion of the Doig Formation (Allan and Creaney, 1991; Riediger et al., 1990; Riediger, 1997; Ejezie, 2007), which unconformably overlies the Montney Formation across most of the basin, including the study area. In up-dip Alberta portions of the basin, located over 50 km to the northeast of the studied wells, some oil has migrated into the Montney Formation from unconformably overlying Jurassic source rocks (Riediger et al., 1990; Ejezie, 2007), but the volume is considered to be insignificant compared to the overall volume within Triassic reservoirs (Allan and Creaney, 1991). Recent organic petrography presented in Beaton et al. (2010) further confirmed the limited presence of alginate in the studied samples. The Montney Formation in the study area is in the oil window.

Vitrinite reflectance

Results for two new pellets from wells intercepting the Triassic Montney Formation in the Fox Creek and petrographic data from 4 wells analyzed in a previous study of the Montney by the Alberta Geological Survey (Beaton et al., 2010) are summarized in Table 1.2 and plotted in Figure 1.4).

The %VRo of new and vintage data suggest early mature to mature oil window.

Table 1.2: Vintage %VRo data from the Montney Formation in the Fox Creek area.

Historical Montney Formation Reflectance Data

Pellet#	C#	Well# on Map	Depth (m)	Latitude	Longitude	mean %BRo	mean $\%VRo_{eqv}$
	C-590365	1	2166.3	54.32032	-116.767	0.73	0.79
	C-590368	3	2656.4	54.06814	-116.996	0.89	0.96
	C-598640	4	2105.1	54.37978	-116.868		1.05
	C-579980	5	2304	54.53546	-117.665	0.45	0.55

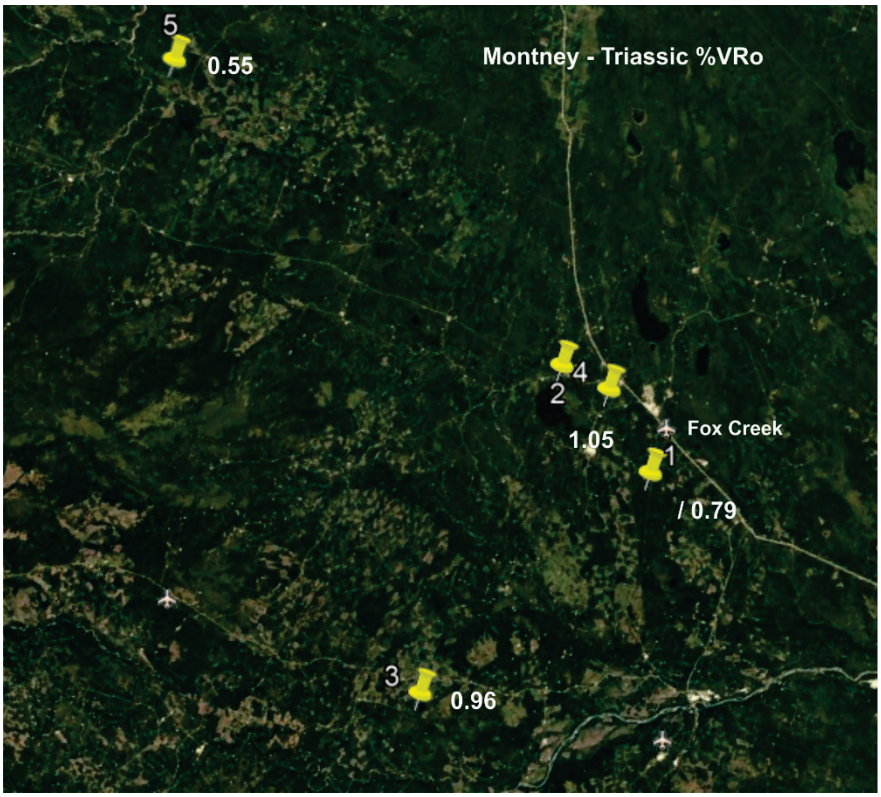

Figure 1.4: Spatial distribution of average %VRo data for the Montney Formation in the Fox Creek area. The yellow pins correspond to well locations. For well #1, the first value is the new petrographic data and the second is the vintage data.

Nordegg and/or Gordondale members (Jurassic)

The Nordegg Member of the Fernie Formation is Early Jurassic in age. The "typical" Nordegg Member consists of dark grey to black, platy to medium-bedded, cherty and phosphate limestones, with 40-90% chert occurring as layers exhibiting pinch and swell, lenticular beds and nodules; chert dark grey to black with blue tints. Interbeds of platy, dark grey, and black silty shales and papery black shales are also present in small amounts. In the best-exposed field occurrences, the Nordegg Member consists of three major units: a basal brown shale, a middle chert and limestone unit, and an upper interval of platy, oolitic and silty limestone. These three units can be easily recognized using gamma-ray logs, as they appear to be two highly radioactive units separated by a low radioactive carbonate unit. The thickness of the Nordegg Member is between 10 to 70 m, with a progressive thickening to the northwest.

In the Fox Creek area, the "calcareous" component of the Nordegg progressively disappears and the unit consists predominantly of organic-rich fine-grained clastic and shales, known as the Gordondale Member of the Fernie Formation. The Gordondale lithology consists of fine-grained, organic-rich, phosphatic, and calcareous mudstones and shales associated with shelf ramp facies. The Gordondale Member ranges in thickness from a maximum of 50 m near the eastern subcrop erosional extent to a minimum of 15 m in the west, near the foothills disturbed belt. While the definition of the stratigraphy of the Fernie Formation base has a complex history, we will continue to use the Nordegg as most reports dealing with that rock succession in the Fox Creek area are using this terminology.

The Nordegg (or Gordondale) Member is considered as a potential, organic-rich shale reservoir of gas, condensate, and oil. However its overall reservoir characteristics are little known (Isinguzo, 2017). One important aspect of this unit is the fact that the Type II kerogen of the shale is rich in sulfur and it is one of the typical example of the Type II-S organic matter (e.g. Fig. 1.1) that starts generating hydrocarbons at a lower thermal regime (Riediger and Bloch, 1995). However, it was argued that most of the generated oil was trapped in the unit because of permeability barriers (Riediger et al., 1990).

Organic petrology

The predominant organic maceral in the Gordondale Member in the study area is solid bitumen and liptinite, with minor amounts of zooclast and inertinite (Kondla et al., 2017; Isinguzo, 2017; Fig. 1.5). Solid bitumen is mainly dispersed within the clay-rich matrix and concentrated in larger pores associated with mineral grains and inertinite (Fig. 1.5). Solid bitumen abundance varies between samples, with some showing clay-rich matrix nearly completely saturated with solid bitumen (Fig. 1.5). Textural variations in bitumen due to incomplete consolidation cause variations in measured bitumen reflectance variations between the matrix bitumen and the concentrated, larger-pore-filling variety. Matrix bitumen generally has lower reflectance due to incomplete surface consolidation and poor surface quality (Kondla 2017; Sanei et al., 2015b). The physical alteration of the liptinite macerals caused by thermal degradation into bitumen makes visual identification of the original kerogen source difficult. However, occasional remnants of marine algae can be seen under ultraviolet light. Unidentifiable yellow to red fluorescing fragments of algal remnants and other liptinitic matter known as liptodetrinite are dispersed throughout the clay-rich matrix. High-reflecting, refractory organic macerals are present mainly as phosphate-rich fish bone fragments and partly as inertinite (hydrogen-poor kerogen).

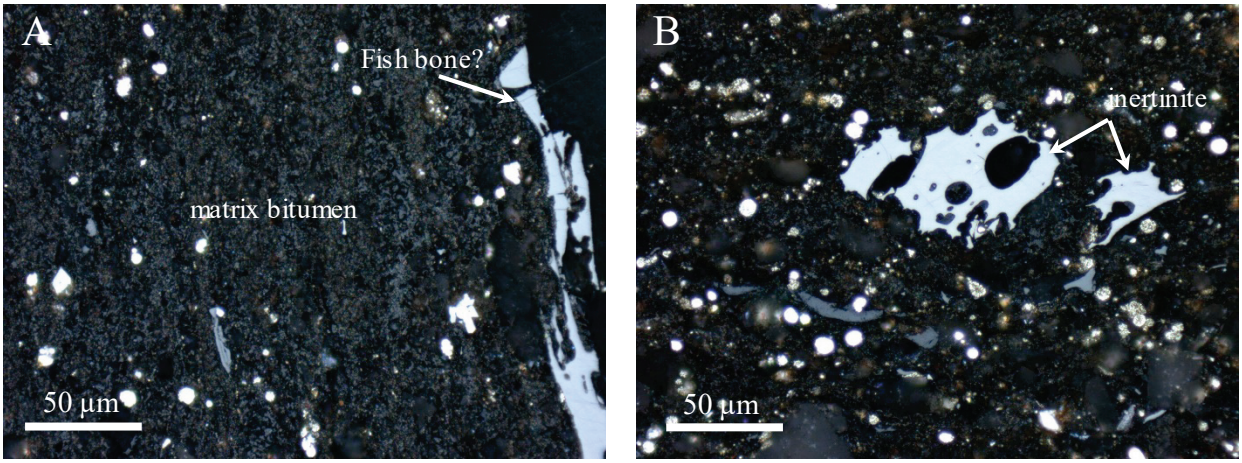

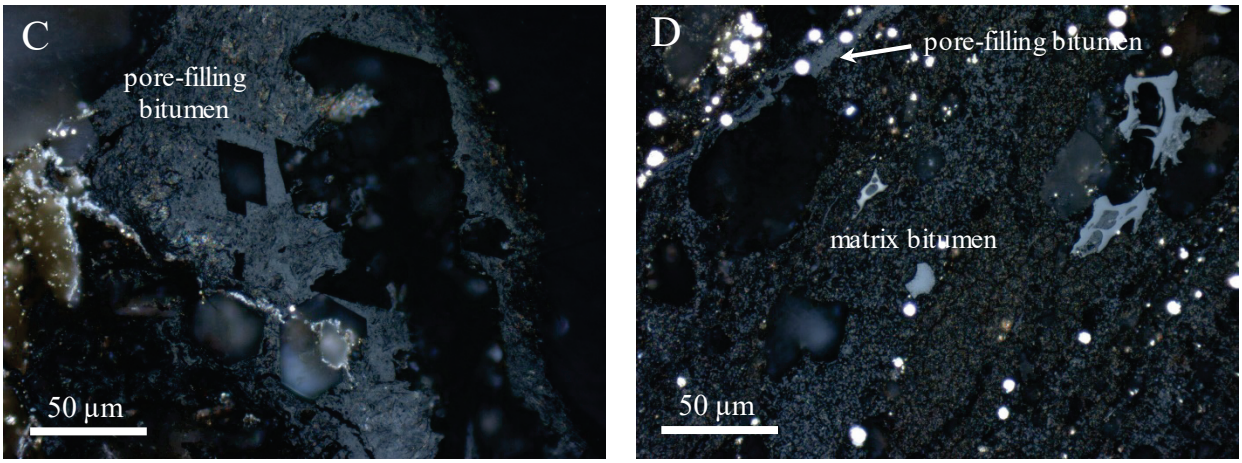

Figure 1.5: Organic petrography photomicrographs of selected Gordondale samples in the study area. All images took with white incident light under oil immersion ×50 objective. The majority of organic matter macerals in the studied samples are solid bitumen as the matrix or pore-filling bitumen. Inertinite and fishbone (?) are the other macerals present in the studied samples. (A) matrix bitumen adsorbed on the clay matrix with fishbone (?) particles; (B) big pieces of inertinite particles with solid bitumen accumulations; (C) pore-filling solid bitumen enclosed large matrix minerals such as dolomite and (D) disseminated matrix bitumen in the rock matrix with pore-filling solid bitumen filled larger pores.

Vitrinite reflectance

A new sample from the Nordegg / Gordondale Member has been examined petrographically. Data is presented in Table 1.3 and located on Figure 1.6.

Table 1.3: New %VRo data from the Nordegg Member in the Fox Creek area

New Nordegg/Gordondale members data

Pellet#	C#	Well# on Map	Depth (m)	Latitude	Longitude	mean %BRo	mean $\%VRo_{eqv}$
016/09	C-603817	1	2162 – 2167	54.366	-117.085	0.71	0.77

A total of 125 measurements were made on bitumen from the pellet, the vitrinite reflectance (%VRo) ranging from 0.55% to 1.07% with an average of 0.77% with a unimodal distribution.

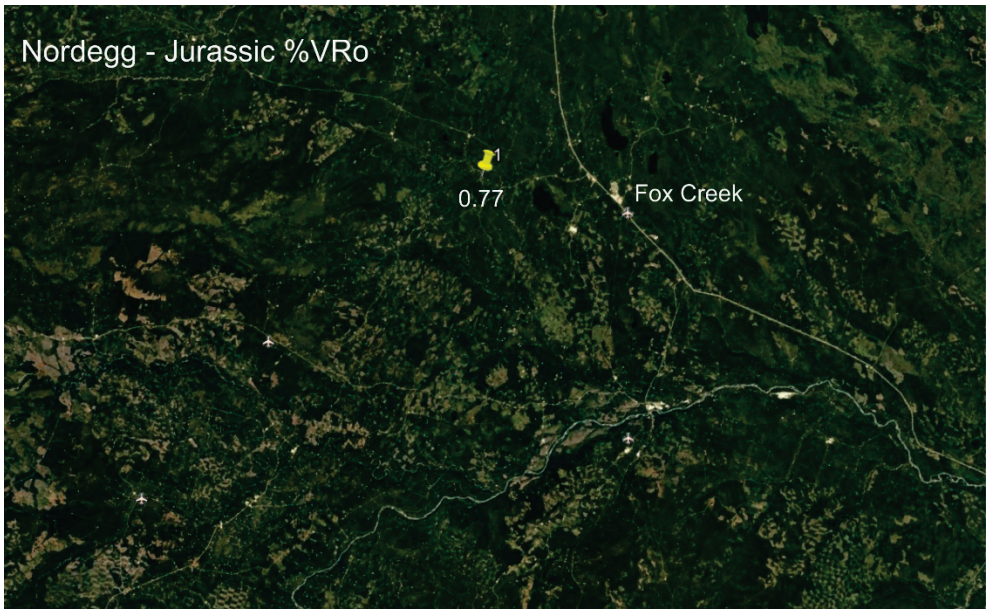

Figure 1.6: %VRo data for the Nordegg Member in the Fox Creek area. The yellow pin corresponds to the well location.

The organic matter of the Nordegg/Gordondale members is dominated by Type II-S sulfur-rich kerogen. Based on the zonation of Figure 1.1, the data indicate a syn-oil peak window. Samples of the Nordegg Member from 2 nearby wells (Fig. 2.8) were analyzed with Rock-Eval (Table 2.6); the Tmax for the unit suggests oil window conditions, in agreement with vitrinite reflectance.

The Mannville Group (Cretaceous)

The Mannville Group is of Cretaceous age and consists of interbedded non-marine sandstone and shale overlain by a thin, non-marine calcareous sandstone member, which is in turn overlain by marine shale, glauconitic sandstone, and non-marine salt-and-pepper sandstone in southern and central Alberta. In east-central and northeastern Alberta, the marine sequence is overlain by nearshore and non-marine sequence having a diachronous contact with the marine sequence. The internal stratigraphy of the Mannville Group is complex and characterized by rapid lateral and vertical facies changes associated with its largely non-marine-dominated facies assemblage, with a complex transition to a marine-dominated domain further north and east (Hayes et al., 1994).

The Mannville Group reaches a maximum thickness of 700 m in the Rocky Mountain Foothills to less than 40 m at its type locality. It is widely distributed in the Western Canada Sedimentary Basin and occurs only in the sub-surface in the Fox Creek area. The Mannville Group hosts numerous conventional oil and gas fields, as well as major coal resources (Smith et al., 1994). The Mannville Group is famous as it contains the oil sands of the McMurray Formation.

Organic petrology

The Mannville Group samples are composed of an alternation of coal layers and fine-grained organic-rich layers. Vitrinite, alginite, and solid bitumen are the dominant organic macerals in the studied samples with less contribution from inertinite maceral group (fusinite) (Fig. 1.7). In fine-grained intervals, alginite macerals are partially transformed into bitumen (Fig. 1.7C) with orange fluorescence color (Fig. 1.7D). The fluorescence color of alginite macerals is in accordance with the thermal maturity of samples in the oil window. In other fine-grained intervals,

alginite macerals completely turned to solid bitumen but preserved the original shape of algae (Fig. 1.7E). In coarse-grained intervals, solid bitumen occurred as pore-filling solid bitumen (Fig. 1.7F).

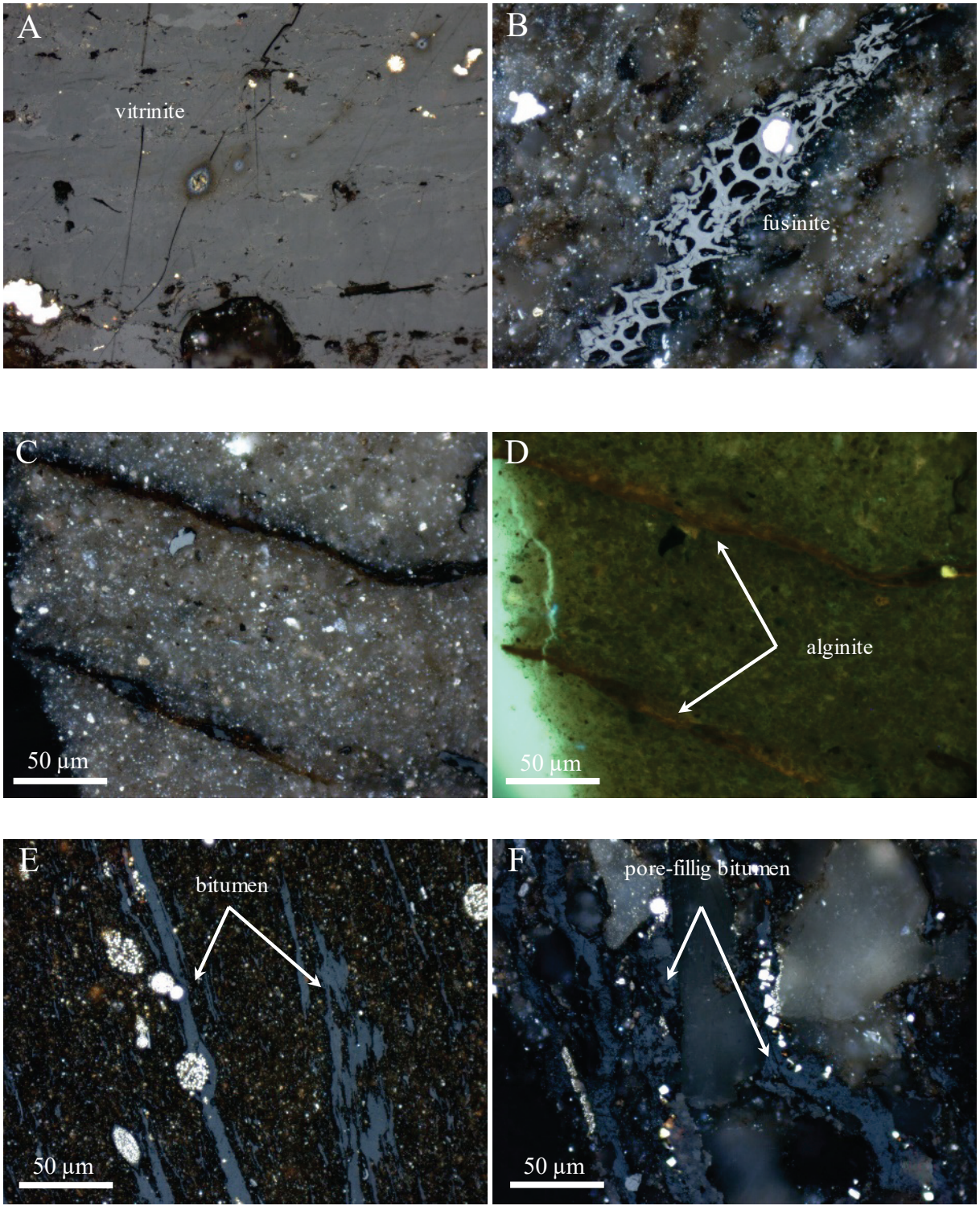

Figure 1.7. Organic petrography photomicrographs of selected Manville Group samples in the study area. All images took with white incident light under oil immersion ×50 objective. The majority of organic matter macerals in the studied samples are vitrinite, solid bitumen as *in situ* or migra-bitumen, as well as inertinite (fusinite). (A) vitrinite maceral in a coal-rich interval; (B) large piece of fusinite in a coarse-grained matrix; (C) alginite macerals partially transformed into bitumen; (D) same view as (C), but under ultraviolet light: alginite macerals exhibit orange fluorescence color that corresponds to the thermal maturity of samples; (E) large alginite macerals transformed into solid bitumen; (F) pore-filling solid bitumen in a coarse-grained interval.

Vitrinite reflectance

New reflectance data for the Mannville Group comes from 5 pellets prepared from one well. Data are presented in Table 1.4 and shown on the map of the Fox Creek area (Fig. 1.8). Note that the sample at 2503.6 m is a coal sample and measurements were taken on vitrinite.

Table 1.4 New %VRo data from the Mannville Group in the Fox Creek area.

New Mannville Group Reflectance Data

Pellet#	C#	Well# on Map	Depth (m)	Latitude	Longitude	mean %VRo	mean %BRo	mean $\%VRo_{eqv}$
011/20	C-420167		2503.6			0.86		0.86
012/20	C-420168		2507.5				0.76	0.82
013/20	C-420169	1	2510.7	54.17102	-117.185		0.92	0.99
014/20	C-420170		2512.1				0.77	0.83
015/20	C-420172		2518.3				0.98	1.05

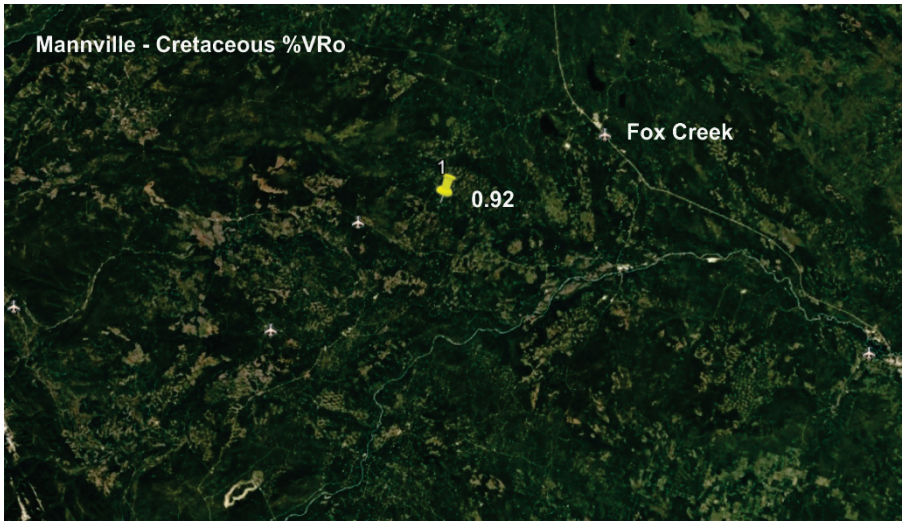

Figure 1.8: Mean %VRo for the Mannville Group in the Fox Creek area. The yellow pin corresponds to the well location

2. Organic matter in the Fox Creek area: programmed pyrolysis (Rock-Eval)

This activity aims at recognizing the type of organic matter and its level of thermal maturation for various stratigraphic units in the Fox Creek area. The goal of this study is to characterize and compare best-known hydrocarbon source rocks of the area to be able to identify the origin of an eventual migration of hydrocarbons from these units towards shallow aquifers. For this initial work, results consist of vintage data of programmed pyrolysis analyses (Rock-Eval) from rock units of the study area, mainly from the Duvernay Formation (Upper Devonian), but some data from the Montney Formation and Nordegg Member are presented and discussed. Other units will likely be synthesized as the project matures and samples from eventual coal intervals in the Paskapoo Formation are obtained during monitoring well drilling.

Programmed pyrolysis (Rock-Eval) and hydrocarbon generation

The Rock-Eval analysis provides a fast and reliable characterization of the quantity and quality of sedimentary organic matter, as well as its thermal maturity. A typical Rock-Eval experiment (Behard et al., 2001) starts with the heating of a pulverized rock sample at 300°C for 3 min in a helium atmosphere, when naturally occurring free hydrocarbons are volatilized. During the next stage, the temperature is steadily increased to 600°C at a rate of 25°C/min and decomposition of solid kerogen occurs. The final stage involves oxidation and combustion of the residual organic matter at 600°C. The amount of hydrocarbons volatilized at 300°C and evolved from kerogen at 300°C to 600°C are recorded as the S1 and S2 peaks, respectively. The temperature measured at the maximum of the S2 peak is referred to as Tmax. The quantity of organic CO_2 generated from 300°C to 390°C, determined by a thermal conductivity detector, corresponds to the S3 peak. The percentage of carbon in CO_2 formed during oxidation at 600°C and in the hydrocarbon peaks, S1 and S2 are used to define the total organic carbon content (TOC), expressed as a weight percentage. The determination of the quality of organic matter is based upon the calculation of Hydrogen (HI) and Oxygen (OI) indices (HI = (S2/TOC) × 100, OI = (S3/TOC) × 100) which are related to the atomic H/C and O/C ratios (Espitalié et al., 1977). The precision and utility of the Rock-Eval results are dependent on a few factors, in particular the presence of enough organic matter to generate a reliable S2 peak from which many important parameters are calculated (TOC, Tmax, HI). The work by Dewing and Sanei (2009) has demonstrated that S2 value below 0.35 mg HC/ g rock is likely to generate unreliable results. In our analysis, these low values will be removed from the dataset, as well as any Tmax value lower than 400°C, which is the lowest normal value of “pristine” organic matter.

The HI versus OI cross plots ("pseudo van Krevelen diagrams") can be used as an organic matter type indicator at low and moderate maturities. The Tmax is an indicator of relative thermal maturity. According to Espitalié et al. (1985), the oil window (Fig. 2.1) is defined by the following Tmax ranges: 440°-448°C (Type I), 435°-455°C (Type II), 425°-455°C (Type II-S) and 435°-470°C (Type III).

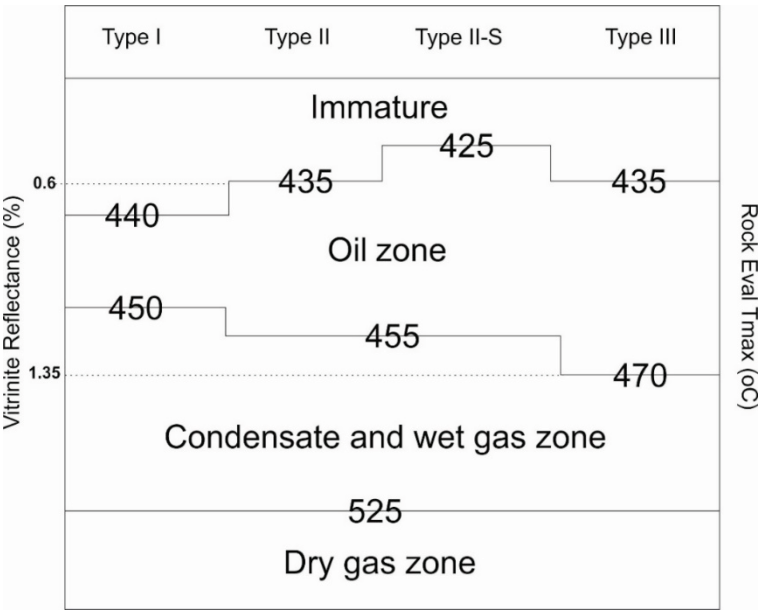

Figure 2.1: Hydrocarbon zones as a function of organic matter types and Rock-Eval Tmax (°C) data. Added to the figure are, for reference, the equivalent Vitrinite Reflectance (%) values for the commonly assumed range of oil window.

Duvernay Formation

A total of 223 Rock-Eval analyses from 4 wells (see Table 2.1) have been evaluated and are reported in Table 2.2. Out of these, 15 did not qualify as valuable based on their S2 and Tmax criteria discussed above (they are identified in yellow in Table 2.2). The hydrogen index (HI) is reported against the oxygen index (OI) in 2 pseudo Van Krevelen diagrams (only wells #3 and #4 had enough data) in Figure 2.2 to display the type of organic matter, whereas the HI versus Tmax plots for the same two wells is presented in Figure 2.3, illustrating the thermal stage with respect to organic matter type.

For both wells, the data on the pseudo Van Krevelen diagrams plot near the lower left side in the domain common to both Type I and Type II organic matter (Fig. 2.2). This is expected for organic material past the oil window as a significant part of the hydrogen in the kerogen has been expelled as hydrocarbons. The data for wells #3 and #4 on the HI vs Tmax diagram plot for both wells in the wet gas domain, with well #4 being slightly more advanced in that domain (Fig. 2.3).

Table 2.1. List and locations of wells – Duvernay Formation

Well ID	Well Name	Well# on Map	Latitude	Longitude
100132505919W500	CELTIC KAYBOBS 13-25-59-19	1	54.13485	-116.724
100012406123W500	AOSC GRIZZLY 1-24-61-23	2	54.28662	-117.305
100051106018W500	HUSKY KAYBOBS 5-11-60-18	3	54.17385	-116.598
100081506218W500	CHEVRON HZ FOXCK 8-15-62-18	4	54.35982	-116.604

Table 2.2: Summary of Rock Eval 6 data for 4 wells in the Fox Creek area. In yellow, data not used because of too low S2 (<0.35 mg HC/g TOC) or Tmax (<400°C) (Jiang et al. 2016; GSC database).

C#	Well# on Map	Interval (m)	TOC wt. %	Tmax °C	S1 mg HC/g	S2 mg HC/g	S3 mg CO_2/g	HI mg HC/g TOC	OI mg CO_2/g TOC
C-590329	1	3213.8	4.77	462	13.3	4.31	0.29	90	6
C-594262	2	3706.35	4.57	504	0.21	1.11	0.44	24	10
C-590353	2	3681.3	0.86	311	1.59	1.07	0.32		
C-590354	2	3684.05	1.67	332	2.75	1.27	0.31		
C-590355	2	3687.1	2.04	308	3.11	1.23	0.24		
C-590356	2	3690.25	2.71	301	1.24	1.27	0.25		
C-590357	2	3694.85	2.06	324	0.81	1.02	0.27		
C-590358	2	3696.35	1.78	309	1	0.96	0.3		
C-590359	2	3699.55	2.62	329	1.12	1.33	0.27		
C-590360	2	3701.45	4.34	487	0.77	1.58	0.22	13	5
C-590361	2	3703.8	4.75	491	0.26	1.29	0.21	27	4
C-590361x	2	3703.8	4.77	497	0.01	1.02	0.23	21	5
C-590362	2	3704.1	3.44	475	0.79	1.38	0.22	40	6
C-590363	2	3704.55	0.64	433	0.38	0.25	0.16		
C-590365	2	3706.35	4.04	497	0.3	1.02	0.22	25	5
C-590366	2	3708.4	4.21	485	0.72	1.33	0.2	32	5
C-590367	2	3709.85	4.19	498	0.48	1.27	0.23	30	5
C-590368	2	3710.65	5.57	498	0.24	1.43	0.21	26	4
C-590369	2	3711.4	2.66	505	0.34	0.91	0.23	34	9
C-590370	2	3711.9	5.43	499	0.65	1.72	0.22	32	4
C-590371	2	3712.8	5.38	492	0.21	1.34	0.29	25	5
C-590372	2	3713.8	3.02	495	0.75	1.2	0.24	40	8
C-590373	2	3714.8	2.9	503	0.58	0.98	0.17	34	6
C-590374	2	3716.1	0.71	431	0.28	0.28	0.18		
C-590375	2	3718.6	0.07	433	0.32	0.12	0.15		
C-590376	2	3723.3	0.22	432	0.54	0.15	0.2		
C-590377	2	3723.6	2.61	515	0.59	0.89	0.26	34	10
C-590378	2	3725.05	3.45	517	0.84	1.33	0.22	39	6
C-590378x	2	3725.05	3.21	560	0.02	0.74	0.25	23	8
C-598640	2	3706.35	4.57	504	0.21	1.11	0.44	24	10
C-598640	2	3706.35	4.57	469	0.67	1.66	0.34	36	7
C-598640	2	3706.35	4.48	489	0.07	1.1	0.3	25	7
C-594410	2	4037.65	2.7	296	0.26	0.23	0.53	9	20
C-598640	2	4056.47	4.73	292	0.4	0.24	0.61	5	13
C-598641	2	4055.5	4.35	601	0.31	0.35	0.59	8	1
	mean well 2			**504**				**29**	**6**

C#	Well# on Map	Interval (m)	TOC wt. %	Tmax °C	S1 mg HC/g	S2 mg HC/g	S3 mg CO_2/g	HI mg HC/g TOC	OI mg CO_2/g TOC
C-594276	3	3052.26	1.14	448	2.1	0.72	0.23	63	20
C-594293	3	3066.02	4.02	463	4.22	3.98	0.38	99	9
C-594392	3	3083.18	5.74	464	12.73	5.84	0.39	102	7
C-594258	3	3048.27	0.61	307	1.94	0.9	0.43		
C-594259	3	3049.22	0.34	307	0.58	0.53	0.53		
C-594260	3	3050.37	0.59	310	0.82	0.97	0.43		
C-594261	3	3051.22	1.37	309	2.37	1.61	0.33		
C-594262	3	3052.26	1.14	448	2.1	0.72	0.23	63	20
C-594263	3	3053.05	2.93	462	4.9	2.36	0.26	81	9
C-594264	3	3054.08	4.39	462	5.69	4.07	0.26	93	6
C-594265	3	3055.13	2.41	453	7.2	2.01	0.3	83	12
C-594266	3	3056.2	3.31	462	6.58	3.11	0.31	94	9
C-594267	3	3057.05	4.77	465	3.87	4.82	0.33	101	7
C-594268	3	3058.07	3.24	463	3.73	3.02	0.26	93	8
C-594269	3	3059.14	4.63	460	3.66	3.99	0.32	86	7
C-594270	3	3060.1	2.35	456	7.3	2.01	0.26	86	11
C-594271	3	3061.07	4.95	467	4.05	4.19	0.32	85	6
C-594272	3	3062.09	6.03	467	7.12	6.11	0.32	101	5

C-594273	3	3063.05	4.3	465	7.29	3.99	0.48	93	11
C-594274	3	3063.95	3.93	463	6.02	3.91	0.26	99	7
C-594275	3	3064.93	4.06	463	6.91	3.64	0.32	90	8
C-594276	3	3066.02	4.02	463	4.22	3.98	0.38	99	9
C-594277	3	3067.05	3.06	460	4.7	3.2	0.35	105	11
C-594278	3	3068.17	2.72	456	4.28	2.89	0.37	106	14
C-594279	3	3069.14	2.45	458	3.48	2.47	0.42	101	17
C-594280	3	3070.19	3.04	465	3.6	2.95	0.39	97	13
C-594281	3	3071.17	5.19	466	5.69	5.18	0.32	100	6
C-594282	3	3072.2	5.57	467	5.31	5.51	0.32	99	6
C-594283	3	3073.18	5.69	467	7.95	5.72	0.33	101	6
C-594284	3	3074.15	5.6	467	6.5	5.61	0.35	100	6
C-594285	3	3075.12	5.66	469	4.35	5.31	0.33	94	6
C-594286	3	3076.2	5.47	468	6.05	5.77	0.32	105	6
C-594287	3	3077.18	6.1	469	5.42	6.07	0.31	99	5
C-594288	3	3078.17	5.14	466	4.46	5.21	0.32	101	6
C-594289	3	3079.42	6.34	470	3.9	5.95	0.33	94	5
C-594290	3	3080.32	0.55	440	1.34	0.39	0.21	71	38
C-594291	3	3081.18	3.06	464	4.56	2.73	0.32	89	10
C-594292	3	3082.15	3.16	465	4.15	3.15	0.3	100	9
C-594293	3	3083.18	5.74	464	12.73	5.84	0.39	102	7
C-594294	3	3084.17	4.47	464	6.24	4.45	0.36	100	8
C-594295	3	3085.05	2.23	467	1.76	1.84	0.31	83	14
	mean well 3			**462**				**93**	**10**

C#	**Well# on Map**	**Interval (m)**	**TOC** wt. %	**Tmax** °C	**S1** mg HC/g	**S2** mg HC/g	**S3** mg CO_2/g	**HI** mg HC/g TOC	**OI** mg CO_2/g TOC
C-579958	4	2989.17	3.85	453	2.67	4.78	0.28	124	7
C-579959	4	2990.38	4.16	455	5.88	5.1	0.3	123	7
C-579960	4	2991.77	3.11	456	3.19	4.1	0.3	132	8
C-579961	4	2992.75	3.67	457	5.34	4.2	0.33	114	9
C-579962	4	2994.65	1.77	450	2.57	2.29	0.36	129	20
C-579963	4	2994	2.03	455	2.37	2.25	0.32	111	16
C-579964	4	2995.55	1.44	452	1.94	2.03	0.33	141	23
C-579964	4	2995.55	1.63	450	2.4	2.01	0.34	123	21
C-579964	4	2995.55	1.57	451	2.39	2.06	0.28	131	18
C-579964	4	2995.55	1.38	450	2.31	2.23	0.28	162	20
C-579965	4	2996.5	2.08	442	3.33	2.08	0.4	100	19
C-579966	4	2997.69	2.18	457	2.37	2.84	0.33	130	15
C-579967	4	2999.27	1.98	449	3.13	2.84	0.39	143	20
C-579968	4	3000.53	4.16	459	4.89	5.16	0.34	124	8
C-579969	4	3002.04	2.87	455	2.86	4.07	0.3	142	10
C-579970	4	3003.59	3.39	455	4.98	4.25	0.28	125	8
C-579971	4	3004.93	2.34	459	1.99	2.65	0.36	113	11
C-579972	4	3006.55	3.74	452	4.21	4.85	0.27	130	7
C-579973	4	3007.92	5.16	459	7.44	5.78	0.29	112	6
C-579974	4	3009.28	4.03	460	5.89	4.96	0.25	123	6
C-579976	4	3011.91	4.17	455	5.72	5.5	0.27	132	6
C-579977	4	3013.58	3.41	459	3.75	3.98	0.25	117	7
C-579978	4	3014.53	3.57	458	6.75	4.61	0.31	129	9
C-579979	4	3016.1	4.72	460	6.28	5.79	0.28	123	6
C-579980	4	3016.29	4.86	460	6.37	5.99	0.28	123	6
C-579981	4	3016.53	4.25	459	4.61	5.18	0.32	122	8
C-579982	4	3016.71	3.3	460	3.13	4.92	0.3	149	9
C-579983	4	3016.93	4.2	459	4.83	5.27	0.25	125	6
C-579984	4	3017.2	5.27	458	6.65	6.38	0.34	121	6
C-579985	4	3017.33	2.34	459	2.46	3.04	0.33	130	14
C-579986	4	3018.9	2.44	457	3.32	3.86	0.27	158	11
C-579987	4	3020.43	5.53	461	6.49	6.45	0.29	117	5
C-579988	4	3021.53	5.1	460	5.69	6.69	0.28	131	5
C-579988	4	3021.53	5.24	461	5.55	5.71	0.27	109	5
C-579988	4	3021.53	5.3	462	5.65	6.32	0.24	119	5
C-579988	4	3021.53	5.33	459	5.15	7.11	0.22	133	4
C-579988	4	3021.53	5.26	461	5.6	5.81	0.3	110	5
C-579988	4	3021.53	5.26	461	5.57	5.82	0.28	110	5

C-579988	4	3021.53	5.29	462	5.59	6.44	0.24	122	5
C-579988	4	3021.53	5.34	462	5.62	6.38	0.24	119	4
C-579988	4	3021.53	5.34	460	5.33	6.87	0.24	129	4
C-579988	4	3021.53	5.37	460	5.3	6.97	0.24	130	5
C-579988	4	3021.53	5.21	460	5.66	5.66	0.34	109	7
C-579988	4	3021.53	5.24	460	5.75	5.59	0.32	107	6
C-579988	4	3021.53	5.31	462	5.8	6.18	0.27	116	5
C-579988	4	3021.53	5.28	461	5.73	6.24	0.29	118	5
C-579988	4	3021.53	5.32	460	5.58	6.43	0.27	121	5
C-579988	4	3021.53	5.37	461	5.56	6.38	0.29	119	5
C-579989	4	3022.8	5.38	461	4.56	6.56	0.29	122	5
C-579990	4	3023.9	4.81	461	6.57	5.81	0.28	121	6
C-579991	4	3024.9	1.53	449	3	1.75	0.3	114	20
C-579992	4	3027.05	1.47	461	1.6	2.45	0.35	167	24
C-579993	4	3028.53	2.61	462	2.41	3.6	0.35	138	13
C-579994	4	3029.15	0.23	441	0.52	0.3	0.25		
C-579995	4	3030.65	0.15	430	0.18	0.13	0.27		
C-579996	4	3033.4	0.1	431	0.12	0.11	0.26		
C-579997	4	3034.65	0.16	446	0.12	0.18	0.34		
C-579998	4	3036.05	0.16	442	0.23	0.21	0.32		
C-586298	4	2989.3	3.39	452	6.44	3.81	0.32	112	9
C-586299	4	2989.6	3.09	450	6.92	4.04	0.4	131	13
C-586300	4	2989.8	3.15	453	4.7	3.54	0.27	112	9
C-586301	4	2990.3	3.02	454	2.82	3.35	0.25	111	8
C-586302	4	2990.4	3.05	452	4.89	3.57	0.29	117	10
C-586303	4	2990.55	1.69	455	2.27	1.71	0.32	101	19
C-586304	4	2990.8	3.52	455	3.98	4.1	0.24	116	7
C-586305	4	2991	3.85	457	5.12	3.7	0.59	96	15
C-586306	4	2991.2	2.52	452	2.78	3.12	0.24	124	10
C-586307	4	2991.45	3.33	455	3.53	4.77	0.19	143	6
C-586308	4	2991.65	3.54	454	3.06	4.87	0.24	138	7
C-586309	4	2991.85	2.82	453	4.34	3.68	0.22	128	8
C-586310	4	2992.25	2.76	457	2.97	3.35	0.37	121	13
C-586311	4	2992.45	2.86	456	2.82	3.78	0.27	132	9
C-586312	4	2992.7	3.49	457	2.99	4.25	0.37	122	11
C-586313	4	2992.9	3.3	460	2.18	3.98	0.29	121	9
C-586314	4	2993.25	3.6	458	4.26	4.02	0.5	112	14
C-586315	4	2993.4	2.67	455	2.77	3	0.36	112	13
C-586316	4	2994	3.25	458	3.53	3.93	0.29	121	9
C-586317	4	2994.17	3.42	458	4.61	4.12	0.26	120	8
C-586318	4	2994.4	1.79	454	2.5	2.13	0.27	119	15
C-586319	4	2994.6	1.7	454	1.56	1.93	0.28	114	16
C-586320	4	2994.8	2.09	456	2.48	2.39	0.26	114	12
C-586321	4	2995.5	1.98	456	2.28	2.55	0.26	129	13
C-586322	4	2995.75	1.69	447	2.77	2.15	0.28	127	17
C-586323	4	2995.9	1.58	450	1.47	1.64	0.25	104	16
C-586324	4	2996.2	1.81	451	2.11	1.93	0.28	107	15
C-586325	4	2996.4	1.87	451	2.54	2.37	0.26	127	14
C-586326	4	2997	2.09	457	1.87	2.51	0.27	120	13
C-586327	4	2997.5	1.89	453	2.55	2.1	0.3	111	16
C-586328	4	2997.8	2.12	451	3.35	2.74	0.3	129	14
C-586329	4	2998	2.01	451	3.11	2.39	0.3	119	15
C-586330	4	2998.3	2.26	454	3.23	3.05	0.27	135	12
C-586331	4	2998.4	1.79	454	2.63	2.5	0.25	140	14
C-586332	4	2998.6	1.57	447	1.96	1.94	0.29	124	18
C-586333	4	2998.85	1.96	452	2.72	2.54	0.3	130	15
C-586334	4	2999	1.9	452	2.71	2.36	0.3	124	16
C-586335	4	2999.8	2.08	450	2.91	2.87	0.31	138	15
C-586336	4	3000.2	2.14	454	2.98	2.81	0.32	131	15
C-586338	4	3001.2	3.08	456	3.1	3.03	0.34	98	11
C-586339	4	3001.4	4.03	459	4.5	4.86	0.31	121	8
C-586340	4	3001.6	3.23	456	3.04	3.7	0.29	115	9
C-586341	4	3001.9	3.12	452	5.58	3.63	0.27	116	12
C-586342	4	3002.2	2.86	453	4.09	3.81	0.28	133	10
C-586343	4	3003	3.31	456	3.86	3.92	0.28	118	8

C-586344	4	3003.4	3.35	456	3.38	4.01	0.28	120	8
C-586345	4	3003.6	2.65	454	4.05	3.16	0.26	119	10
C-586346	4	3003.8	2.82	456	2.6	3.62	0.22	128	8
C-586347	4	3004	3.05	453	5.37	3.73	0.26	122	9
C-586348	4	3004.2	3.1	454	4.42	3.82	0.24	123	8
C-586349	4	3004.6	3.16	457	2.33	3.57	0.24	113	8
C-586350	4	3004.8	2.78	456	4.14	3.53	0.28	127	10
C-586351	4	3005.2	3.37	461	2.73	4.05	0.28	120	8
C-586352	4	3005.4	3.44	459	2.2	4.15	0.28	121	8
C-586353	4	3005.6	2.05	460	1.74	2.42	0.26	118	13
C-586354	4	3006.1	3.35	456	3.86	4.07	0.24	121	7
C-586355	4	3006.3	5.96	459	3.79	7.37	0.26	124	4
C-586356	4	3006.6	3.8	454	3.44	4.57	0.21	120	6
C-586357	4	3006.85	3.26	459	4.89	3.86	0.24	118	7
C-586358	4	3007.2	1.75	457	2.89	1.96	0.25	112	14
C-586359	4	3007.4	3.06	455	4.05	3.63	0.24	118	8
C-586360	4	3007.6	4.61	462	6.39	5.18	0.25	112	5
C-586361	4	3008	3.76	461	5.2	4.93	0.23	131	6
C-586362	4	3008.2	4.02	461	8.18	4.83	0.27	120	7
C-586363	4	3008.4	4.06	458	6.56	5.29	0.24	130	6
C-586364	4	3008.8	3.74	461	5.13	4.65	0.24	124	6
C-586365	4	3009	3.53	455	5.9	3.54	0.25	100	7
C-586366	4	3009.2	2.91	456	6.5	3.22	0.25	110	9
C-586367	4	3009.6	3.05	459	3.59	3.65	0.24	120	8
C-586368	4	3010	5.71	461	6.3	6.67	0.31	117	5
C-586369	4	3010.2	4.8	456	5.05	4.25	0.31	89	6
C-586370	4	3010.4	6.22	460	7.27	7.42	0.32	119	5
C-586371	4	3010.8	3.95	459	6.63	4.94	0.27	125	7
C-586372	4	3011	4.4	460	3.52	5.21	0.23	118	5
C-586373	4	3011.2	3.08	457	5.81	3.45	0.25	112	8
C-586374	4	3011.4	4.06	457	9.37	4.61	0.25	114	6
C-586375	4	3011.6	4.12	459	5.35	4.93	0.21	120	5
C-586376	4	3011.7	4.62	458	5.94	6.05	0.23	131	5
C-586377	4	3012	3.53	456	5.07	4.01	0.25	114	7
C-586378	4	3012.1	2.75	456	4.14	3.19	0.23	116	11
C-586379	4	3012.4	3.88	458	3.27	4.69	0.24	121	6
C-586380	4	3012.6	4.12	462	3.23	5.21	0.2	126	5
C-586381	4	3012.8	4.39	458	6.19	5.38	0.26	123	6
C-586383	4	3013.4	3.55	459	4.25	4.22	0.21	119	6
C-586384	4	3013.6	3.51	457	5.02	3.83	0.24	109	7
C-586385	4	3014	4.21	459	4.07	4.92	0.25	117	6
C-586386	4	3014.4	4.38	460	4.32	5.37	0.2	123	5
C-586387	4	3014.6	3.45	458	6.61	4.04	0.43	117	12
C-586388	4	3015	3.11	459	4.01	3.07	0.24	99	8
C-586390	4	3015.4	3.51	458	5.16	3.99	0.21	114	6
C-586391	4	3015.8	0.45	407	0.29	0.2	0.27		
C-586392	4	3016	4.79	459	7.44	5.49	0.24	115	5
C-586393	4	3016.2	4.72	460	5.47	5.58	0.21	118	4
C-586395	4	3016.8	3.24	459	3.08	4.25	0.25	131	8
C-586397	4	3017.2	4.85	460	3.94	5.63	0.19	116	4
C-586399	4	3017.8	3.04	457	2.95	3.68	0.24	121	8
C-586401	4	3018.2	2.41	454	4.44	3.19	0.34	132	14
C-586403	4	3018.8	2.62	455	3.55	3.19	0.24	122	9
C-586405	4	3019.4	4.46	460	3.58	5.56	0.21	125	5
C-586407	4	3020	4.79	460	7.23	5.61	0.3	117	6
C-586409	4	3020.8	5.35	461	6.31	6.3	0.3	118	6
C-586411	4	3021	5.59	462	5.26	6.45	0.23	115	4
C-586415	4	3021.8	5.23	461	5.96	6.18	0.28	118	5
C-586417	4	3022.8	5.27	460	6.01	6.16	0.25	117	5
C-586419	4	3023.2	5.6	462	5.86	6.7	0.3	120	5
C-586423	4	3024.4	4.2	461	4.75	5.19	0.22	124	5
C-586425	4	3025	1.55	447	3.56	2.02	0.19	130	12
C-586427	4	3025.6	2.27	456	4.06	2.59	0.23	114	10
C-586429	4	3026.2	4.46	460	4.92	4.72	0.48	106	11
C-586431	4	3026.6	3.01	458	3.62	4.03	0.33	134	11

C-586433	4	3026.9	2.47	459	3.52	3	0.3	121	12
C-586435	4	3027.4	4.95	459	4.82	5.76	0.22	116	4
C-586437	4	3028.2	3.32	459	3.5	4.26	0.25	128	8
C-586439	4	3028.6	3.21	463	3.56	3.91	0.33	122	10
C-586441	4	3029	0.23	262	0.42	0.29	0.22		
C-586443	4	3031	0.15	352	0.22	0.3	0.3		
C-586445	4	3033	0.25	378	0.89	0.66	0.38		
C-586447	4	3035	0.32	381	0.58	0.43	0.35		
	mean well 4		**3.5**	**456**				**121**	**9**

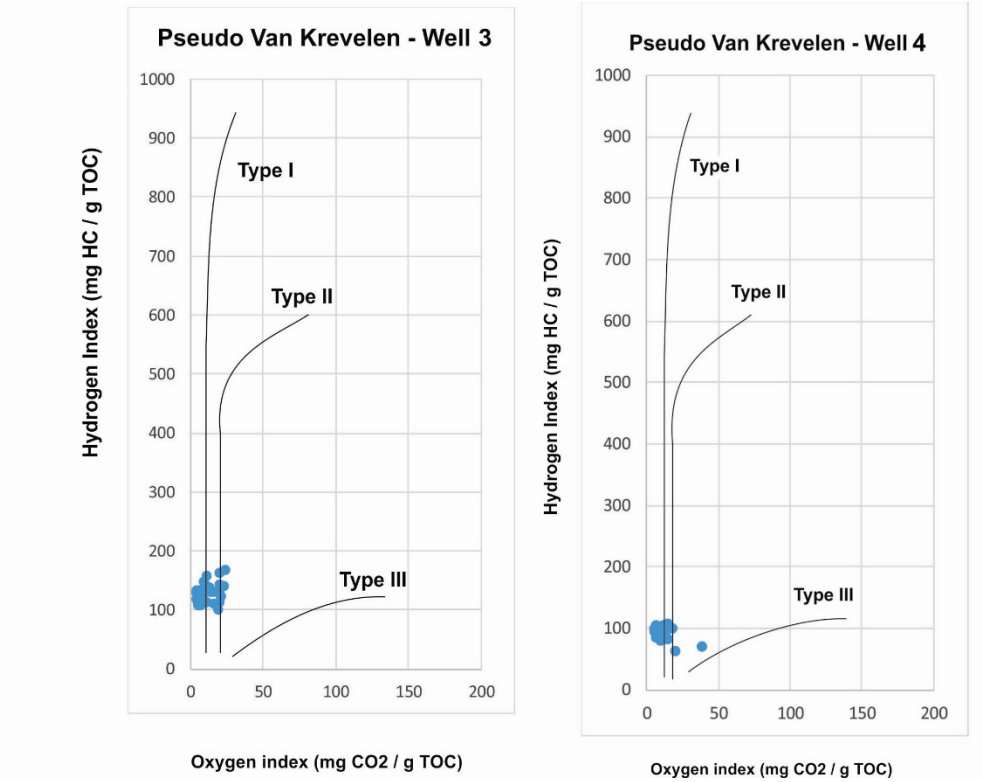

Figure 2.2. Pseudo Van Krevelen diagram for wells #3 and #4

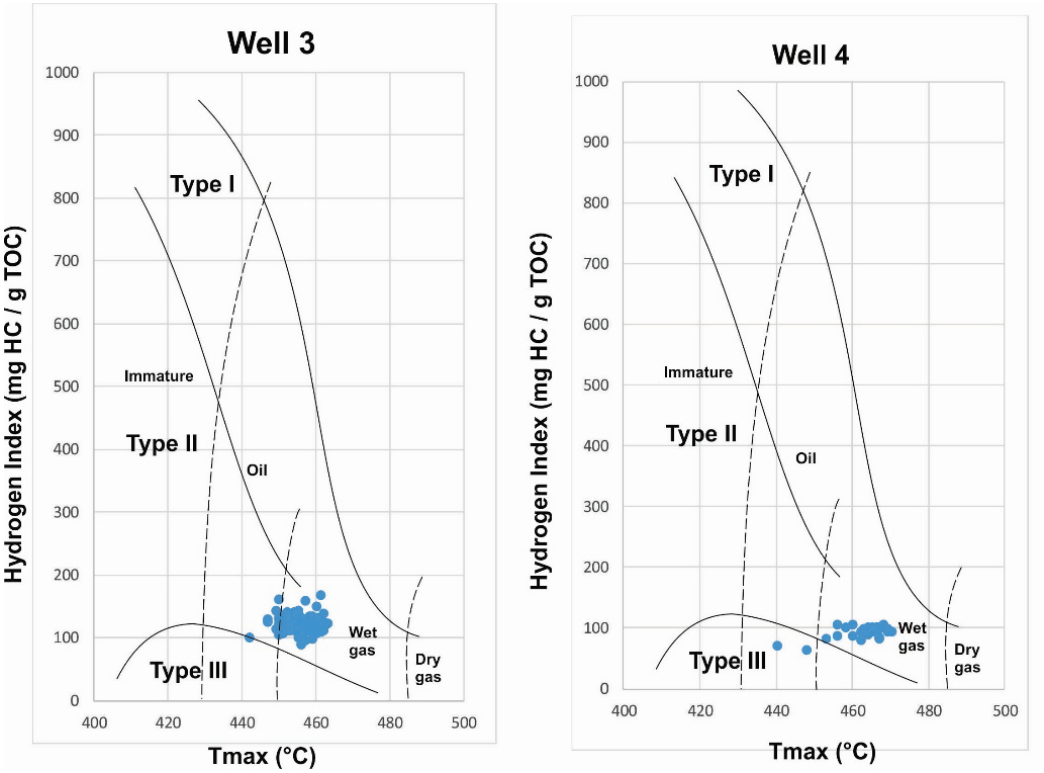

Figure 2.3. HI vs Tmax diagram for wells #3 and #4

The average Tmax values are plotted on the map of the Fox Creek area (Fig. 2.4). Note that well #1 has only one Rock-Eval value. Most of the wells are also characterized petrographically (section 1) and there is a good agreement between the measured %VRo values and the Tmax results. Indeed, the Tmax data also indicate that the Duvernay Formation spans from the early condensate-wet gas zone in the eastern part of the study area to possibly the dry gas zone towards its western limit. The spatial distribution of results indicates, as for the %VRo map (Figure 1.3), that there is a westerly increase in thermal maturation.

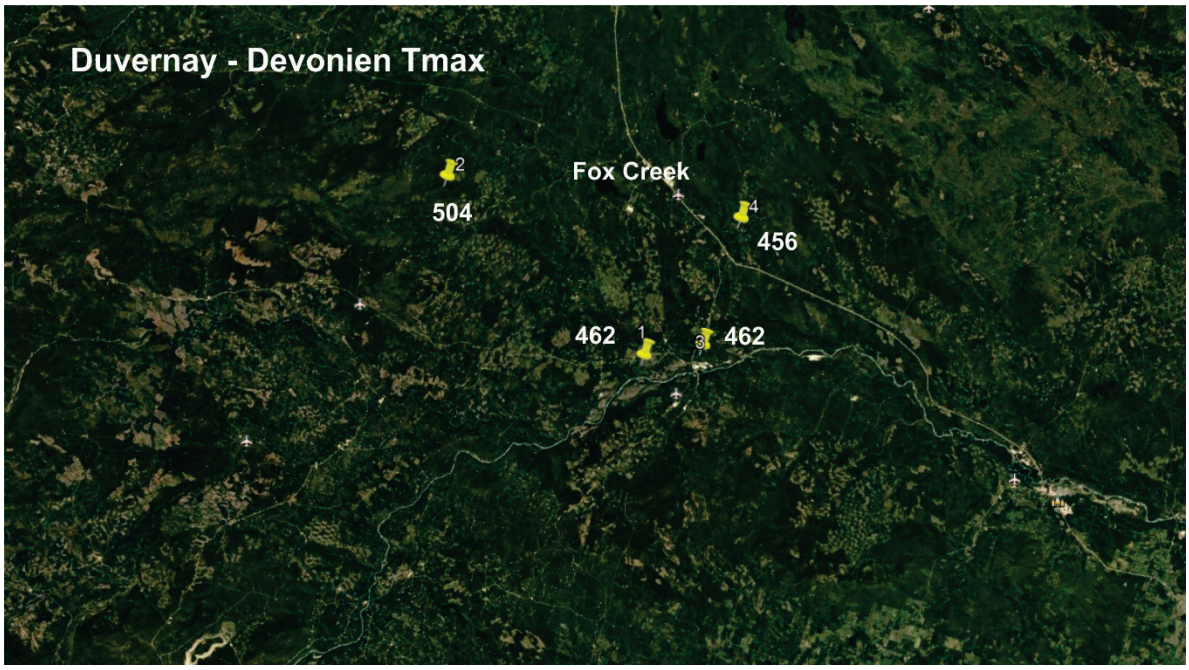

Figure 2.4: Spatial distribution of average Tmax data for the Duvernay Formation in the Fox Creek area. The yellow pins correspond to well locations.

Montney Formation

Twenty-one (21) Rock-Eval data obtained from 7 wells in the Fox Creek area (see Table 2.3) are presented in Table 2.4. Their spatial distribution is shown in Figure 2.5. As with the Duvernay, samples highlighted in yellow have not passed the quality criteria and are not considered any further.

Table 2.3: List and locations of available wells for the Montney Formation.

Well ID	Well Name	Well# on Map	Latitude	Longitude
100112406220W500	1976082 KAYBOBS 11-24-62-20	1	54.37986	-116.86765
102113406119W500	BURLINGTON ETAL 102 FOXCK 11-34-61-19	2	54.32032	-116.76767
100151906022W500	DELPHI BIGSNE 15-19-60-22	3	54.20831	-117.28781
100040605920W500	ACL FIR 4-6-59-20	4	54.06814	-116.99589
100111405723W500	TALISMAN WILDR 11-14-57-23	5	53.92805	-117.31407
100071406425W500	DELPHI SIMONN 7-14-64-25	6	54.53546	-117.66498
100113406119W500	ACL FOXCK 11-34-61-19	7	54.32025	-116.76781

Table 2.4: Summary of Rock-Eval6 data for the Montney Formation for 7 wells in the Fox Creek area. Rejected data are shown in yellow, due to their too low S2 (<0.35 mg HC/ g TOC) or Tmax (<400°) values. Samples number without C-number are from the Alberta Geological Survey (AGS).

C/AGS#	Well# on Map	Interval m	TOC wt. %	Tmax °C	S1 mg HC/g	S2 mg HC/g	S3 mg CO_2/g	HI mg HC/g TOC	OI mg CO_2/g TOC
C-534007	1	2105.1	0.26	411	0.4	0.57	0.29	219	112
8800	1	2081.0	7.05	443	1.36	19.33	0.38	220	4
	mean well #1			**427**					
C-533970	2	2166.3	0.45	440	0.55	0.53	0.22	117	49
C-533971	2	2171.4	0.06	436	0.05	0.23	0.20		
C-533972	2	2180.4	0.37	417	0.68	0.72	0.22	195	59
	mean well #2			**429**					
C-603757	3	2583.1	0.29	405	0.44	0.65			
C-603758	3	2589.0	0.63	421	0.63	0.85	0.14	224	48
C-603759	3	2596.3	0.46	430	0.55	0.59	0.15	135	24
	mean well #3			**419**			0.11	128	24
8808	4	2643.9	6.67	476	0.33	2.52	0.43	38	6
8813	4	2656.4	0.11	421	0.02	0.09	0.15	82	136
	mean well #4								
8819	5	3013.3	0.13	352	0.02	0.08	0.23	62	177
8891	6	2289.0	11.65	438	2.01	52.8	0.67	447	6
8893	6	2291.5	0.35	427	0.35	0.57	0.23	163	66
8894	6	2295.2	0.22	424	0.07	0.31	0.18	141	82
8895	6	2297.3	0.81	437	0.4	2.91	0.12	359	15
8897	6	2304.0	0.97	437	0.5	4.2	0.11	433	11
8898	6	2306.9	0.79	437	0.47	3.56	0.14	451	18
	mean well #6			**435**					
	7	2166.3		440	0.45	0.53	0.22	118	49
	7	2171.4		436	0.06	0.23	0.20	383	333
	7	2180.4		417	0.37	0.72	0.22	195	59
	mean well #7			**429**					

Although the very limited number of data points precludes a formal interpretation of the Tmax spatial distribution, these data suggest that the Montney Formation in the Fox Creek area is largely immature to early mature (Tmax < 435°C). The origin of organic matter in the Montney Formation has been a matter of debate in recent years (Crombez et al., 2016; Euzen et al., 2018; Chalmers and Bustin, 2012; Sanei et al., 2015; Wood et al, 2018, 2020). Although a limited amount of organic petrography evidence showed the occurrence of primary organic matter in the Montney Formation (Beaton et al., 2010), however, almost the majority of organic matter in the Montney Formation is migra-bitumen (Sanei et al., 2015; Wood et al., 2018, 2020). Therefore, the Rock-Eval data for Montney Formation cannot be used accurately for kerogen type determination and thermal maturity.

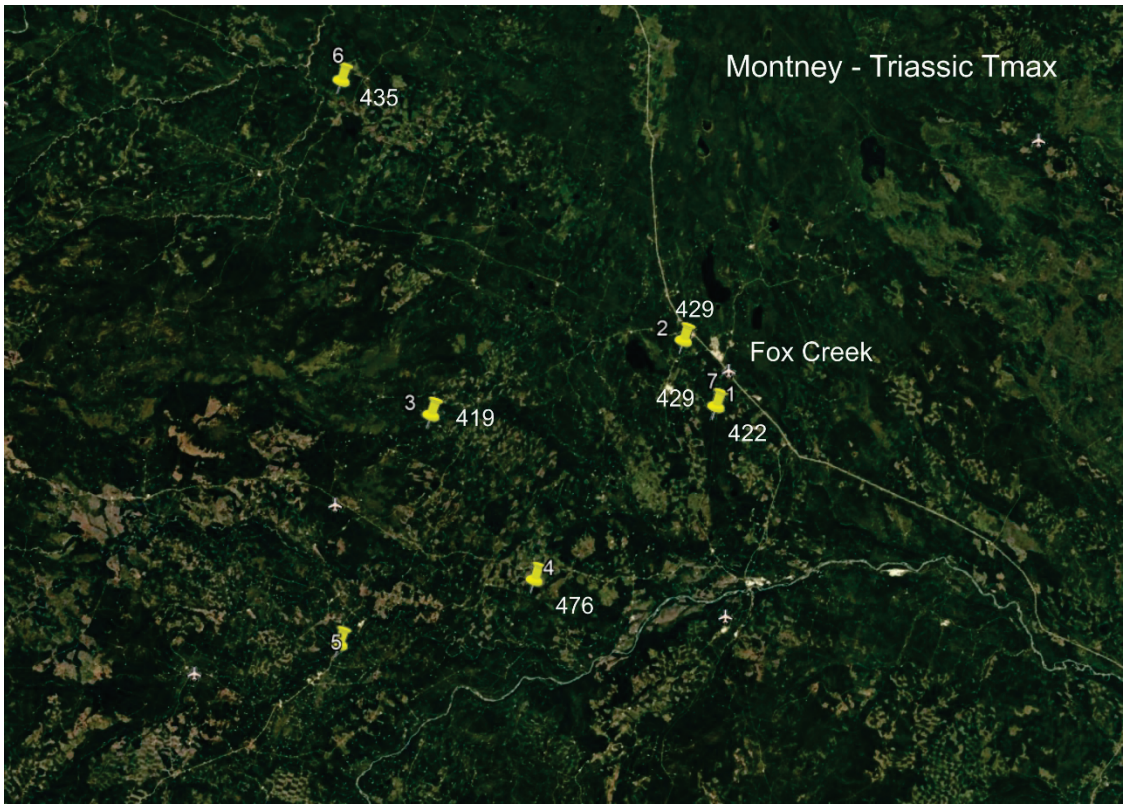

Figure 2.5. Spatial distribution of average Tmax data for the Montney Formation in the Fox Creek area. The yellow pins correspond to well locations.

Even if data are relatively scarce, pseudo Van Krevelen (Fig. 2.6) and Tmax vs HI (Fig. 2.7) diagrams have been constructed. They also suggest that the kerogen in the Montney Formation is a mixture of Type II and III organic matter and hydrocarbons range from immature to early mature conditions.

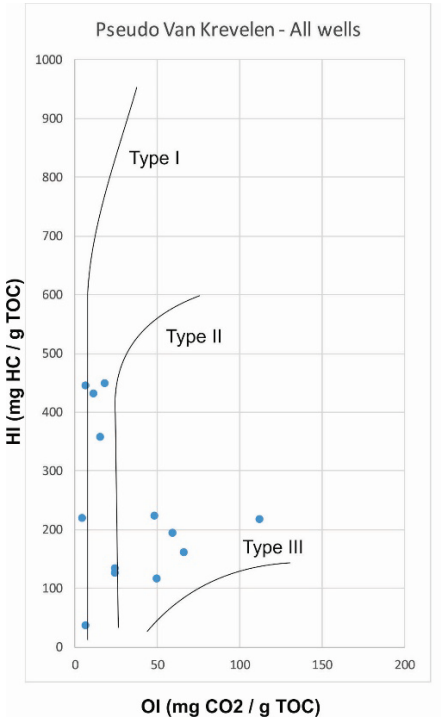

Fig. 2.6 Pseudo Van Krevelen diagram for the Montney Formation from available data in the study area.

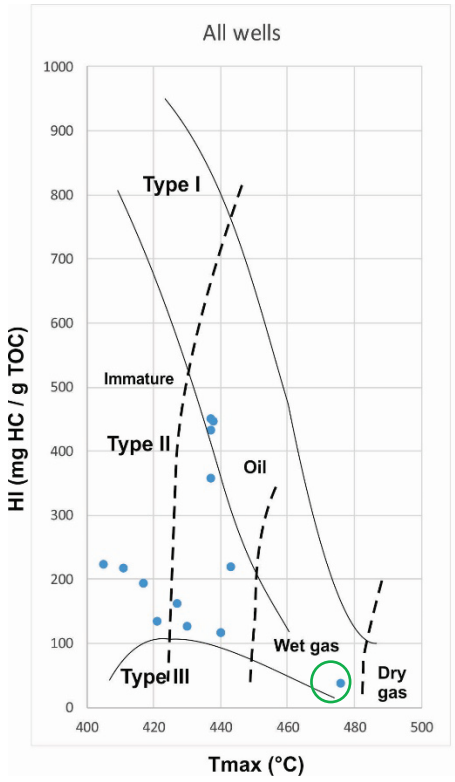

Fig. 2.7. The Tmax vs HI diagram for the Montney Formation from available data in the study area. There is an anomalous value near the transition between wet and dry gas that comes from a single analysis from well #4 (circled in green).

Nordegg Member

Two wells in the Fox Creek area have provided some Rock-Eval data for the Nordegg Member (Table 2.5 and 2.6). For both wells, samples were collected at about 2 km in depth. Of note, only one data is available for well #1. Data are plotted on the map of the area (Fig. 2.10).

Table 2.5: List and locations of wells for the Nordegg Member

Well ID	Well Name	Well# on Map	Latitude	Longitude
100112406220W500	1976082 KAYBOBS 11-24-62-20	1	54.3798	-116.868
100042806220W500	1976082 KAYBOBS 4-28-62-20	2	54.3868	-116.948

C#	Well# on Map	Interval m	TOC wt. %	Tmax °C	S1 mg HC/g	S2 mg HC/g	S3 mg CO_2/g	HI mg HC/g TOC	OI mg CO_2/g TOC	PI S1/(S1+S2)
C-534005	1	2080.9	8.79	443	1.36	19.33	0.38	220	4	0.06
C-583671	2	2114.2	9.86	445	4.44	18.71	0.57	190	6	0.2
C-583671	2	2114.2	11.15	444	4.66	18.98	0.58	170	5	0.21
C-583672	2	2114.5	8.57	442	2.96	14.89	0.53	173	6	0.17
C-583672	2	2114.5	7.56	445	2.73	12.71	0.58	168	8	0.18
C-583673	2	2116.8	6.07	446	1.76	9.41	0.48	155	8	0.16
C-583673	2	2116.8	6.49	441	1.88	9.58	0.5	148	8	0.16
C-583674	2	2117.8	10.51	446	2.65	19.54	0.62	186	6	0.12
C-583674	2	2117.8	10.04	447	2.61	19.22	0.58	191	6	0.12
C-583675	2	2118	9.83	449	2.11	15.35	0.51	156	5	0.12
C-583675	2	2118	9.95	440	2.12	15.74	0.51	158	5	0.12
C-583676	2	2119	13.66	447	3.68	29.74	0.65	218	5	0.11
C-583676	2	2119	12.82	446	4.05	30.22	0.59	236	5	0.12
	mean well 2			**445**				**179**	**6**	**0.15**

The Rock-Eval data suggest high TOC, S1, and S2 values, indicative of great source rock. The production index (PI = S1/[S1+S2]) is a measure of the transformation of the organic matter into hydrocarbons with initial generation at a ratio of 0.1. The single value from well #1 suggests immature conditions with a PI of 0.06, whereas data from well #2 offer PI ranging from 0.11 to 0.2 (average of 0.15), suggesting a very early stage of hydrocarbon generation. Pseudo Van Krevelen and Tmax versus HI diagrams are presented in Figures 2.8 and 2.9. Indeed in Figure 2.8, data appear in the fields of Type I / II, while in Figure 2.9, all data plots in the field corresponding to the Type II organic matter for shales in the oil window. The spatial distribution for data of the Nordegg Member is shown in Fig. 2.10

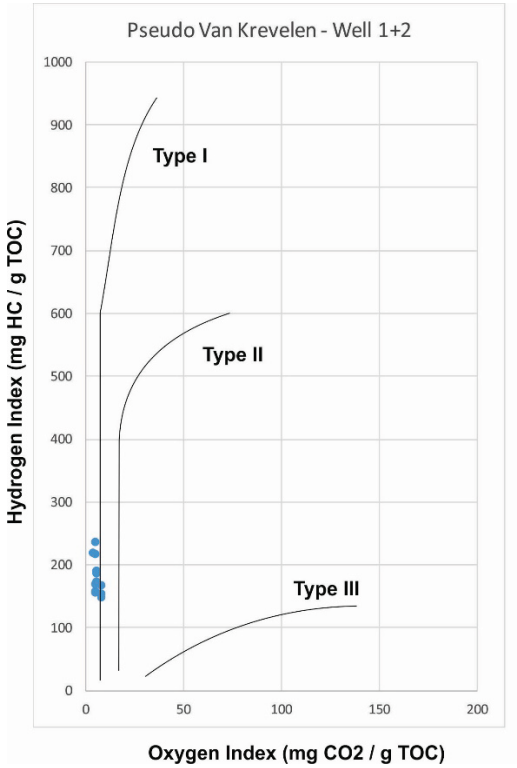

Figure 2.8 Pseudo Van Krevelen diagram for the Nordegg Member using available data in the study area.

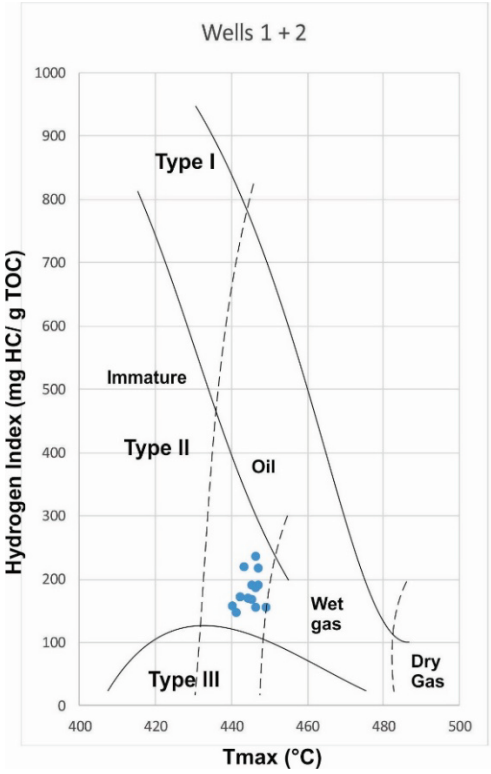

Fig. 2.9 HI vs Tmax diagram for the Nordegg Member using available data in the study area.

The Tmax data (from 2 wells), although very limited in number, suggest that the Nordegg Member in the Fox Creek area is mature (Tmax ≈ 445°C).

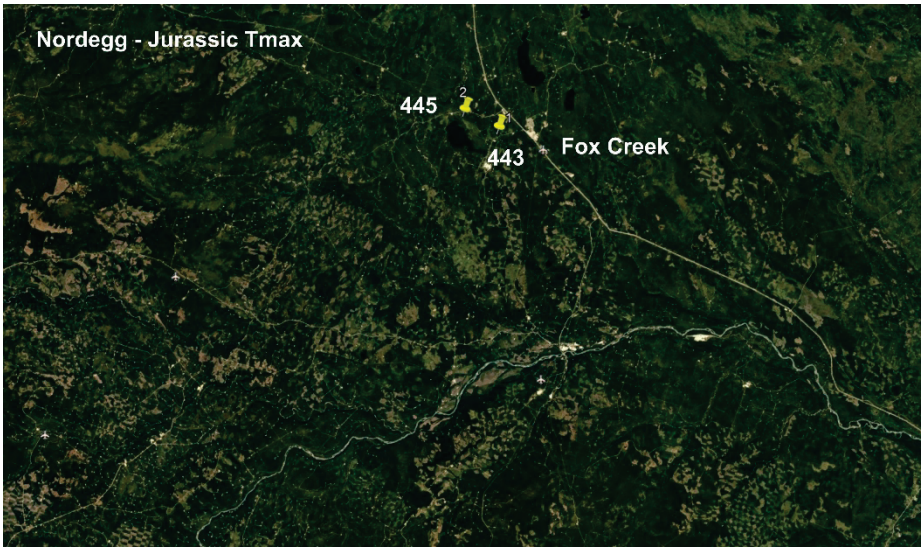

Figure 2.10: Spatial distribution of average Tmax data for the Nordegg Member in the Fox Creek area. The yellow pins correspond to well locations.

3. Gas composition and carbon isotopes for wells in the Fox Creek area

This section aims to complement the previously presented analyses on the organic matter, which allowed us to characterize the type of organic material in sedimentary units and to evaluate the thermal rank of that organic matter in order to generate knowledge on which unit and what type of hydrocarbons (oil, wet gas, and dry gas) should be expected from the sub-surface. We had access to composition and isotope results of gas samples collected in isotubes at various depths from 7 wells (Table 3.1) drilled in the area of interest between 2008 and 2017. Their spatial distribution is shown in Figure 3.1. One (well #5) is located north 40 km of Grande Prairie.

Table 3.1. Wells with gas hydrocarbons composition and $\delta^{13}C$ ratios in the general area.

Well ID	Well Name	Well# on Map	Latitude	Longitude
100070206318W500	SCL HZ FOXCK 8-34-62-18 (FOX CREEK 19)	1	54.4197	-116.613
100011806117W500	SCL FOXCK 1-18-61-17W5 (FOX CREEK 2)	2	54.27135	-116.532
100041906422W500	SCL HZ 102 MCKINLEY 5-30-64-22	3	54.54685	-117.326
100041606420W500	SCL HZ KAYBOB 4-16-64-20	4	54.51215	-116.975
100121908107W600	SCL HZ KAYBOB 15-22-63-20	5	56.03899	-119.095
100012906320W503	SCL HZ KAYBOB 1-29-63-20	6	54.48954	-116.986
100023206320W500	SCL KAYBOB 10-5-6-20	7	54.48954	-116.986

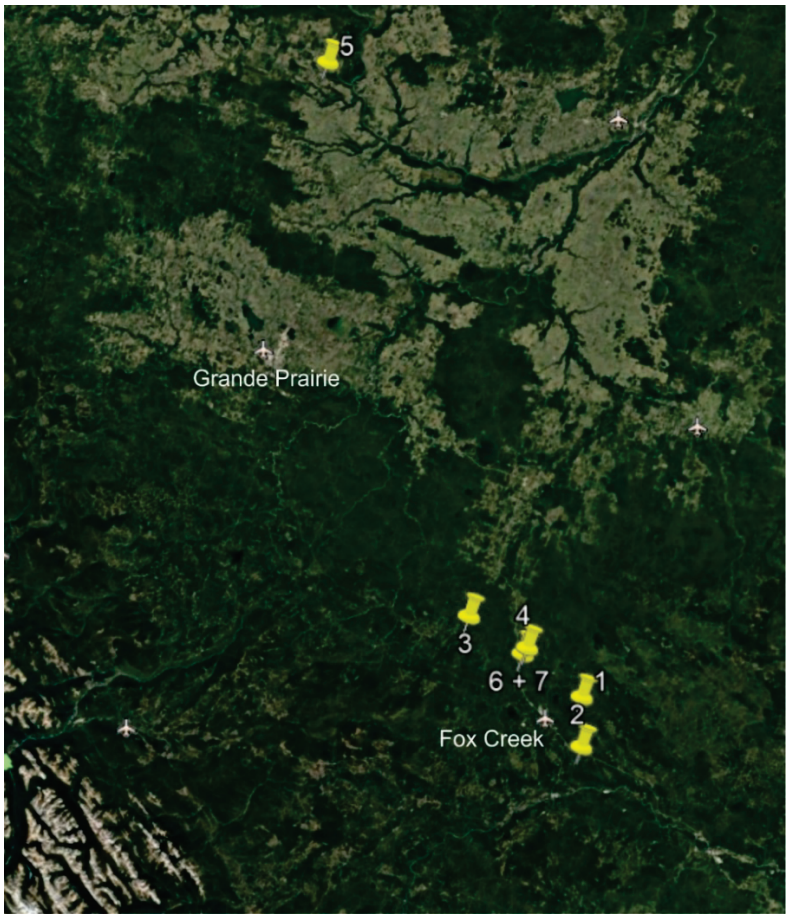

Figure 3.1. Location of 7 wells with gas composition and carbon isotope ratios, 6 in the Fox Creek area and one 40 km north of Grande Prairie.

The data available include the gas composition of C1, C2, and C3 (i.e. of methane, ethane, and propane) and their carbon isotope ratios when enough gas was available. From this data set, some ratios were calculated: gas wetness (C1/[C2+C3]), iso-butane over n-butane (iC4/nC4), $\Delta^{13}C$ ($\delta^{13}C_{methane}$ - $\delta^{13}C_{ethane}$) (Appendix 1). The vertical variations of gas composition, isotopic ratios, and other tracers are presented in various diagrams of Appendices 2 to 10. The stratigraphic assignment is provided in Appendix 1, and all measured depths were transferred into true vertical depths using the azimuth and inclination data. Only meaningful, representative, or interesting relationships will be illustrated and discussed in this section. Topics to be discussed are the following: 1) $\delta^{13}C$-methane versus gas wetness, 2) $\delta^{13}C$-methane versus depth, 3) $\delta^{13}C$-ethane versus depth, 4) $\delta^{13}C$-ethane versus $\delta^{13}C$-propane, 5) depth versus iC4/nC4, 6) depth versus $\delta^{13}C$-methane - $\delta^{13}C$-ethane, 7) isotopic partial rollover and secondary cracking) gas (C1 and C2) isotope ratios versus sedimentary units.

$\delta^{13}C$-methane versus gas wetness

The $\delta^{13}C$-methane versus gas wetness diagram (Bernard et al., 1978) is commonly used to distinguish between the microbial and thermogenic source of methane. For all wells, the data suggest a strongly dominant thermogenic source. However, two wells also offer $\delta^{13}C$-methane ratios that plot outside the field of thermogenic source, but their wetness ratio values are still compatible with a dominant thermogenic origin. For these two wells, these slightly divergent values are found at the top of the sedimentary succession that was sampled for gas, although the sample

depth is over 1 km for both (1110 and 1575 m; Kabob 15-22-63-20 and Kabob 1-29-63-20, respectively). For all other wells, the first collected samples are always > 2 km. Figure 3.2 presents the two different situations. Individual graphs for each well are provided in Appendix 2.

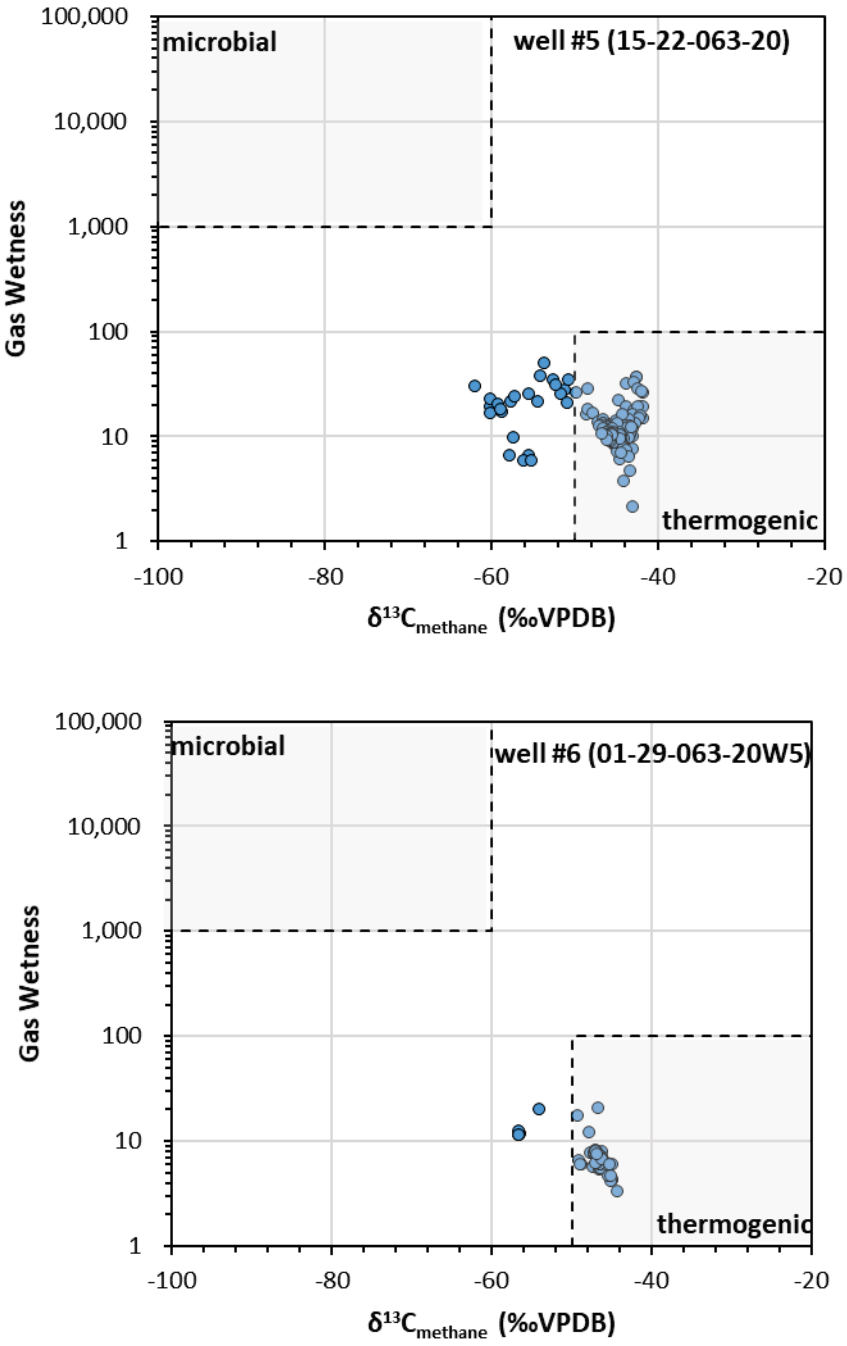

Figure 3.2. Bernard diagrams for wells #5 (top) and #6 (bottom), wells location are provided in Table 3.1 and on the map of Figure 3.1.

$\delta^{13}C$-methane versus depth

At least three patterns can be seen from this dataset. Wells #2 and #4 display irregular distribution of data points, with no visible trends. Wells # 3, 5, and 7 offer distinct relationships of either progressively heavier (#3 and 5) or lighter (#7) ratios with depth (Fig. 3.3). Wells #1 and 6 display more or less perfectly developed progressive enrichment in heavy carbon isotope with depth up to a point (variable) at which an inverse trend is observed and after the reverse tendency (Fig. 3.3). . Individual graphs for each well are provided in Appendix 3.

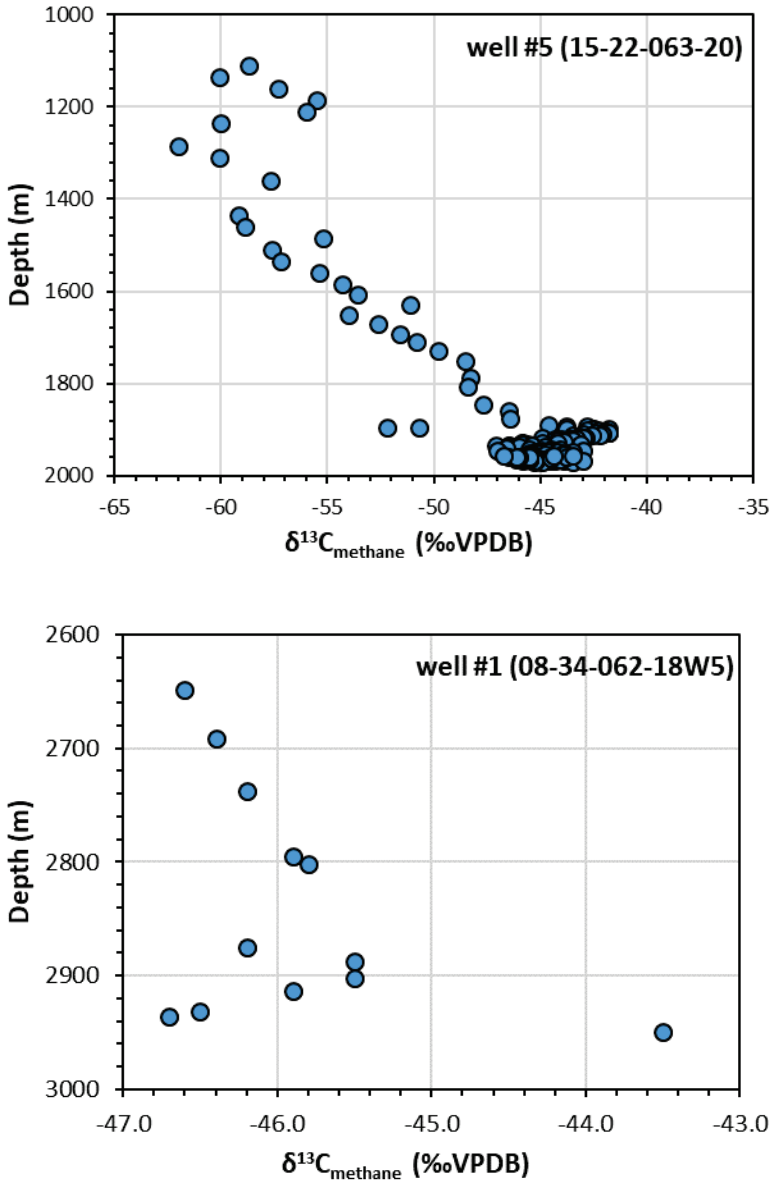

Figure 3.3. $\delta^{13}C$-methane progressively heavier trend with depth for wells #5 (top) and inverted trends of well #1 (bottom). Wells location is shown in Fig. 3.1. Individual graphs for each well are provided in Appendix 3.

$\delta^{13}C$-ethane versus depth

As seen in Appendix 4, except for three wells, all show a progressive enrichment of heavy carbon isotope in ethane with depth. Wells #1, 4, and 5 display the same pattern as observed for the evolution of carbon isotopes of methane with depth, with an initial enrichment in heavy isotopes then a reverse tendency towards a lighter isotope ratio. This is related to the secondary cracking effect (Fig. 3.4).

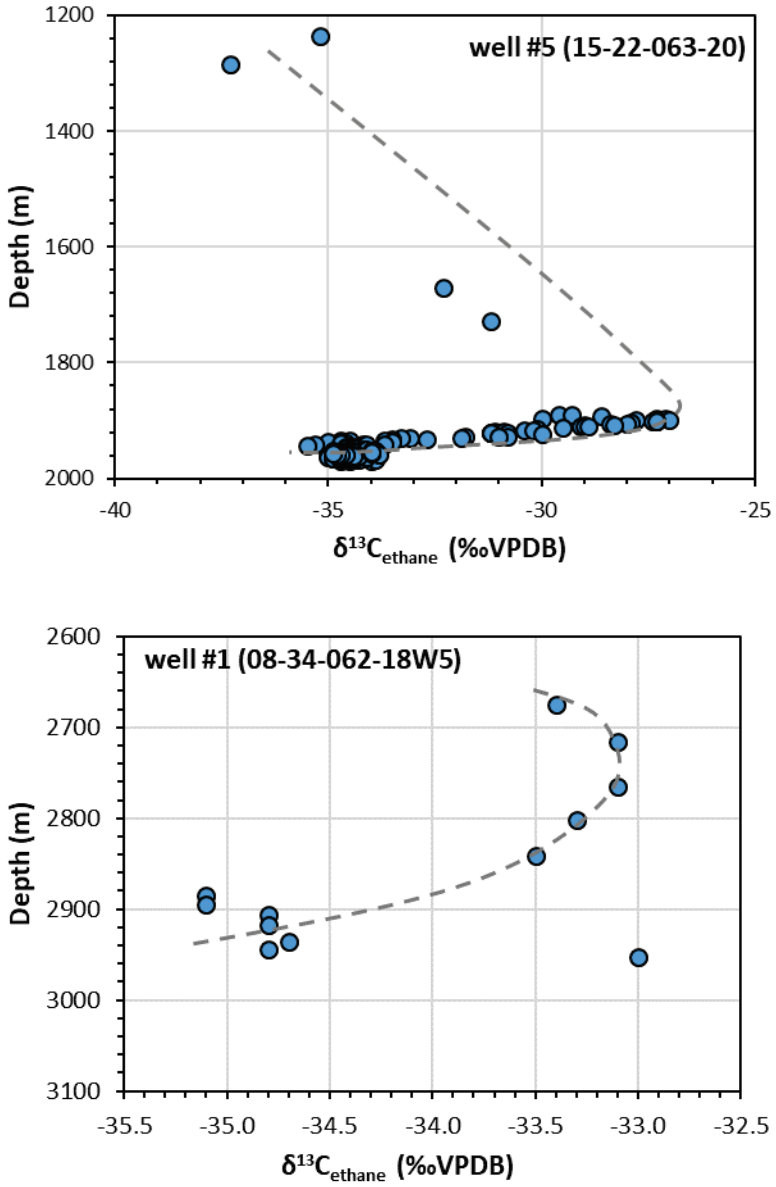

Figure 3.4 Potential partial isotopic rollover recorded by $\delta^{13}C$-ethane, same wells as on Fig. 3.3 (wells #5 on top and well #1 at the bottom).

δ^{13}C-ethane versus δ^{13}C-propane

Carbon isotope ratios of propane are not available for each well and definitively not for all samples. Wells with no evidence of isotope reversal display a statistically robust positive correlation ($R^2 = 0.84$) between δ^{13}C-ethane and δ^{13}C-propane ratios (top graph of Figure 3.5 shows an example). On the other hand, data showing a possible isotopic rollover are characterized by no correlation between ethane and propane carbon isotope ratios (the bottom graph of Figure 3.5 provides an example of such behaviour). Individual graphs for each well are provided in Appendix 3.

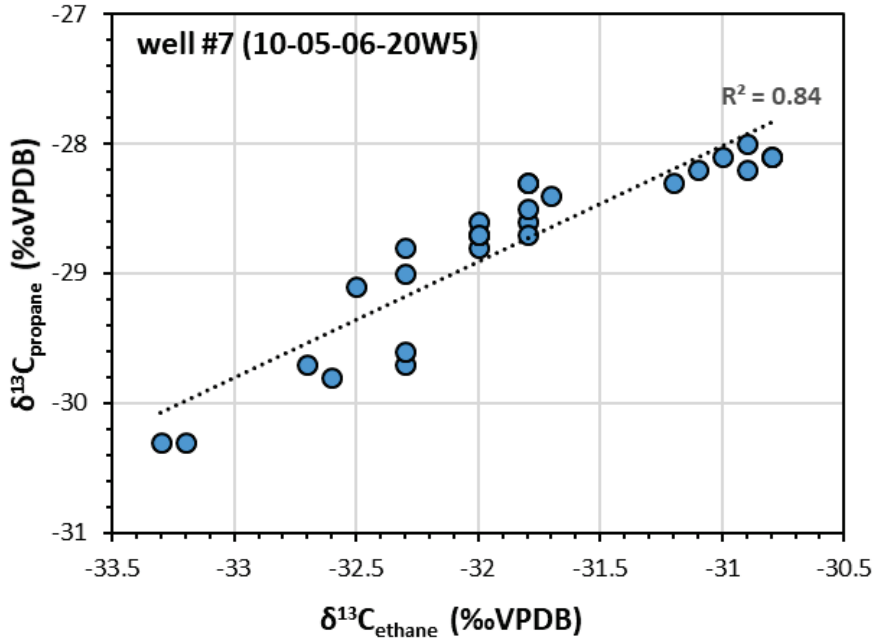

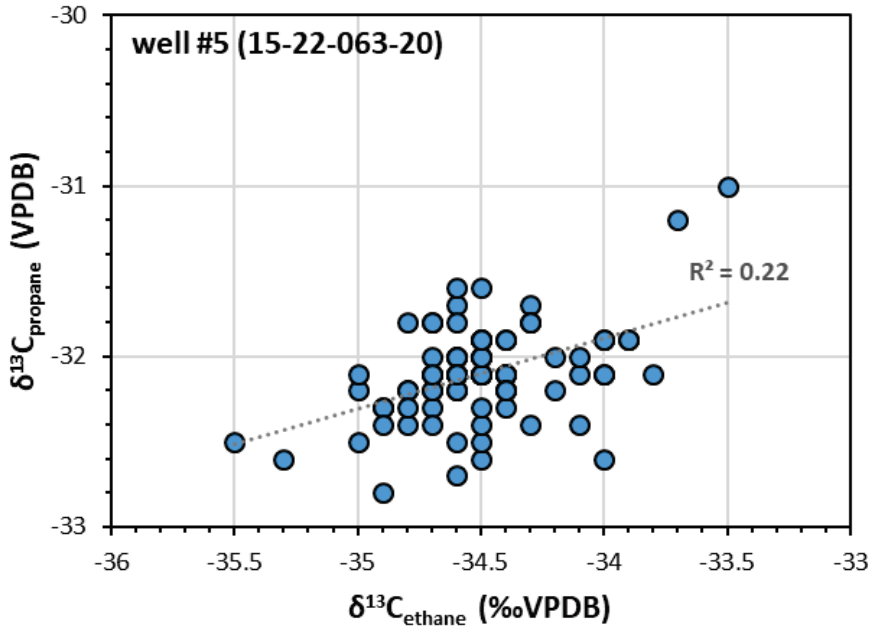

Figure 3.5: δ^{13}C-ethane versus δ^{13}C-propane diagrams with, on top (well #7), a significant correlation between the isotopic ratios for the two gas and bottom, well #5 with no statistically significant correlation. The well at the bottom shows the isotopic record of secondary cracking based on δ^{13}C-ethane with depth (Fig. 3.4).

Depth versus iC4/nC4

In their study of the Utica Shales in Quebec, Chatellier et al. (2013) have shown that the evolution of the ratios of the two isomers of butane with depth mimics that of the carbon isotopic ratios of ethane with depth, with a reversal tendency at the same depths. Butane occurs under two main structural isomers, n-butane (or normal – chain-like) and isobutene (or branched - with T shaped for carbon molecule structure). Chatellier et al (2013) have noticed a reversal in the increasing iC4/nC4 ratio with depth followed by a decreasing ratio in the isotopic reversal zone. This could indicate that secondary cracking of wet gas in the overpressure zone has some role in the transition from one isomer to the other, as iC4 is less stable than nC4.

Wells #1 and #5 show the effect of ratio reversal (shown in Fig. 3.4): the vertical evolution of the iC4/nC4 ratio suggests a reversal of the trend at the same depth where the trend for the δ^{13}C ratio of ethane is inverted (Fig. 3.6). Individual graphs for each well are provided in Appendix 6.

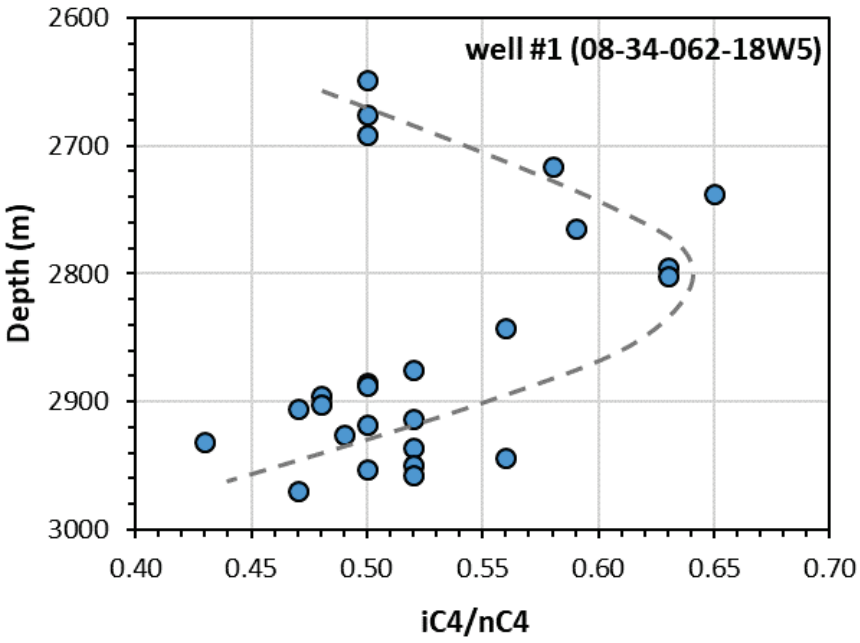

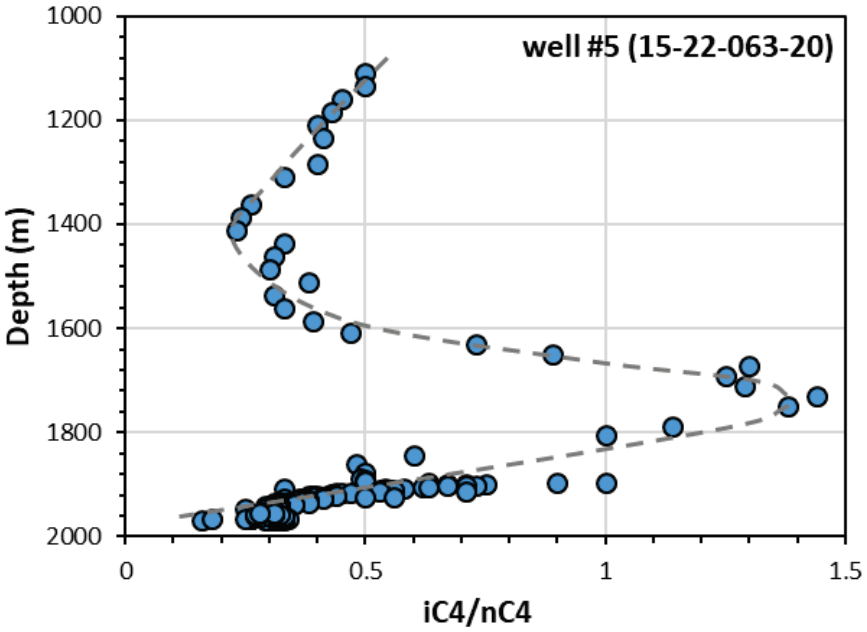

Figure 3.6: Vertical trend of iC4/nC4 ratio with depth. The two presented wells have trends suggesting butane ratio reversal. The evolving trend of iC4/nC4 is reversed in the interval where the carbon isotope trend of ethane is reversed. The location of wells #1 (top) and #5 (bottom) is provided in Fig. 3.1.

Depth versus [δ^{13}C-methane - δ^{13}C-ethane]

As temperature increases with depth, secondary cracking of higher hydrocarbons will take place at some point and produce isotopically lighter daughter C2+ products, which will ultimately result in partial or complete isotope rollover with δ^{13}C of methane. For wells with enough pairs of [δ^{13}C-methane and δ^{13}C-ethane] values, a decreasing trend is locally present with depth (Fig. 3.7 provides an example for well #7 and Appendix 7 provides graphs for three other wells).

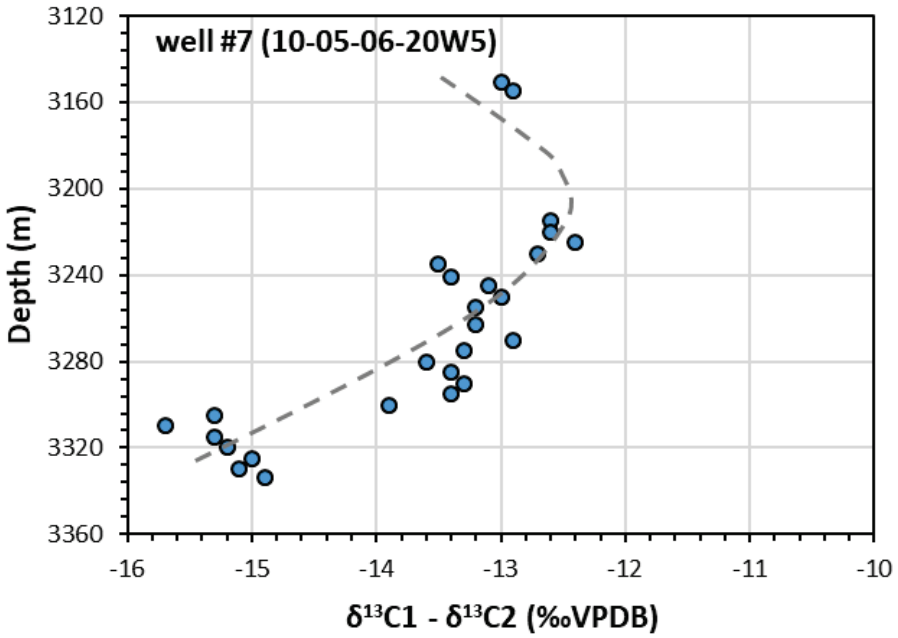

Fig. 3.7: Depth versus [δ^{13}C-methane - δ^{13}C-ethane] values for well #7. The location of this well is shown in Fig. 3.1.

Isotopic partial rollover and secondary cracking

The identification of an isotopic rollover and hence of secondary cracking can only be recognized if the dataset covers intervals that span this transition. As seen in the previous sections, some depth intervals are either too short or too deep to cover the transition. For this particular dataset, the relationship of progressively heavier (less negative) carbon isotope ratios for methane to ethane and propane (i.e. δ^{13}C1 > δ^{13}C2 > δ^{13}C3), characteristics of full isotopic rollover in highly mature basins (Zumberge et al., 2012), is not observed.

The previously used parameters (δ^{13}C ethane, iC4/nC4, and [δ^{13}C-methane - δ^{13}C-ethane are here plotted against gas wetness to identify the presence of an isotopic rollover and secondary cracking (Zumberge et al., 2012). The gas wetness ratio diminishes with increasing temperature, as secondary cracking of oil will increase the concentration of C2+ given a thermogenic source of hydrocarbons.

Figure 3.8 presents the best case in our dataset for δ^{13}C ethane versus gas wetness, other diagrams being rather inconclusive (see Appendix 8). For well #5, the dataset covers a wide spectrum of wetness ratios, over which the sudden decrease in wetness ratio is associated with ethane becoming isotopically lighter.

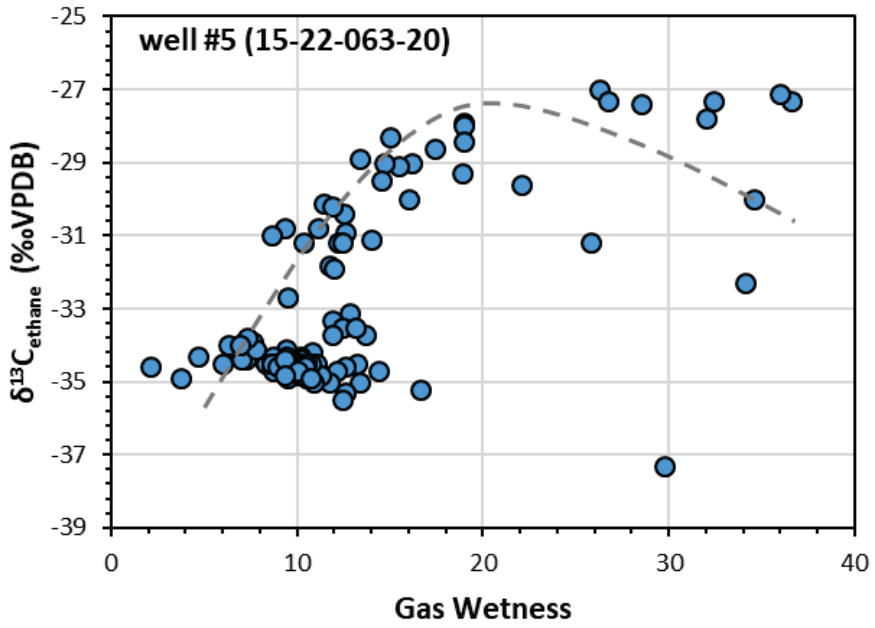

Figure 3.8: Isotopic rollover for well #5 at gas wetness of about 20 where secondary cracking produces isotopically lighter ethane.

For the same well, the relationships between iC4/nC4 ratios and wetness (Appendix 9) also suggest secondary cracking of wet gas (top graph of Fig. 3.9) at approximately the same wetness value of 20 – 30 as in Fig. 3.8. However, well #1 where secondary cracking is recorded in butane ratio vs depth (Fig. 3.6), does not show the inverted trend (bottom graph of Fig.3.9).

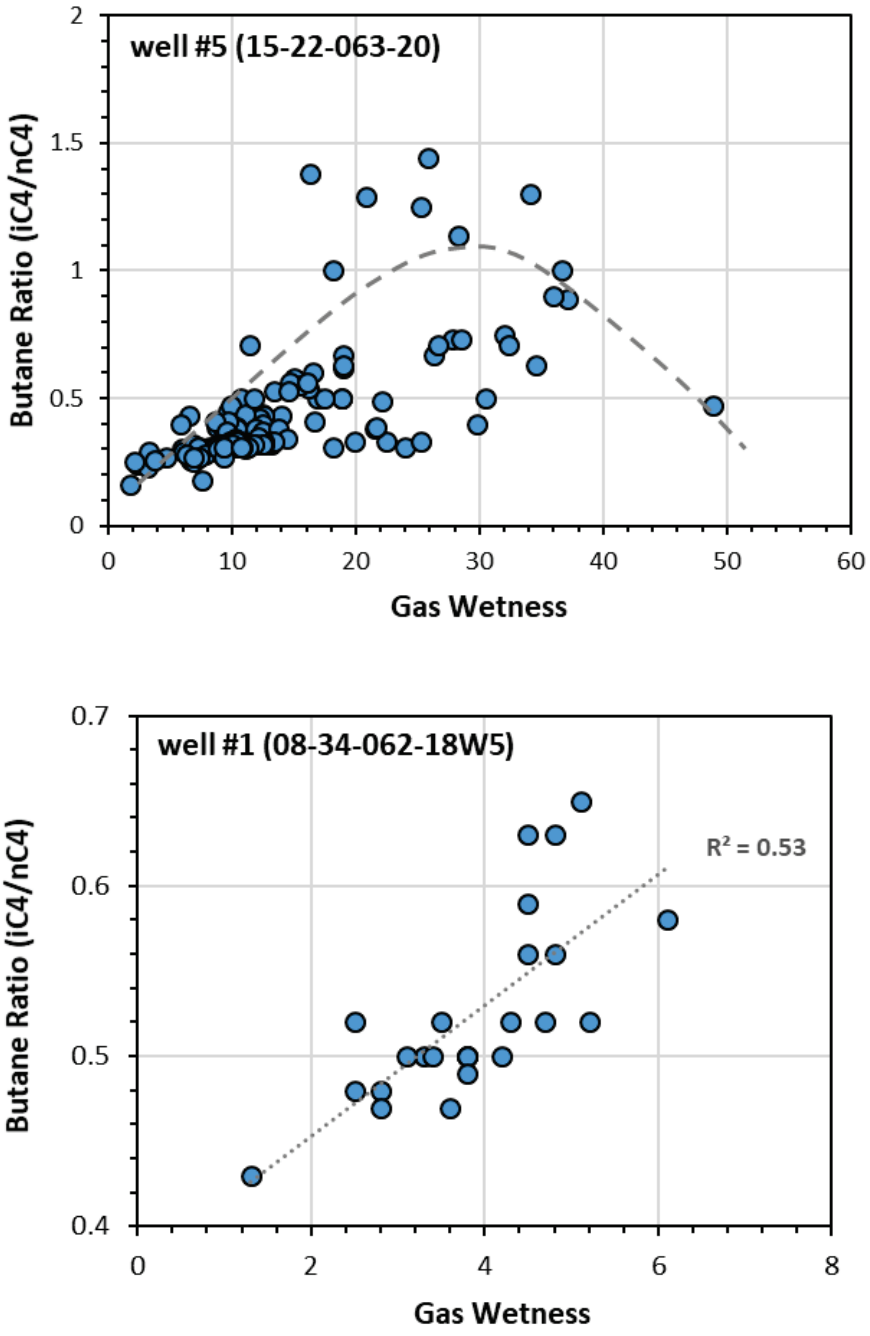

Figure 3.9: Top graph: the inverted trend for well #5 of iC4/nC4 ratios with respect to wetness; bottom graph: linear relationship for well #1, which seemingly shows partial rollover based on butane ratio versus depth (Fig. 3.6).

Another set of parameters that is useful in recognizing secondary cracking is the difference between $\delta^{13}C1$ and $\delta^{13}C2$. As conditions for secondary cracking are met, the $\delta^{13}C2$ (and $\delta^{13}C3$) ratios will progressively become lighter up to a point where it becomes lighter than that of methane. As with other approaches, a complete set of data

covering the interval where secondary cracking occurs would be required to detect a rollover. Our dataset, to the contrary, is rather incomplete, as $\delta^{13}C2$ values were not analyzed at all depths and not even for all wells, and cover only deeper, likely post-secondary cracking zones. Only two wells have a robust correlation ($R^2 > 0.6$) between evolving $\delta^{13}C1 - \delta^{13}C2$ values with respect to decreasing wetness, (suggesting partial rollover ($\delta^{13}C1 - \delta^{13}C2 < 0$). They are shown in Figure 3.10. Graphs for the remaining wells are provided in Appendix 10.

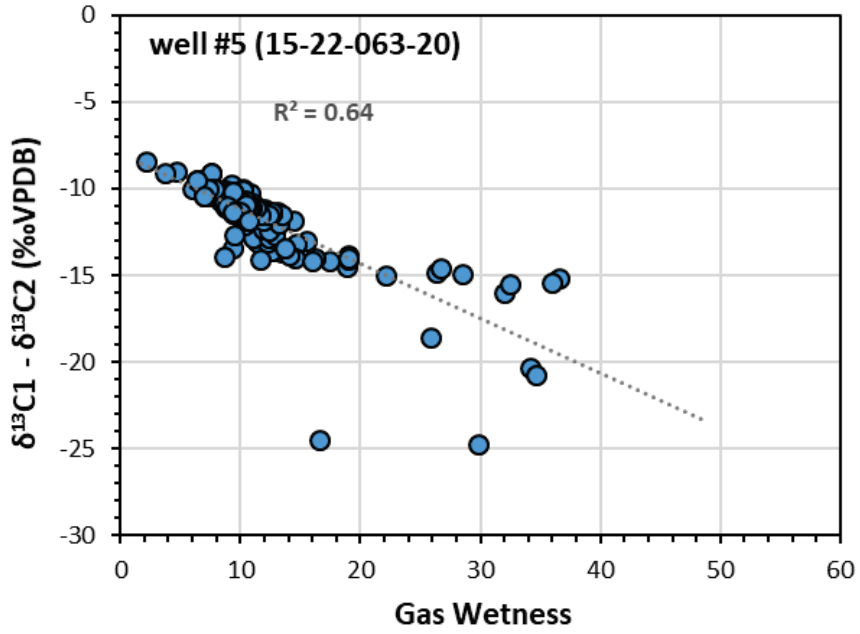

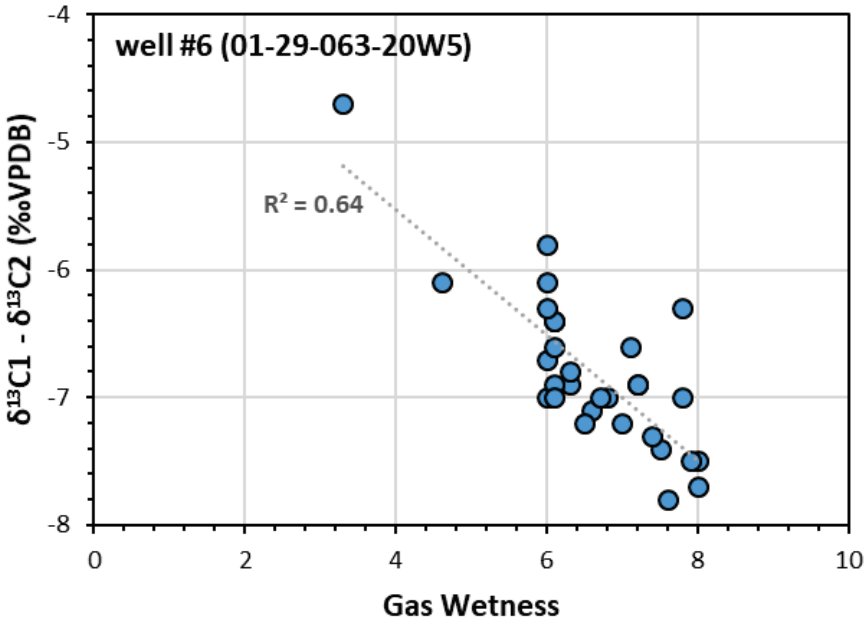

Figure 3.10: Identification of secondary cracking and incomplete reversal based on the evolution of the difference of $\delta^{13}C1$ and $\delta^{13}C2$ with respect to gas wetness. The complete reversal would result in $\delta^{13}C1 - \delta^{13}C2$ being over a value of zero. The location of wells #5 (top) and #6 (bottom) is shown in Fig. 3.1.

Methane and ethane carbon isotope ratios versus sedimentary units

It is of interest to contrast the $\delta^{13}C1$ and $\delta^{13}C2$ isotope gas ratios of various potential source rock units to eventually help identify the source of eventual dissolved hydrocarbons in groundwater. We currently do not have such data for the very shallow coals of the Paskapoo Formation, in which the regional aquifer is located; every coal bed intercepted in the shallow drilling program will be characterized. Units for which we currently have data are the Duvernay Formation, the Montney Formation, the Nordegg Member and its Fernie Formation, the Gething Formation, and the Mannville Group. Data is presented in Table 3.2 and plotted on area maps in Figures 3.11 to 3.16.

Table 3.2: Summary of methane and ethane $\delta^{13}C$ ratios for various units for individual wells. (std is the standard deviation and n is number of results).

Unit/age	Well	$\delta^{13}C$ methane	$\delta^{13}C$ ethane
Duvernay / Devonian	2	**mean -44.2** **Std 0.3** **n=23**	**mean -32.8** **std 0.45** **n = 21**
	3	**mean -45.9** **std 0.53** **n = 10**	**mean -34.7** **std 0.61** **n = 9**
	4	**mean -45.5** **std 0.41** **n = 47**	**mean -33.2** **std 0.3** **n = 47**
	7	**Mean -46.2** **Std N/A** **n = 2**	**Mean -33.3** **Std N/A** **n = 2**
Montney / Triassic	4	**mean -46.3** **std 0.82** **n = 15**	**mean -39.1** **std 0.93** **n = 11**
	6	**mean -46.3** **std: 0.71** **n=29**	**mean -39.5** **std 0.29** **n = 29**
Nordegg / Jurassic	4	**mean -46.9** **std 0.29** **n = 6**	**mean -40.6** **std 0.17** **n = 6**
	5	**mean -45.1** **std 0.85** **n=51**	**mean -34.5** **std 0.27** **n = 51**
Fernie / Jurassic	4	**mean -46.6**	**mean -35.5**

		std: 0.23	**std 2.72**
		n = 11	**n = 11**
	5	**mean -44.4**	**mean -32.6**
		std 1.35	**std 2.41**
		n = 72	**n = 66**
Gething / Cretaceous	5	**mean -45**	**Mean -28.2**
		std 2.61	**std 1.17**
		n = 12	**n = 9**
	6	**Mean -46.7**	
		std: 0.61	
		n=27	
Mannville / Cretaceous	5	**mean -50.6**	
		std 2.22	
		n = 11	

The Duvernay Formation is the unit for which there is most data (Table 3.2 and Fig. 3.11); there are minor variations in $\delta^{13}C$ ratios for both methane and ethane. However, all wells are located at a close distance and concentrated in the eastern domain of the study area.

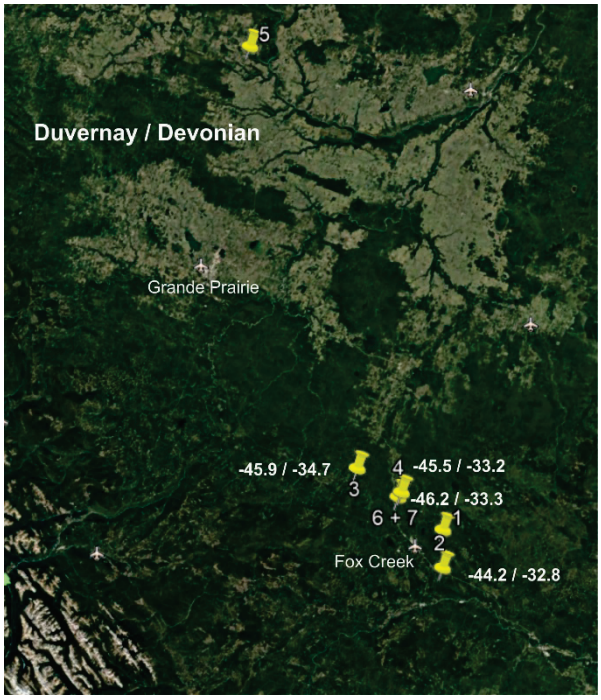

Fig. 3.11: Spatial distribution of the mean $\delta^{13}C$ ratios for methane (first number) and ethane (second number) in the Duvernay Formation.

The Montney Formation has $\delta^{13}C$ ratios that are statistically similar for both methane and ethane (Fig. 3.12). For well #4 in which the Duvernay Formation is also present, the Montney is slightly more negative (isotopically lighter) reflecting its shallower depth in the subsurface.

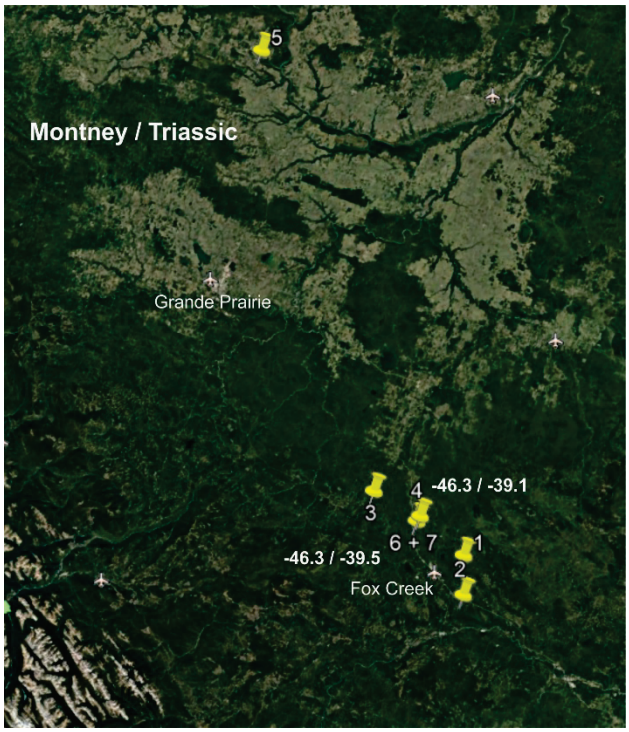

Fig. 3.12: Spatial distribution on $\delta^{13}C$ ratios for methane (first number) and ethane (second number) in the Montney Formation.

The Nordegg Member is only present in two wells (Table 3.2); Figure 3.13 shows that $\delta^{13}C$ ratios for methane and ethane in well #4 are statistically similar to those of the Montney from the same well. However, values for well #5, located much further north, are slightly less negative (isotopically heavier) for both methane and ethane, which could indicate slightly deeper paleoburial depth even if samples are from similar actual depths (see Appendix 1).

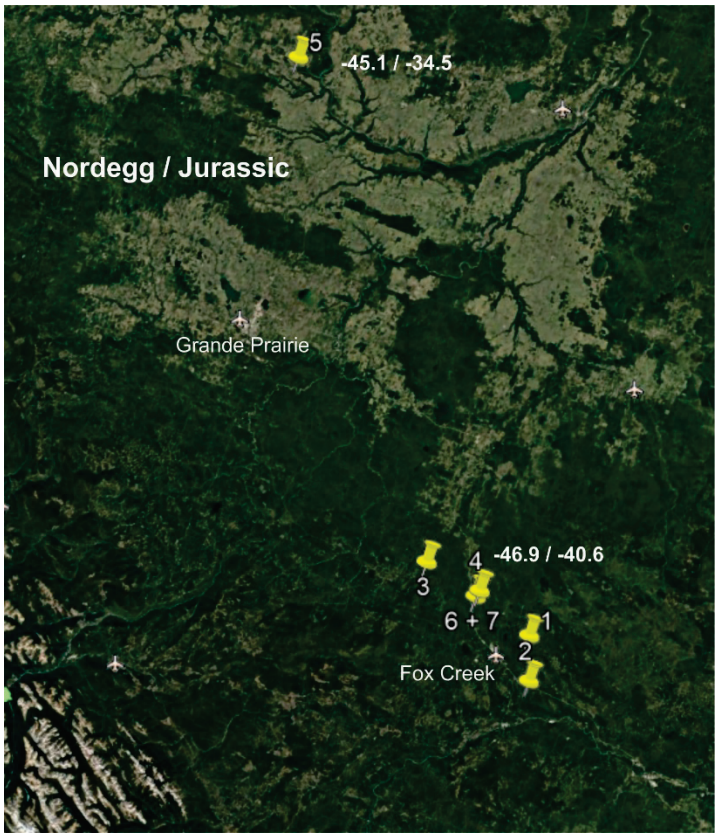

Fig. 3.13: Spatial distribution of $\delta^{13}C$ ratios for methane (first number) and ethane (second number) in the Nordegg Member.

Samples from wells #4 and 5 assigned to the Fernie Formation, containing the Nordegg Member (Fig. 3.14), are located in fact a few meters above those of the Nordegg Member (see Appendix 1). On a well-to-well basis (Table 3.2), methane $\delta^{13}C$ ratios are statistically similar. However, ethane $\delta^{13}C$ ratios from the Fernie Formation are isotopically heavier compared to those of the Nordegg Member, in line with the partial isotopic reversal visible on Fig. 3.4 for well #1 and #5

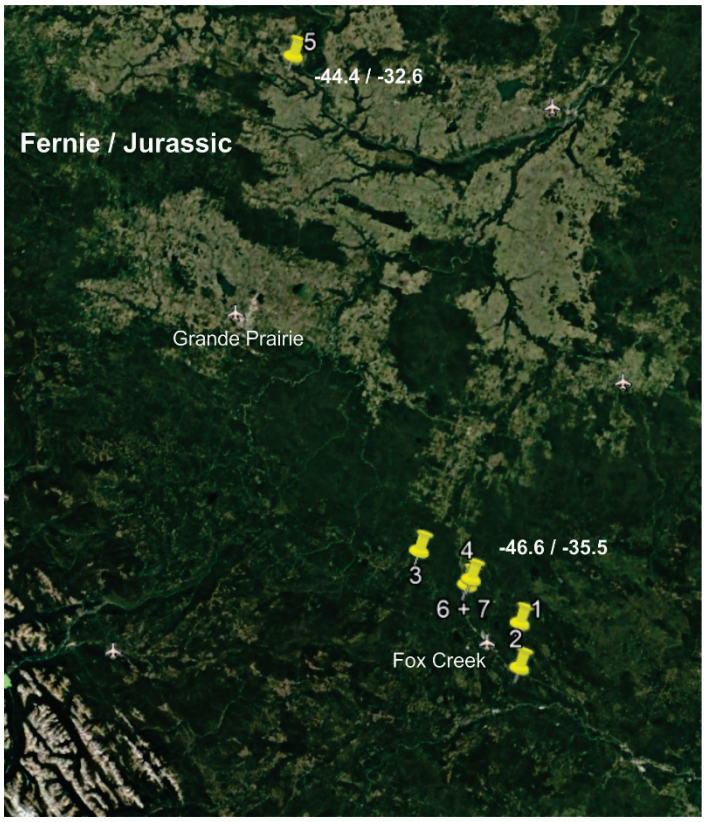

Fig. 3.14: Spatial distribution of $\delta^{13}C$ ratios for methane (first number) and ethane (second number) in the Fernie Formation, containing the Nordegg Formation.

The Gething Formation of the Mannville Group is present in wells # 5 and #6 (Table 3.2 and Fig. 3.15), but ethane $\delta^{13}C$ ratios are only available in well #5. The methane $\delta^{13}C$ ratios are statistically similar to those of the Fernie Formation in well #5. However, the ethane $\delta^{13}C$ ratios are significantly isotopically heavier compared to those of the deeper Fernie Formation and Nordegg Member, providing more evidence for the partial isotopic rollover (Fig. 3.4 for well #5).

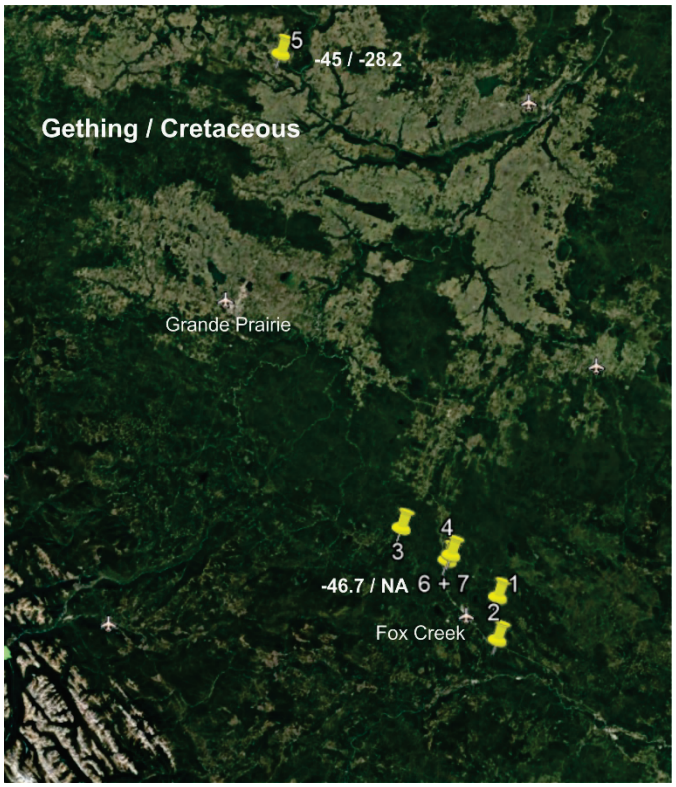

Fig. 3.15: Spatial distribution of $\delta^{13}C$ ratios for methane (first number) and ethane (second number) in the Gething Formation. NA is for "not available".

The undifferentiated Mannville Group has been sampled in well #5, and only methane $\delta^{13}C$ ratios are available. The Mannville samples are above those of the Gething Formation (see Appendix 1), which is at the base of the Mannville Group (see Fig. 1). The methane $\delta^{13}C$ data of the Mannville Group (Table 3.2 and Fig. 3.16) are statistically different from those of the Gething Formation: they are more negative (isotopically lighter), in accordance with slightly shallower burial depths. Such a trend is clearly visible in the data from overlying units (Appendix 1).

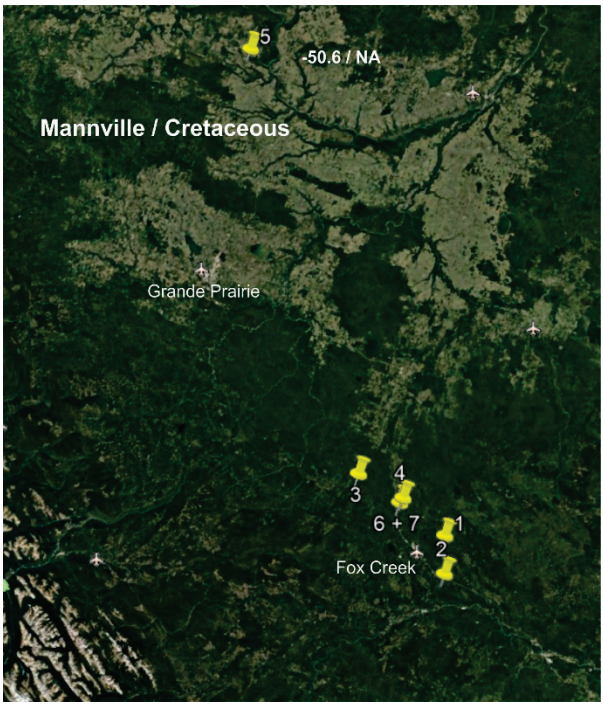

Fig. 3.16: Spatial distribution of $\delta^{13}C$ ratios for methane (first number) and ethane (second number) in the Mannville Group, NA is for "not available".

CONCLUSIONS

This report synthesizes new and vintage data on organic matter-rich intervals in the sub-surface of the Fox Creek area in west-central Alberta, as well as presents composition and isotopic values of gas sampled at various depths.

The organic matter composition and vitrinite reflectance thermal maturation data are available, from the oldest to the youngest: the Duvernay Formation, Montney Formation, Nordegg Member, and Mannville Group. Samples have been collected from organic-rich intervals, with only data from the Duvernay Formation being statistically significant and having a relatively good spatial coverage over the study area. The dominant organic matter in the Duvernay Formation is composed of solid bitumen as *in situ* bituminized algae to pore- and fracture-filling solid bitumen. Although the Montney Formation organic matter is generally composed of migra-bitumen, organic-rich intervals of the Montney Formation in the study area contain a minor amount of alginite macerals. The dominant maceral in the Nordegg Member of the Fernie Formation is bitumen, with a lesser amount of inertinite macerals and fishbone. Solid bitumen in the Nordegg samples either occurs as disseminated matrix bitumen or pore-filling solid bitumen. The Mannville Group is composed of intermittent intervals of coal-bearing strata with fine-grained organic-rich intervals. The dominant macerals in the Mannville Group samples are vitrinite, inertinite, and solid bitumen as *in situ* bituminized algae or pore-filling solid bitumen.

The reflectance data (vitrinite and vitrinite-equivalent) indicate that all units are mature and have generated hydrocarbons. The deepest and the likely more mature unit, the Duvernay Formation, shows vitrinite-equivalent data suggestive of the end of the oil zone in the eastern part of the study area and of the condensate zone in the western part. This is coherent with the produced hydrocarbons in the area. The limited data for the shallower units are all indicative of the oil window.

Rock-Eval data were synthesized from historical data from the GSC database. A significant number of analytical results are available for the Duvernay Formation; the Tmax data suggest that the unit belongs to the condensate zone, almost reaching the dry gas zone in the westernmost domain. Results from the overlying Montney Formation and Nordegg Member are less abundant, with the Tmax data suggestive of the oil window. All these results are in agreement with the vitrinite-equivalent reflectance data.

A significant database of gas composition (C1-C5) and $\delta^{13}C$ isotopic composition of methane, ethane, and propane samples is available. However, most of the wells are located near the eastern limit of the study area (and one well is located north of Grande Prairie). Most of the wells have available data for only a short interval (few have data distributed over a significant depth interval). Nonetheless, all units with some source rocks potential have had isotube gas samples analyzed. All $\delta^{13}C$ methane and wetness values indicate an obvious thermogenic source of the gas, even if the shallowest samples for two wells (at circa 1000 and 1500 samples depth) have $\delta^{13}C$ values slightly more negative than the classical thermogenic field (yet their wetness ratio is consistent with a thermogenic origin). Other plots, including $\delta^{13}C$ ethane versus depth, $\delta^{13}C$ ethane versus wetness, iC4/nC4 versus depth, iC4/nC4 versus wetness, and $\delta^{13}C$-methane - $\delta^{13}C$-ethane versus depth, indicate or strongly suggest that partial isotopic rollover occurred at depth, but was never fully complete (i.e. $\delta^{13}C$ of ethane was never more negative than $\delta^{13}C$ of methane). This observation indicates that the eastern part of the study area is not overmature and agrees with the thermal conditions recorded by organic matter reflectance and Rock-Eval data. Given the poor spatial distribution of our gas dataset, the conditions for the western sector of the study area could not be assessed.

This study indicates that all Upper Devonian to Cretaceous potential source rock units of the study area has entered the oil window with the maximal thermal conditions found in the Duvernay Formation, suggestive of the end of the condensate zone in the western end of the study area. There is some significant overlap of $\delta^{13}C$ values of methane for deeper units in the study area and a partial isotopic rollover was observed for $\delta^{13}C$ values of ethane, supported by butane ratios with depth. Therefore, in the eventual presence of permeable natural pathways connecting any of

the examined deep units to the shallow aquifers, identifying the source or provenance of dissolved hydrocarbons in shallow groundwater would be difficult. Shallower source rock units (Cretaceous and Cenozoic coals) have not been covered in this study and are likely to have very different $\delta^{13}C$ values for alkanes.

ACKNOWLEDGEMENTS

This study was made possible through the efficient and diligent efforts of Pat Webster and Richard Fontaine (GSC-Calgary) for searching organic matter samples in the GSC collection for the preparation of new pellets for organic petrography. Andy Mort (GSC-Calgary) is thanked for providing raw gas data for wells in the study area. Elena Konstantinovskaya (University of Alberta) provided the stratigraphic assignment, as well as azimuth and deviation data for the wells with gas data. Jean-Sébastien Marcil (Derena Geoscience) kindly provided the spreadsheet for transferring measured depth to true vertical depth. Sincere thanks to Dennis Jiang for his review of this report.

References

Alberta Geological Survey (2019). Alberta Table of Formations. Alberta Energy Regulator, https://ags.aer.ca/publications/Table_of_Formations_2019.html

Allan, J., Creaney, S., 1991. Oil families of the Western Canada basin. Bulletin of Canadian Petroleum Geology, v. 39, p. 107–122.

Beaton, A.P., Pawlowicz, J.G., Anderson, S.D.A., Berhane, H. and Rokosh, C.D. 2010. Organic petrography of the Montney Formaiton in Alberta: shale gas data release. Energy Resources Conservation Board and Alberta Geological Survey, Open File Report 2010-07, 129 p.

Behar, F., Beaumont V., Penteado, H.L. de B., 2001. Rock-Eval 6 technology: performances and developments. Oil Gas Science and Technology, Revue Institut français du pétrole, v. 56, p. 111–134.

Bertrand, R., 1990. Correlations among the reflectance of vitrinite, chitinozoans, graptolites and scolecodonts. Organic Geochemistry, v. 15, p. 565–574.

Bernard, B.B., Brooks, J.M. and Sackett, W.M. 1978. Light hydorcarbons in recent Texas continental shelf and slope sediments. Journal of Geophysical Research – Ocean, v. 83, Issue C8, p. 4053-4061.

Chalmers, G.R.L., Bustin, R.M., 2012. Geological evaluation of Halfway-Doig-Montney hybrid gas shale-tight gas reservoir, northeastern British Columbia. Marine and Petroleum Geology, v. 38, 53–72.

Chatellier, J.Y., Ferworn, K., Larsen, N.L., Ko, S., Flek, P.. Molgat, M. and Anderson, I. 2013. Overpressure in Shale Gas: When Geochemistry and Reservoir Engineering Data Meet and Agree, in J.Y. Chatellier and D. Jarvie, eds. Critical assessment of shale gas resource play. AAPG Memoir 103, p. 45-69.

Corlett, H., Schultz, R., Branscombe, P., Hauck, T., Haug, K., MacCormack, K. and Shipman, T. 2018. Subsurface faults inferred from reflection seismic, earthquakes, and sedimentological relationships: Implications for induced seismicity in Alberta, Canada. Marine and Petroleum Geology, v. 93, p. 135-144.

Crombez, V., Baudin, F., Rohais, S., Riquier, L., Euzen, T., Pauthier, S., Ducros, M., Caron, B., Vaisblat, N., 2017. Basin scale distribution of organic matter in marine fine-grained sedimentary rocks: insight from sequence stratigraphy and multi-proxies analysis in the Montney and Doig formations. Marine and Petroleum Geology, v. 83, p. 382–401.

Dewing, K. and Sanei, H. 2009, Analysis of large thermal maturity datasets: Examples from the Canadian Arctic Islands; International Journal of Coal Geology, v. 77, p. 436-448.

Ejezie, N., 2007. Triassic Oil Families and Possible Source Rocks, Peace River Embayment Area, Alberta, Canada. Unpublished M.Sc. Thesis. University of Calgary, Calgary, Alberta, Canada.

Espitalié, J., Laporte, J.L., Madec, M., Marquis, F., Leplat, P., Paulet, J. and Boutefeu, A. 1977. Rapid Method for Source Rock Characterization and for Determination of Their Petroleum Potential and Degree of Evolution. Revue de l'Institut Français du Pétrole, v. 32, p. 23-42.

Espitalié, J., Deroo, G. and Marquis, F. 1985. Rock-Eval pyrolysis and its application. Revue de l'Institut Français du Pétrole, v. 40, p. 563-579.

Euzen, T., Moslow, T.F., Crombez, V., Rohais, S., 2018. Regional stratigraphic architecture of the Spathian Deposits in Western Canada—Implications for the Montney resource play. Bulletin of Canadian Petroleum Geology, v. 66, p. 175–192.

Hayes, B.J.R., Christopher, J.E., Rosenthal, R.L., Los, G., McKercher, B., Minken, D., Tremblay, Y.M., Fennel, J., and Smith, D.G. 1994. Chapter 19 - Cretaceous Mannville Group of the Western Canada Sedimentary Basin; in Geological Atlas of the Western Canada Sedimentary Basin, G.D. Mossop and I. Shetsen (comp.), Canadian Society of Petroleum Geologists and Alberta Research Council, https://ags.aer.ca/publications/chapter-19-cretaceous-mannville-group.htm

Isinguzo, N.G. 2017. Characterization of the Lower Jurassic Gordondale Member in West-Central, Alberta, Canada, using Organic Geochemical and Petrophysical Methods. Unpublished MSc. Thesis. University of Calgary. http://dx.doi.org/10.11575/PRISM/5224

Jacob, H., 1989. Classification, structure, genesis and practical importance of natural solid oil bitumen ("migrabitumen"). International Journal of Coal Geology, v. 11, p. 65–79.

Jiang, C; Obermajer, M; Chen, Z; Geological Survey of Canada, Open File 8155, 2016, 532 pages, https://doi.org/10.4095/299332

Knapp, L.J., Harris, N.B. and McMillan, J.M. 2019. A sequence stratigraphic model for the organic-rich Upper Devonian Duvernay Formation, Alberta, Canada. Sedimentary Geology, v. 387, p. 152-181.

Knapp, L.J., Ardakani, O.H., Uchida, S., Nanjo, T., Otomo, C. and Hattori, T., 2020. The influence of rigid matrix minerals on organic porosity and pore size in shale reservoirs: Upper Devonian Duvernay Formation, Alberta, Canada. International Journal of Coal Geology, v. 227, p.103525.

Kondla, D., Sanei, H., Clarkson, C.R. and Goodarzi, F., 2017. High resolution characterization of a core from the Lower Jurassic Gordondale Member, Western Canada Sedimentary Basin. Marine and Petroleum Geology, v. 83, p.50-59.

Mastalerz, M., Drobniak, A., Stankiewicz, A.B., 2018. Origin, properties, and implications of solid bitumen in source-rock reservoirs: a review. International Journal of Coal Geology, v. 195, p. 14–36.

Riediger, C.L., Brooks, P.W., Fowler, M.G., Snowdon, L.R., 1990. Lower and Middle Triassic source rocks, thermal maturation, and oil-source rock correlations in the Peace River Embayment area, Alberta and British Columbia. Bulletin of Canadian Petroleum Geology, v. 38, p. 218–235.

Riediger, C.L., and Bloch, J.D., 1995. Depositional and diagenetic controls on source-rock characteristics of the Lower Jurassic "Nordegg Member", western Canada. Journal of Sedimentary Research, v. A65, p. 112-126.

Riediger, C.L., Fowler, M.G., Snowdon, L.R., Goodarzi, F., and Brooks, P.W., 1990. Source rock analysis of the Lower Jurassic "Nordegg Member" and oil-source rock correlations, northwestern Alberta and northeastern British Columbia. Bulletin of Canadian Petroleum Geology, v. 38A, p. 236-249.

Riediger, C.L., 1997. Geochemistry of potential hydrocarbon source rocks of Triassic age in the Rocky Mountain Foothills of northeastern British Columbia and west-Central Alberta. Bulletin of Canadian Petroleum Geology, v. 45, p. 719–741.

Sanei, H., Wood, J.M., Ardakani, O.H., Clarkson, C.R., Jiang, C., 2015a. Characterization of organic matter fractions in an unconventional tight gas siltstone reservoir. International Journal of Coal Geology, v. 150, p. 296–305.

Sanei, H., Haeri-Ardakani, O.,Wood, J.M., Curtis, M.E., 2015b. Effects of nanoporosity and surface imperfections on solid bitumen reflectance (BRo) measurements in unconventional reservoirs. International Journal of Coal Geology, v. 138, p. 95-102.

Smith, G.G., Cameron, A.R., and Bustin, R.M. 1994. Chapter 33 – Coal resources of the Western Canada Sedimentary Basin; in Geological Atlas of the Western Canada Sedimentary Basin, G.D. Mossop and I. Shetsen (comp.), Canadian Society of Petroleum Geologists and Alberta Research Council, https://ags.aer.ca/publications/chapter-33-coal-resources.htm

Switzer, S.B., Holland, W.G., Christie, D.S., Graf, G.C., Hedinger, A.S., McAuley, R.J., Wierzbicki, R.A., Packard, J.J., 1994. Chapter 12 - The Woodbend-Winterburn strata of the Western Canada Sedimentary Basin; in Geological Atlas of the Western Canada Sedimentary Basin G.D. Mossop and I. Shetsen (comps.), Canadian Society of Petroleum Geologists and Alberta Research Council, https://ags.aer.ca/publications/chapter-12-devonian-woodbend-winterburn-strata.htm

Van de Wetering, N., Sanei, H. and Mayer, B., 2016. Organic matter characterization in mixed hydrocarbon producing areas within the Duvernay Formation, Western Canada Sedimentary Basin, Alberta. International Journal of Coal Geology, v. 156, p.1-11.

Wood, J.M., Sanei, H., Ardakani, O.H., Curtis, M.E., Akai, T., Currie, C., 2018. Solid bitumen in the Montney Formation: diagnostic petrographic characteristics and significance for hydrocarbon migration. International Journal of Coal Geology, v. 198, p. 48–62.

Wood, J.M., Ardakani, O.H., Sanei, H., Curtis, M.E., Royer, D. 2020. Application of paleoporosity and bitumen saturation concepts to tight-gas accumulations containing solid bitumen. International Journal of Coal Geology, v. 228, p. 103547.

Zumberge, J., Ferworn, K., and Brown, S. 2012. Isotopic reversal (‘rollover’) in shale gases produced from the Mississippian Barnett and Fayetville formations. Marine and Petroleum Geology, v. 31, p. 43-52.

Appendix 1. Hydrocarbon gas composition and isotopic values of selected well in the study area

Well	Formation	MD[1] m	TVD[2] m	Gas Units	C1 ppm	C2 ppm	C3 ppm	C1/(C2+C3)	iC4	nC4	iC4/nC4	δ^{13}C1 ‰VPDB	δ^{13}C2 ‰VPDB	δ^{13}C1-δ^{13}C2 ‰VPDB
1	Woodbend	2710	2649	98	93	19	9	3.3	2	4	0.50			
	Woodbend	2738	2675	101	628	107	57	3.8	9	18	0.50	-46.6	**-33.4**	-13.2
	Woodbend	2756	2691	102	381	64	35	3.8	6	12	0.50			
	Woodbend	2784	2716	110	2660	307	133	6.1	18	31	0.58	-46.4	-33.1	-13.3
	Woodbend	2812	2737	130	1820	246	112	5.1	17	26	0.65			
	Woodbend	2840	2765	110	1110	164	84	4.5	13	22	0.59	-46.2	**-33.1**	-13.1
	Woodbend	2868	2795	119	909	134	70	4.5	12	19	0.63			
	Woodbend	2896	2802	73	1140	161	76	4.8	12	19	0.63	-45.9	**-33.3**	-12.6
	Woodbend	2924	2842	120	913	138	63	4.5	9	16	0.56	-45.8	**-33.5**	-12.3
	Woodbend	2952	2875	92	352	84	57	2.5	10	19	0.52			
	Woodbend	2960	2885	110	1160	255	119	3.1	15	30	0.50	-46.2	-35.1	-11.1
	Woodbend	2965	2888	100	1450	300	131	3.4	16	32	0.50			
	Cooking Lake	2971	2895	131	1080	257	122	2.8	15	31	0.48	-45.5	-35.1	-10.4
	Cooking Lake	2977	2902	132	688	181	96	2.5	13	27	0.48			
	Cooking Lake	2983	2906	114	1110	267	131	2.8	17	36	0.47	-45.5	-34.8	-10.7
	Cooking Lake	2989	2913	131	2200	437	196	3.5	25	48	0.52			
	Cooking Lake	2995	2918	166	3520	679	269	3.8	30	60	0.50	-45.9	-34.8	-11.1
	Beaver Hill	3001	2926	115	1260	289	142	3.8	19	39	0.49			
	Beaver Hill	3007	2931	102	41	17	14	1.3	3	7	0.43			
	Beaver Hill	3013	2936	170	5880	866	266	5.2	25	48	0.52	-46.5	-34.7	-11.8
	Beaver Hill	3019	2944	120	2970	469	154	4.8	15	27	0.56	-46.7	-34.8	-11.9
	Beaver Hill	3025	2949	170	1890	294	105	4.7	12	23	0.52			
	Beaver Hill	3031	2953	130	1470	249	102	4.2	12	24	0.50	-43.5	-33.0	-10.5
	Beaver Hill	3037	2957	110	1180	195	82	4.3	11	21	0.52			
	Beaver Hill	3043	2970	204	825	157	72	3.6	9	19	0.47			

[1]Measured Depth

[2]True Vertical Depth

well	Formation	TVD m	Gas Units	C1 ppm	C2 ppm	C3 ppm	C1/(C2+C3)	iC4	nC4	iC4/nC4	δ^{13}C1 ‰VPDB	δ^{13}C2 ‰VPDB	δ^{13}C3 ‰VPDB	δ^{13}C1-δ^{13}C2 ‰VPDB
2	Duvernay	3047	144	6960	484	107	11.8	9	16	0.56	-44.5	-33.1		
	Duvernay	3049	178	5280	375	86	11.5	7	14	0.50	-44.1	-33.2		
	Duvernay	3050	193	7160	497	100	12.0	7	13	0.54	-44.2	-32.9		
	Duvernay	30534	200	9270	611	123	12.6	9	16	0.56	-44.3	-33.3		
	Duvernay	3055	105	1350	95	22	11.5	2	4	0.50	-44.0			
	Duvernay	30575	166	11700	846	163	11.6	12	19	0.63	-44.1	-33.0		
	Duvernay	3060	194	10700	780	152	11.5	11	19	0.58	-44.3	-33.1		
	Duvernay	30625	219	16900	1280	250	11.0	19	30	0.63	-44.3	-33.3	-30.6	-11.0
	Duvernay	3065	200	16700	1260	247	11.1	18	30	0.60	-44.3	-33.3	-30.6	-11.0
	Duvernay	30675	276	16100	1210	238	11.1	18	28	0.64	-43.7	-32.8	-30.2	-10.9
	Duvernay	3070	299	17700	1350	263	10.9	21	36	0.58	-44.6	-33.3	-30.6	-11.3
	Duvernay	30725	323	17800	1360	265	11.0	21	36	0.58	-44.6	-33.3	-30.8	-11.3
	Duvernay	3075	311	17700	1340	260	11.1	20	35	0.57	-44.7	-33.0	-30.3	-11.7
	Duvernay	30825	150	6170	598	158	8.2	15	27	0.56	-44.0	-32.7		
	Duvernay	3085	132	6250	615	162	8.0	15	26	0.58	-43.8	-32.2		
	Duvernay	30875	133	5940	611	166	7.6	16	29	0.55	-43.7	-32.5		
	Duvernay	3090	188	7430	719	198	8.1	20	38	0.53	-43.5	-32.3	-29.7	-11.2
	Duvernay	30925	206	8180	747	199	8.6	20	35	0.57	-43.9	-32.3	-29.8	-11.6
	Duvernay	3095	377	26700	2150	430	10.3	36	58	0.62	-44.5	-32.4	-29.6	-12.1
	Duvernay	30975	133	5550	486	130	9.0	13	28	0.46	-44.3	-32.2		
	Duvernay	3100	250	12400	972	227	10.3	22	38	0.58	-44.5	-32.2	-29.6	-12.3
	Duvernay	3102	193	9960	784	197	10.2	21	38	0.55	-44.3	-32.1	-29.4	-12.2
	Duvernay	3105	57	1160	111	32	8.1	4	7	0.57	-43.8			

Well	Formation	MD m	TVD m	Gas Units	C1 ppm	C2 ppm	C3 ppm	C1/(C2+C3)	iC4	nC4	iC4/nC4	δ^{13}C1 ‰VPDB	δ^{13}C2 ‰VPDB	δ^{13}C3 ‰VPDB	δ^{13}C1-δ^{13}C2 ‰VPDB
3	Ireton	3150	3131	40	555	47	14	9.1	1	3	0.33	-46.8			
	Ireton	3180	3160	28	561	47	12	11.0	1	2	0.5	-48.3			
	Ireton	3210	3190	50	1120	77	23	11.2	3	4	0.75	-46.6			
	Ireton	3240	3218	51	920	69	20	10.3	3	4	0.75	-46.7			
	Ireton	3270	3244	66	215	24	10	6.3	2	3	0.66				
	Ireton	3300	3271	130	4930	340	86	11.6	8	13	0.62	-46.3	-34.6		-11.7
	Duvernay	3306	3273	263	8110	802	196	8.1	14	28	0.5	-46	-35.2		-10.8
	Duvernay	3312	3281	322	13900	1450	364	7.7	30	57	0.53	-46.6	-35.5		-11.1

	Duvernay	3318	3289	330	42	11	4	2.8	nd	2					
	Duvernay	3324	3298	251	6610	915	260	5.9	19	25	0.76	-46	-35.2		-10.8
	Duvernay	3330	3308	256	9310	1110	325	6.5	30	61	0.49	-45.8	-34.9		-10.9
	Duvernay	3336	3316	187	4200	580	198	5.4	20	43	0.47	-45	-34.4		-10.6
	Duvernay	3342	3324	106	2100	311	125	4.8	14	31	0.45	-45.5	-34		-11.5
	Duvernay	3348	3332	61	2180	305	91	5.3	8	15	0.53	-46.8	-34.9		-11.9
	Duvernay	3356	3340	32	2490	377	112	5.1	9	19	0.47	-45.7	-33.8		-11.9
	Duvernay	3362	3346	88	1020	190	46	4.3	2	2	1	-45.5			
	Duvernay	3368	3352	74	1990	284	90	5.3	9	18	0.5	-46	-34.1		-11.9
	Duvernay	3374	3355	39	15	7	8	1.0	2	8	0.25				
	Duvernay	3386	3347		65.13	16.53	9.26	2.5	1.27	2.86		-46.06	-34.95	-31.57	-11.11
	Duvernay	3386	3347		65.56	16.95	8.53	2.6	1.14	2.48		-46.21	-34.96	-31.66	-11.25

Well	Formation	MD	TVD	Gas Units	C1	C2	C3	C1/(C2+C3)	iC4	nC4	iC4/nC4	$\delta^{13}C1$	$\delta^{13}C2$	$\delta^{13}C3$	$\delta^{13}C1$-$\delta^{13}C2$
		m	m		ppm	ppm	ppm					‰VPDB	‰VPDB	‰VPDB	‰VPDB
4	Fernie	1875	1855	766	17000	1050	367	12.0	38	76	0.50	-46.7	-32.2		-14.5
	Fernie	1880	1860	234	12000	606	182	15.2	16	33	0.48	-46.3	-32.4		-13.9
	Fernie	1885	1862	246	6190	357	129	12.7	13	28	0.46	-46.9	-33.4		-13.5
	Fernie	1890	1866	195	11300	678	238	12.3	24	53	0.45	-46.4	-34.1		-12.3
	Fernie	1895	1871	274	15300	866	285	13.3	26	60	0.43	-46.6	-34.7		-11.9
	Fernie	1900	1876	184	7980	447	182	12.7	20	47	0.43	-46.4	-34.4		-12.0
	Fernie	1905	1884	100	2300	153	66	10.5	7	17	0.41	-47.0	-35.2		-11.8
	Fernie	1910	1888	169	2520	165	68	10.6	7	17	0.41	-46.4	-36.2		-10.2
	Fernie	1915	1894	151	3760	244	106	10.7	11	28	0.39	-46.8	-37.9		-8.9
	Fernie	1920	1898	339	20200	1470	504	10.2	37	102	0.36	-46.5	-39.7		-6.8
	Fernie	1925	1903	518	26100	1880	619	10.4	43	127	0.34	-46.5	-40.1		-6.4
	Nordegg	1930	1908	717	56000	3960	1200	10.9	76	226	0.34	-47.0	-40.6		-6.4
	Nordegg	1935	1912	645	44300	2960	910	11.4	60	189	0.32	-47.4	-40.8		-6.6
	Nordegg	1940	1915	568	40100	3020	954	10.1	62	196	0.32	-46.9	-40.7		-6.2
	Nordegg	1945	1918	580	36100	2710	848	10.1	53	154	0.34	-46.8	-40.7		-6.1
	Nordegg	1950	1920	295	16500	1200	399	10.3	26	87	0.30	-46.9	-40.4		-6.5
	Nordegg	1955	1924	395	25200	2000	619	9.6	33	108	0.31	-46.5	-40.4		-6.1
	Montney	1960	1928	330	21800	1460	563	10.8	41	127	0.32	-46.5	-40.3		-6.2
	Montney	1965	1931	179	8270	820	357	7.0	25	84	0.30	-45.2	-39.9		-5.3
	Montney	1970	1935	317	18800	1200	467	11.2	32	107	0.30	-46.2	-40.3		-5.9
	Montney	1975	1939	141	6330	579	299	7.2	24	87	0.28	-46.0	-39.8		-6.2
	Montney	1980	1944	175	7560	551	276	9.1	23	80	0.29	-45.5	-39.6		-5.9
	Montney	1985	1949	85	2130	198	125	6.6	11	41	0.27	-45.5	-39.2		-6.3
	Montney	1990	1955	80	1280	156	126	4.5	13	48	0.27	-46.9	-39.0		-7.9
	Montney	1995	1960	74	1730	101	70	10.1	8	30	0.27	-47.0	-38.6		-8.4
	Montney	2000	1964	96	1540	86	62	10.4	7	29	0.24	-47.1	-38.0		-9.1
	Montney	2005	1968	74	1260	65	39	12.1	5	18	0.28	-47.1	-38.3		-8.7
	Montney	2010	1972	90	495	24	14	13.0	2	7	0.29	-47			
	Montney	2015	1976	69	1310	62	36	13.4	5	19	0.26	-46.9	-37.6		-9.3
	Montney	2020	1980	112	384	16	8	16.0	1	5	0.20	-47			
	Montney	2025	1984	106	864	39	15	16.0	2	7	0.29	-45.5			
	Montney	2030	1989	105	662	28	10	13.8	1	4	0.25	-44.7			
	Debolt	2035	1995	64	2120	88	33	17.1	4	13	0.31	-44.7	-35.8		-8.9
	Winterburn	2795	2345	80	742	32	9	18.1	nd	2		-49.2			
	Winterburn	2815	2351	80	940	33	9	22.4	1	2	0.50	-49.5			
	Winterburn	2836	2358	69	600	29	11	15.0	3	6	0.50	-47.1			
	Winterburn	2856	2365	100	1140	48	13	18.7	3	5	0.60	-46.8	-30.1		-16.7
	Ireton	2875	2372	161	5300	254	62	16.8	8	10	0.80	-46.2	-30.7		-15.5
	Ireton	2895	2375	74	1210	85	28	10.7	5	6	0.83	-45.0	-30.3		-14.7
	Ireton	2915	2379	69	410	25	8	12.4	2	2	1.00	-46			
	Ireton	2936	2386	79	2720	146	39	14.7	6	8	0.75	-45.5	-31.0		-14.5
	Ireton	2955	2391	106	3640	213	58	13.4	9	10	0.90	-45.7	-31.1		-14.6
	Ireton	2975	2396	74	41	3	nd	13.7	nd	nd					
	Ireton	2997	2400	63	748	44	14	13.4	3	3	1.00	-45.9			
	Ireton	3015	2404	69	1200	64	18	14.6	3	4	0.75	-46.1	-31.5		-14.6
	Ireton	3034	2407	106	1130	60	15	15.1	3	3	1.00	-46.0	-31.8		-14.2
	Ireton	3055	2411	75	1560	96	25	12.9	4	4	1.00	-45.6	-32.0		-13.6
	Ireton	3095	2416	106	1380	122	40	8.5	7	9	0.78	-44.6	-32.3		-12.3
	Ireton	3105	2417	80	1900	108	28	14.0	4	5	0.80	-45.7	-32.2		-13.5
	Duvernay	3115	2418	65	2550	154	45	12.8	7	9	0.78	-45.8	-32.3		-13.5
	Duvernay	3135	2420	69	1520	87	25	13.5	4	5	0.80	-46.4	-32.4		-14
	Duvernay	3155	2421	85	19600	1500	404	10.3	45	80	0.56	-45.7	-33.0	-30.3	-12.7
	Duvernay	3175	2421	95	2170	156	39	11.1	4	7	0.57				
	Duvernay	3195	2421	1102	82000	7260	1710	9.1	160	258	0.62	-45.6	-33.2	-30.6	-12.4
	Duvernay	3217	2421	757	45500	4090	1090	8.8	118	203	0.58	-45.6	-33.0	-30.1	-12.6
	Duvernay	3240	2421	891	43300	3430	898	10.0	100	176	0.57	-45.7	-33.2	-30.4	-12.5
	Duvernay	3260	2421	807	43700	3580	952	9.6	108	190	0.57	-45.8	-33.2	-30.1	-12.6

	Duvernay	3280	2421	891	38000	3030	785	9.9	86	152	0.56	-45.9	-33.1	-30.3	-12.8
	Duvernay	3300	2421	840	54300	4990	1360	8.6	153	280	0.55	-45.4	-33.0	-30.2	-12.4
	Duvernay	3340	2421	807	na	na	na		na	na					
	Duvernay	3380	2422	769	61500	4990	1200	8.6	118	201	0.59	-46.1	-33.4	-30.6	-12.7
	Duvernay	3450	2422	936	41200	3550	909	9.3	95	168	0.57	-45.4	-33.2	-30.7	-12.2
	Duvernay	3500	2424	908	14400	1370	504	7.7	67	126	0.53	-44.4	-32.8	-30.5	-11.6
	Duvernay	3550	2424	640	16200	1230	338	10.3	38	70	0.54	-45.7	-33.1	-30.4	-12.6
	Duvernay	3600	2425	724	56100	4850	1300	9.1	148	265	0.56	-44.7	-32.8	-29.8	-11.9
	Duvernay	3650	2426	945	85800	7180	1780	9.6	181	319	0.57	-45.3	-33.0	-30.5	-12.3
	Duvernay	3700	2425	960	24500	2910	1100	6.1	164	329	0.50	-43.7	-32.7	-30.4	-11
	Duvernay	3750	2425	951	86400	7200	1810	9.6	186	332	0.56	-45.3	-33.0	-30.6	-12.3
	Duvernay	3800	2425	949	87700	7900	2040	8.8	214	385	0.56	-45.5	-33.1	-30.2	-12.4
	Duvernay	3851	2425	1086	33300	2800	699	9.5	70	118	0.59	-45.6	-33.2	-30.3	-12.4
	Duvernay	3900	2426	1166	72800	6150	1490	9.5	148	252	0.59	-45.9	-33.1	-30.6	-12.8
	Duvernay	3950	2426	1100	59700	5160	1290	9.3	130	232	0.56	-45.9	-33.2	-30.6	-12.7
	Duvernay	4000	2426	1211	16600	1590	407	8.3	52	112	0.46				
	Duvernay	4050	2427	1150	136000	12300	3180	8.8	327	594	0.55	-45.6	-33.4	-30.6	-12.2
	Duvernay	4100	2427	1064	125600	11000	2860	9.1	302	557	0.54	-45.6	-33.2	-29.9	-12.4
	Duvernay	4150	2427	980	106500	8860	2250	9.6	231	410	0.56	-45.7	-33.3	-30.2	-12.4
	Duvernay	4200	2427	1480	122900	10800	2840	9.0	296	541	0.55	-45.5	-33.3	-30.4	-12.2
	Duvernay	4250	2427	1333	103500	9100	2380	9.0	252	467	0.54	-45.5	-33.2	-30.2	-12.3
	Duvernay	4300	2426	1372	112500	10600	2830	8.4	294	556	0.23	-45.4	-33.4	-30.5	-12
	Duvernay	4350	2426	1216	48600	4530	1250	8.4	136	260	0.52	-45.6	-33.5	-29.1	-12.1
	Duvernay	4400	2426	948	39700	3140	743	10.2	72	131	0.55	-45.9	-33.7	-30.4	-12.2
	Duvernay	4450	2426	830	66000	5560	1410	9.5	134	213	0.63	-45.5	-33.3	-30.3	-12.2
	Duvernay	4500	2426	651	60800	5300	1410	9.1	153	280	0.55	-45.3	-33.3	-30.6	-12
	Duvernay	4550	2426	1232	91000	8440	2160	8.6	217	395	0.55	-45.6	-33.4	-30.7	-12.2
	Duvernay	4600	2426	1450	100100	9390	2550	8.4	271	517	0.52	-45.6	-33.2	-30.6	-12.4
	Duvernay	4650	2427	1139	82800	8050	2150	8.1	223	417	0.53	-45.7	-33.3	-30.5	-12.4
	Duvernay	4700	2427	970	61700	5310	1420	9.2	153	287	0.53	-45.6	-33.3	-30.9	-12.3
	Duvernay	4750	2427	960	80400	7080	1880	9.0	200	379	0.53	-45.5	-33.3	-30.7	-12.3
	Duvernay	4800	2427	1065	70300	6400	1660	8.7	171	314	0.54	-45.8	-33.4	-30.7	-12.4
	Duvernay	4804	2427	3062	253100	25400	6750	7.9	658	1160	0.58	-45.6	-33.5	-30.6	-12.1
	Duvernay	4850	2428	1237	100700	9390	2600	8.4	274	516	0.53	-45.5	-33.4	-30.3	-12.1
	Duvernay	4900	2428	1170	82300	7460	2040	8.7	216	415	0.52	-45.6	-33.2	-30.6	-12.4
	Duvernay	4950	2428	1120	77500	7100	1980	8.5	214	417	0.52	-45.5	-33.5	-30.3	-12
	Duvernay	5000	2428	1029	62500	5180	1330	9.6	136	247	0.55	-45.7	-33.7	-30.2	-12
	Duvernay	5050	2428	1310	51500	4800	1310	8.4	138	263	0.52	-45.7	-33.6	-30.7	-12.1
	Duvernay	5100	2428	1154	32900	3020	857	8.5	97	185	0.52	-45.7	-33.5	-30.8	-12.2
	Duvernay	5150	2428	1143	42500	3820	1070	8.7	119	227	0.52	-45.9	-33.5	-30.7	-12.4
	Duvernay	5166	2429	3048	231300	23300	6180	7.8	606	1090	0.55	-45.3	-33.7	-31.1	-11.6
	Duvernay	5166	2429	6005	295300	87100	29700	2.5	3110	5190	0.60	-45.4	-33.6	-30.7	-11.8

Well	Formation	MD	TVD	Gas Units	C1	C2	C3	C1/(C2+C3)	C4	nC4	C4/nC4	$\delta^{13}C1$	$\delta^{13}C2$	$\delta^{13}C3$	$\delta^{13}C1$-$\delta^{13}C2$
		m	m		ppm	ppm	ppm					‰VPDB	‰VPDB	‰VPDB	‰VPDB
5	Bad Heart	110	110	77	1400	55	28	16.9	5	10	0.50	-58.7			
	Muskiki	135	135		2610	95	44	18.8	6	12	0.50	-60.1			
	Cardium	160	160	70	1070	69	41	9.7	5	11	0.45	-57.3			
	Cardium	185	185	93	864	81	51	6.5	6	14	0.43	-55.5			
	Kaskapau	210	210	80	995	100	71	5.8	8	20	0.40	-56.0			
	Kaskapau	235	235	155	5610	219	119	16.6	12	29	0.41	-60.0	-35.2		-24.5
	Kaskapau	260	260	184	9	nd	1	9.0	nd	2					
	Kaskapau	285	285	284	6700	361	199	29.8	21	53	0.40	-62.0	-37.3		-24.7
	2nd White Specks	310	310	287	740	18	15	22.4	1	3	0.33	-60.1			
	2nd White Specks	335	335	396	61	2	2	15.3	nd	2					
	2nd White Specks	360	360	100	794	43	77	6.6	12	47	0.26	-57.7			
	2nd White Specks	385	385	370	120	14	38	2.3	8	34	0.24				
	Dunvegan	410	410	426	224	21	49	3.2	9	39	0.23				
	Dunvegan	435	435	336	6690	154	182	19.9	27	83	0.33	-59.2			
	Dunvegan	460	460	125	5820	144	177	18.1	26	83	0.31	-58.9			
	Shaftesbury	485	485	246	517	27	60	5.9	14	47	0.30	-55.2			
	Shaftesbury	510	510	94	6440	154	146	21.5	18	48	0.38	-57.6			
	Fish Scale	535	535	106	7410	161	148	24.0	18	59	0.31	-57.2			
	Fish Scale	560	560	87	4960	108	89	25.2	11	33	0.33	-55.4			
	Viking	585	585	100	5540	154	102	21.6	13	33	0.39	-54.3			
	Mannville	610	608	188	0800	159	62	48.9	7	15	0.47	-53.6			
	Mannville	635	630	544	4760	118	53	27.8	8	11	0.73	-51.1			
	Mannville	660	651	100	7410	149	51	37.1	8	9	0.89	-54.0			
	Mannville	685	671	209	7200	393	112	34.1	13	10	1.30	-52.6	-32.3		-20.3
	Mannville	710	692	236	6660	192	72	25.2	10	8	1.25	-51.6			
	Mannville	735	710	121	4830	168	64	20.8	9	7	1.29	-50.8			
	Mannville	760	729	271	1000	325	102	25.8	13	9	1.44	-49.8	-31.2		-18.6
	Mannville	785	750	188	3300	140	63	16.3	11	8	1.38	-48.5			
	Mannville	810	768	82	28	2	2	7.0	nd	nd					
	Mannville	835	788	114	6220	163	57	28.3	8	7	1.14	-48.3			
	Mannville	860	805	94	3630	142	58	18.2	8	8	1.00	-48.4			
	Mannville	885	825	82	45	3	2	9.0	nd	nd					
	Mannville	910	845	105	3800	166	65	16.5	6	10	0.60	-47.7			
	Gething	935	860	111	2530	150	80	11.0	10	21	0.48	-46.5			
	Gething	960	876	126	2330	141	76	10.7	10	20	0.50	-46.4			
	Gething	985	889	666	12500	835	183	22.1	19	39	0.49	-44.6	-29.6		-15
	Gething	987	891	476	0200	425	116	18.9	14	28	0.50	-43.8	-29.3		-14.5
	Gething	989	892	94	405	18	4	18.4	nd	1					
	Gething	991	893	281	5260	245	58	17.4	6	12	0.50	-42.8	-28.6		-14.2
	Gething	994	895	193	3970	105	25	30.5	2	4	0.50	-52.2			
	Gething	996	896	364	8820	204	51	34.6	5	8	0.63	-50.7	-30.0		-20.7
	Gething	998	897	326	12900	790	110	36.6	9	9	1.00	-42.5	-27.3		-15.2
	Gething	2000	897	453	12400	789	112	36.0	9	10	0.90	-42.5	-27.1		-15.4
	Gething	2002	898	479	6320	200	40	26.3	4	6	0.67	-41.8	-27.0		-14.8
	Gething	2004	899	479	2400	330	58	32.0	6	8	0.75	-43.8	-27.8		-16
	Gething	2006	900	437	15200	668	110	32.4	10	14	0.71	-42.8	-27.3		-15.5
	Fernie	2008	901	136	14500	738	122	28.5	11	15	0.73	-42.3	-27.4		-14.9
	Fernie	2010	902	196	13700	758	131	26.7	12	17	0.71	-41.9	-27.3		-14.6
	Fernie	2012	903	255	6830	298	61	19.0	6	9	0.67	-42.0	-27.9		-14.1
	Fernie	2014	905	296	0500	462	90	19.0	8	13	0.62	-41.8	-28.0		-13.8
	Fernie	2016	906	281	2800	561	112	19.0	10	16	0.63	-42.4	-28.4		-14
	Fernie	2018	907	124	824	51	13	12.9	1	3	0.33				
	Fernie	2020	907	134	5460	292	71	15.0	7	12	0.58	-41.8	-28.3		-13.5
	Fernie	2022	908	134	6370	317	76	16.2	7	13	0.54	-43.0	-29.0		-14
	Fernie	2024	909	202	5580	291	70	15.5	6	11	0.55	-42.1	-29.1		-13
	Fernie	2026	911	176	7720	420	106	14.7	10	18	0.56	-42.2	-29.0		-13.2
	Fernie	2028	911	86	4660	273	76	13.4	8	15	0.53	-42.6	-28.9		-13.7
	Fernie	2030	912	125	5360	289	80	14.5	8	15	0.53	-43.5	-29.5		-14
	Fernie	2032	914	156	3360	234	62	11.4	5	7	0.71	-43.2	-30.1		-13.1
	Fernie	2034	915	154											
	Fernie	2036	916	140	6400	390	122	12.5	11	25	0.44	-43.3	-30.4		-12.9
	Fernie	2038	916	113	5060	322	104	11.9	10	22	0.45	-42.9	-30.2		-12.7
	Fernie	2040	917	171	2460	183	66	9.9	7	15	0.47	-43.0			
	Fernie	2042	918	198	5590	303	97	14.0	9	21	0.43	-44.9	-31.1		-13.8
	Fernie	2044	919	177	6000	355	121	12.6	12	28	0.43	-43.6	-30.9		-13.6
	Fernie	2046	920	61	4640	279	102	12.2	10	24	0.42	-44.3	-31.2		-13.1
	Fernie	2048	920	169	4000	261	100	11.1	11	25	0.44	-43.6	-30.8		-12.8
	Fernie	2050	921	166	4730	278	102	12.4	10	25	0.40	-44.0	-31.2		-12.8
	Fernie	2052	921	198	3080	214	85	10.3	9	23	0.39	-43.3	-31.2		-12.1
	Fernie	2054	922	235	2660	181	75	10.4	8	21	0.38	-44.3			
	Fernie	2056	923	100	1720	136	61	8.7	7	18	0.39	-44.4			
	Fernie	2058	924	77	2710	198	80	9.7	9	22	0.41	-43.5			

	Fernie	2060	1924	99	6670	328	89	16.0	9	16	0.56	-44.2	-30.0		-14.2
	Fernie	2062	1925	94	565	35	13	11.8	2	4	0.50	-43.9			
	Fernie	2064	1926	75	430	25	12	11.6	2	6	0.33				
	Fernie	2066	1927	109	1850	137	62	9.3	7	19	0.37	-44.2	-30.8		-13.4
	Fernie	2068	1928	100	1430	113	53	8.6	7	17	0.41	-44.9	-31.0		-13.9
5	Fernie	2070	1928	113	2090	125	53	11.7	6	17	0.36	-45.9	-31.8		-14.1
	Fernie	2072	1929	113	4260	242	91	12.8	9	25	0.36	-45.8	-33.1		-12.7
	Fernie	2074	1930	126	3630	217	85	12.0	9	25	0.36	-43.1	-31.9		-11.2
	Fernie	2076	1931	88											
	Fernie	2078	1931	88	4670	283	108	11.9	11	29	0.38	-45.6	-33.3		-12.3
	Fernie	2080	1932	90	5050	297	111	12.4	11	30	0.37	-45.9	-33.5		-12.4
	Fernie	2082	1933	89	1720	125	57	9.5	7	19	0.37	-45.4	-32.7		-12.7
	Fernie	2084	1934	111	2710	144	54	13.7	6	16	0.38	-47.1	-33.7		-13.4
	Fernie	2086	1934	94	823	55	30	9.7	4	13	0.31				
	Fernie	2088	1935	99	8940	474	147	14.4	11	32	0.34	-46.5	-34.7		-11.8
	Fernie	2090	1935	94	3330	187	66	13.2	6	19	0.32	-46.5	-34.5		-12
	Fernie	2092	1936	88	0500	609	190	13.1	14	43	0.33	-44.8	-33.5	-31.0	-11.3
	Fernie	2094	1937	83	2300	706	214	13.4	15	46	0.33	-46.5	-35.0	-32.2	-11.5
	Fernie	2096	1938	83	1000	668	207	12.6	15	45	0.33	-46.1	-34.6	-31.7	-11.4
	Fernie	2098	1938	88	4100	891	277	12.1	20	57	0.35	-46.0	-34.7	-32.3	-11.3
	Fernie	2100	1940	89	1900	1350	394	12.6	27	85	0.32	-46.6	-35.3	-32.6	-11.3
	Fernie	2102	1940	66											
	Fernie	2104	1941	61	7300	1210	397	10.8	31	97	0.32	-44.5	-34.2	-32.2	-10.3
	Fernie	2106	1941	71	7420	575	214	9.4	18	58	0.31	-44.1	-34.1	-32.1	-10
	Fernie	2108	1941	83	1000	185	117	3.3	13	45	0.29				
	Fernie	2110	1942	88	2400	1450	430	11.9	30	95	0.32	-45.5	-33.7	-31.2	-11.8
	Fernie	2112	1943	100											
	Fernie	2114	1944	120	7800	2390	667	12.4	44	139	0.32	-47.0	-35.5	-32.5	-11.5
	Fernie	2116	1945	178	3600	1550	731	6.0	71	243	0.29	-44.5	-34.5	-32.6	-10
	Fernie	2118	1945	251	1790	466	384	2.1	48	190	0.25	-43.0	-34.6	-32.7	-8.4
	Fernie	2120	1946	376	7700	2480	913	8.2	77	252	0.31	-44.9	-34.4	-31.9	-10.5
	Fernie	2122	1947	435	9700	2580	932	8.5	78	253	0.31	-45.2	-34.4	-32.1	-10.8
	Fernie	2124	1948	188	3500	4400	1450	9.1	112	352	0.32	-45.1	-34.6	-32.0	-10.5
	Fernie	2126	1948	355	8800	4880	1610	9.1	122	384	0.32	-44.8	-34.6	-32.1	-10.2
	Fernie	2128	1948	392	0800	5020	1670	9.1	129	411	0.32	-44.7	-34.6	-32.1	-10.1
	Fernie	2130	1949	472	2000	2330	868	6.9	70	216	0.32	-44.2	-34.2	-32.0	-10
	Fernie	2132	1949	586	3700	2320	922	7.3	82	265	0.31	-43.5	-34.1	-32.0	-9.4
	Fernie	2134	1950	326	8600	2500	932	8.3	80	264	0.30	-45.2	-34.5	-32.1	-10.7
	Fernie	2136	1951	456	0700	3430	1210	8.8	101	325	0.31	-45.0	-34.5	-32.1	-10.5
	Fernie	2138	1951	544	9400	3890	1310	9.5	105	340	0.31	-45.5	-34.9	-32.3	-10.6
	Fernie	2140	1951	654	5700	2480	990	7.4	90	297	0.30	-43.9	-33.9	-31.9	-10
	Fernie	2142	1953	628	4700	2380	951	7.4	86	288	0.30	-43.9	-34.0	-31.9	-9.9
	Fernie	2144	1953	604	2400	2200	895	7.2	82	277	0.30	-43.9	-34.0	-32.1	-9.9
	Fernie	2146	1954	676	8800	1860	749	7.2	65	212	0.31	-44.8	-34.4	-32.1	-10.4
	Fernie	2148	1954	694	8800	2450	920	8.6	80	268	0.30	-45.4	-34.6	-32.2	-10.8
	Fernie	2150	1955	768	3200	2760	1010	8.8	87	290	0.30	-45.5	-34.7	-32.2	-10.8
	Fernie	2152	1956	481	3900	2840	1030	8.8	87	294	0.30	-45.4	-34.6	-32.0	-10.8
	Fernie	2154	1956	552	4800	2890	1050	8.8	90	297	0.30	-45.5	-34.7	-32.4	-10.8
	Fernie	2156	1956	705	5100	2920	1060	8.8	91	302	0.30	-45.4	-34.6	-32.0	-10.8
	Fernie	2158	1957	701	5000	2930	1070	8.8	90	304	0.30	-45.4	-34.5	-31.9	-10.9
	Fernie	2160	1957	806	5600	2970	1080	8.8	91	306	0.30	-45.5	-34.5	-32.1	-10
	Fernie	2162	1958	505	6500	3060	1100	8.8	92	307	0.30	-45.4	-34.6	-31.8	-10.8
	Fernie	2164	1959	646											
	Fernie	2166	1959	673	0600	1410	470	11.0	37	125	0.30	-45.3	-34.5	-32.5	-10.8
	Nordegg	2168	1960	720	9900	2640	768	11.7	53	167	0.32	-46.5	-35.0	-32.5	-11.5
	Nordegg	2170	1960	809	8600	2620	786	11.3	57	183	0.31	-45.9	-34.8	-32.4	-11.1
	Nordegg	2172	1961	631	5500	1310	468	8.7	37	121	0.31	-44.6	-34.5	-32.4	-11.1
	Nordegg	2174	1962	705	5300	1300	471	8.6	37	122	0.30	-44.6	-34.4	-32.3	-10.2
	Nordegg	2176	1962	670	8600	2990	940	9.8	68	208	0.33	-45.5	-34.7	-32.1	-10.8
	Nordegg	2178	1962	682	7200	2900	928	9.7	69	218	0.32	-45.1	-34.6	-32.1	-10.5
	Nordegg	2180	1963	716	2200	3940	1200	10.2	85	257	0.33	-45.4	-34.8	-32.2	-10.6
	Nordegg	2182	1963	430	9360	1370	620	4.7	58	214	0.27	-43.3	-34.3	-32.4	-9
	Nordegg	2184	1963	509	2800	2570	858	9.6	67	219	0.31	-44.6	-34.4	-32.1	-10.2
	Nordegg	2186	1963	602	3300	1790	603	9.7	47	152	0.31	-45.6	-34.6	-32.5	-11
	Nordegg	2188	1964	557	8600	2880	912	10.2	69	218	0.32	-45.4	-34.8	-31.8	-10.6
	Nordegg	2190	1964	501	1600	2930	894	10.9	65	208	0.31	-46.1	-35.0	-32.1	-11.1
	Nordegg	2192	1965	557	4650	787	470	3.7	49	187	0.26	-44.0	-34.9	-32.8	-9.1
	Nordegg	2194	1965	764	5700	2010	706	9.5	57	191	0.30	-45.3	-34.6	-32.1	-10.7
	Nordegg	2196	1965	853	3500	2660	895	9.4	70	221	0.32	-45.2	-34.5	-32.3	-10.7
	Nordegg	2198	1965	964	5300	3720	1210	9.2	90	276	0.32	-44.3	-34.5	-32.1	-9.8
	Nordegg	2200	1966	563	9300	3590	1120	10.5	84	266	0.31	-45.8	-34.9	-32.3	-10.9
	Nordegg	2202	1966	678	7000	2110	736	9.5	59	188	0.31	-44.9	-34.5	-32.1	-10.4
	Nordegg	2204	1966	757	2700	4660	1480	10.2	109	319	0.34	-44.3	-34.3	-31.7	-10
	Nordegg	2206	1966	800	6300	4150	1360	10.2	107	328	0.33	-44.5	-34.4	-31.9	-10.1

	Nordegg	2208	1966	928	14500	6930	1250	10.5	99	320	0.31	-45.4	-34.7	-32.1	-10.7
	Nordegg	2210	1968	505	54	16	16	1.7	3	19	0.16				
	Nordegg	2212	1968	675	18700	2410	859	8.8	70	224	0.31	-44.5	-34.4	-32.1	-10.1
	Nordegg	2214	1968	774	13300	1970	708	8.7	58	186	0.31	-44.6	-34.3	-31.8	-10.3
	Nordegg	2216	1968	816											
	Nordegg	2218	1968	933	18300	6240	1170	8.7	98	322	0.30	-45.3	-34.7	-32.0	-10.6
	Nordegg	2220	1968	539	19200	6340	1190	8.7	99	320	0.31	-45.1	-34.5	-32.0	-10.6
	Nordegg	2222	1968	531	11200	3520	1260	8.6	103	338	0.30	-45.1	-34.5	-32.1	-10.6
	Nordegg	2224	1969	626	12600	3670	1300	8.6	107	347	0.31	-44.9	-34.5	-32.0	-10.4
5	Nordegg	2324	1969	331	5200	1160	397	9.8	31	98	0.32	-45.3	-34.7	-32.2	-10.6
	Nordegg	2374	1968	456	6710	661	291	7.0	28	109	0.26	-43.9	-34.4	-32.2	-9.5
	Nordegg	2424	1967	567	11000	2340	752	10.0	57	177	0.32	-45.2	-34.5	-32.0	-10.7
	Nordegg	2474	1967	633	10100	849	324	8.6	28	98	0.29	-45.3	-34.5	-31.9	-10.8
	Nordegg	2524	1969	624	7900	798	348	6.9	35	142	0.25	-43.5	-34.0	-31.9	-9.5
	Nordegg	2574	1967	633	9690	932	350	7.6	32	128	0.18	-43.0	-33.9	-31.9	-9.1
	Nordegg	2624	1965	221	11400	1650	552	9.7	44	143	0.31	-45.9	-34.4	-32.2	-11.5
	Nordegg	2674	1965	441	17700	2070	650	10.2	48	145	0.33	-46.0	-34.7	-31.8	-11.3
	Nordegg	2724	1965	463	15100	1860	616	10.1	51	165	0.31	-45.5	-34.5	-31.6	-11
	Nordegg	2774	1964	499	10700	2190	691	10.7	55	178	0.31	-45.6	-34.5	-31.9	-11.1
	Nordegg	2824	1964	620	18600	3560	1060	10.5	77	231	0.33	-45.5	-34.5	-31.9	-11
	Nordegg	2874	1963	767	7900	1590	714	7.8	74	265	0.28	-44.1	-34.1	-32.4	-10
	Nordegg	2924	1962	572	12500	3240	1020	10.0	81	254	0.32	-45.8	-34.6	-32.2	-11.2
	Nordegg	3024	1961	648	19500	6930	1340	9.4	110	345	0.32	-44.5	-34.3	-31.8	-10.2
	Nordegg	3074	1961	572	13500	3300	1060	10.0	83	261	0.32	-46.1	-34.7	-31.8	-11.4
	Nordegg	3124	1961	498	11800	2670	919	8.9	78	257	0.30	-45.6	-34.6	-32.1	-11
	Nordegg	3174	1960	285	6800	1320	479	9.3	46	171	0.27	-45.8	-34.4	-32.2	-11.4
	Nordegg	3274	1959	441	15700	3340	1050	10.4	81	247	0.33	-45.5	-34.6	-31.6	-10.9
	Nordegg	3274	1959	541	19000	2980	930	10.0	70	218	0.32	-46.0	-34.7	-32.1	-11.3
	Nordegg	3324	1958	419	18200	2190	835	9.3	69	221	0.31	-46.1	-34.8	-32.3	-11.3
	Nordegg	3374	1958	614	13900	1310	584	7.3	61	225	0.27	-43.8	-33.8	-32.1	-10
	Nordegg	3424	1957	419	12400	2290	733	10.7	58	190	0.31	-46.7	-34.9	-32.4	-11.8
	Nordegg	3474	1956	477	9560	993	516	6.3	58	210	0.28	-43.5	-34.0	-32.6	-9.5
	Nordegg	3520	1955	420	9770	964	451	6.9	46	170	0.27	-44.4	-34.0	-32.1	-10.4

Well	Formation	MD	TVD	Gas Units	C1	C2	C3	C1/(C2+C3)	iC4	nC4	iC4/nC4	δ^{13}C1	δ^{13}C2	δ^{13}C3	δ^{13}C1-δ^{13}C2
		m	m		ppm	ppm	ppm					‰VPDB	‰VPDB	‰VPDB	‰VPDB
6	Paddy	1575	1575	63	2180	84	102	11.7	15	51	0.29	-56.5			
	Harmon	1600	1599	720	1800	71	88	11.3	13	44	0.30	-56.6			
	Notikwn	1625	1623	475	2060	76	92	12.3	14	46	0.30	-56.6			
	Spirit River	1650	1647	40	1790	71	87	11.3	13	44	0.30	-56.6			
	Spirit River	1675	1668	40	1660	72	67	11.9	12	43	0.28	-47.8			
	Spirit River	1700	1694	98	5740	219	73	19.7	12	18	0.67	-54.1			
	Spirit River	1725	1715	237	4020	121	73	20.7	13	44	0.30	-46.7			
	Spirit River	1750	1736	87	4190	175	67	17.3	10	16	0.63	-49.2			
	Spirit River	1775	1759	88	646	69	38	6.0	6	10	0.60	-48.7			
	Spirit River	1800	1778	58	1010	104	55	6.4	8	13	0.62	-49.0			
	Spirit River	1825	1792	23	752	82	46	5.9	7	12	0.58	-48.9			
	Spirit River	1850	1808	100	734	113	61	4.2	8	17	0.47	-44.9			
	Spirit River	1875	1822	71	567	88	48	4.2	6	13	0.46	-44.9			
	Gething	1930	1842	80	340	53	29	4.1	4	8	0.50				
	Gething	1932	1844	61	263	25	15	6.6	2	6	0.33				
	Gething	1934	1844	40	144	13	8	6.9	1	3	0.33				
	Gething	1936	1845	56	978	92	37	7.6	3	9	0.33	-47.4			
	Gething	1938	1845	61	1000	92	38	7.7	3	9	0.33	-47.6			
	Gething	1940	1846	79	469	44	18	7.6	2	4	0.50				
	Gething	1942	1846	79	2630	250	96	7.6	7	21	0.33	-46.8			
	Gething	1944	1846	77	1830	174	65	7.7	5	14	0.36	-47.2			
	Gething	1946	1847	118	2620	247	93	7.7	7	20	0.35	-47.0			
	Gething	1948	1847	129	2800	265	100	7.7	7	21	0.33	-47.0			
	Gething	1950	1847	108	2290	280	121	5.7	9	27	0.33	-47.0			
	Gething	1952	1848	108	1210	151	66	5.6	5	15	0.33	-47.0			
	Gething	1954	1848	96	2000	242	103	5.8	8	22	0.37	-47.1			
	Gething	1956	1849	75	1690	207	90	5.7	7	20	0.35	-47.3			
	Gething	1958	1849	73	1710	211	94	5.6	7	23	0.30	-46.3			
	Gething	1960	1849	167	843	109	50	5.3	4	12	0.33	-46.5			
	Gething	1962	1850	145	1210	153	69	5.5	5	17	0.29	-46.3			
	Gething	1964	1850	128	1360	172	79	5.4	6	19	0.32	-46.4			
	Gething	1966	1851	74	1440	180	81	5.5	6	20	0.30	-46.3			
	Gething	1968	1851	61	1330	167	75	5.5	6	19	0.32	-46.4			
	Gething	1970	1852	74	665	86	38	5.4	3	10	0.30	-46.4			
	Gething	1972	1852	75	785	101	45	5.4	4	12	0.33	-46.4			
	Gething	1974	1853	79	796	102	46	5.4	3	12	0.25	-46.4			

	Gething	1976	1853	83	1520	174	73	6.2	5	17	0.29	-46.7			
	Gething	1978	1853	90	1680	190	79	6.2	5	18	0.28	-46.7			
	Gething	1980	1854	80	2770	299	148	6.2	12	41	0.29	-45.6			
	Gething	1982	1854	63	1450	227	126	4.1	11	38	0.29	-45.1			
	Gething	1984	1855	61	1660	233	129	4.6	11	38	0.29	-45.4			
	Gething	1986	1855	71	1350	128	53	7.5	4	12	0.33	-47.1			
	Gething	2011	1859	63	1650	153	64	7.5	5	14	0.36	-47.2			
	Gething	2025	1861	63	1860	173	71	7.6	5	16	0.31	-47.2	-39.4		-7.8
	Montney	2420	1956	309	9030	845	319	7.8	23	72	0.32	-46.2	-39.9	-34.3	-6.3
	Montney	2470	1960	223	3490	398	184	6.0	16	54	0.30	-46.4	-39.7	-34.3	-6.7
	Montney	2520	1960	300	9670	1080	499	6.1	44	150	0.29	-45.9	-39.5	-34.2	-6.4
	Montney	2570	1961	328	9320	1040	479	6.1	42	144	0.29	-45.9	-39.5	-34.3	-6.4
	Montney	2620	1961	226	9490	1070	493	6.1	43	147	0.29	-45.9	-39.3	-34.1	-6.6
	Montney	2670	1961	266	8140	748	297	7.8	23	79	0.29	-46.8	-39.8	-34.2	-7.0
	Montney	2720	1962	269	4730	540	243	6.0	21	75	0.28	-44.9	-39.1	-34.4	-5.8
	Montney	2770	1962	318	13800	1390	558	7.1	42	131	0.32	-46.1	-39.5	-34.3	-6.6
	Montney	2820	1963	225	9480	1050	520	6.0	45	152	0.30	-45.5	-39.4	-34.5	-6.1
	Montney	2870	1963	226	13900	1560	642	6.3	51	171	0.30	-46.4	-39.5	-34.1	-6.9
	Montney	2920	1964	230	13400	1450	593	6.6	46	151	0.30	-46.8	-39.7	-34.1	-7.1
	Montney	2970	1964	275	12600	1320	538	6.8	43	141	0.30	-46.6	-39.6	-34.1	-7.0
	Montney	3020	1964	316	6430	705	317	6.3	26	88	0.30	-46.6	-39.8	-34.2	-6.8
	Montney	3070	1963	251	6710	662	270	7.2	21	70	0.30	-46.8	-39.7	-34.2	-6.9
	Montney	3120	1963	228	5960	589	241	7.2	19	62	0.31	-46.7	-39.8	-34.4	-6.9
	Montney	3170	1964	272	11300	1310	585	6.0	51	165	0.31	-46.5	-39.5	-34.0	-7.0
	Montney	3220	1964	205	11	nd	nd		nd	nd					
	Montney	3270	1965	289	12200	1340	550	6.5	43	141	0.30	-46.7	-39.5	-34.0	-7.2
	Montney	3320	1965	113	2960	334	155	6.1	13	48	0.27	-46.8	-39.9	-34.2	-6.9
	Montney	3370	1965	263	3060	345	158	6.1	14	49	0.29	-47.0	-40.0	-34.1	-7.0
	Montney	3420	1966	267	1150	208	140	3.3	17	65	0.26	-44.2	-39.5	-34.2	-4.7
	Montney	3470	1966	384	641	125	89	3.0	10	39	0.26				
	Montney	3520	1966	313	10600	1060	448	7.0	39	134	0.29	-46.3	-39.1	-33.7	-7.2
	Montney	3570	1966	301	13700	1310	515	7.5	42	139	0.30	-46.6	-39.2	-34.0	-7.4
	Montney	3620	1966	163	16700	1510	569	8.0	45	147	0.31	-47.0	-39.3	-34.0	-7.7
	Montney	3670	1966	240	11100	1000	391	8.0	31	103	0.30	-47.0	-39.5	-34.1	-7.5
	Montney	3720	1966	287	7340	667	263	7.9	21	70	0.30	-46.9	-39.4	-33.8	-7.5
	Montney	3770	1967	350	3560	502	265	4.6	27	106	0.25	-45.0	-38.9	-33.9	-6.1
	Montney	3820	1967	234	10700	1110	477	6.7	42	149	0.28	-46.1	-39.1	-33.9	-7.0
	Montney	3870	1967	235	15800	1530	600	7.4	49	162	0.30	-46.8	-39.5	-33.9	-7.3
	Montney	3920	1967	296	407	106	98	2.0	15	75	0.20				
	Montney	3943	1967	332	10100	1150	525	6.0	47	164	0.29	-45.2	-38.9	-33.7	-6.3

Well	Formation	MD	TVD	Gas Units	C1	C2	C3	C1/(C2+C3)	iC4	nC4	iC4/nC4	$\delta^{13}C1$	$\delta^{13}C2$	$\delta^{13}C3$
		m	m		ppm	ppm	ppm					‰VPDB	‰VPDB	‰VPDB
7	Duvernay	3151	952	52800	4740	1160	8.9	116	183	0.63	-46.2	-33.2	-30.3	-13.0
	Duvernay	3155	840	52200	4680	1150	9.0	116	184	0.63	-46.2	-33.3	-30.3	-12.9
	Waterways	3215	141	2900	452	194	4.5	30	58	0.52	-45.2	-32.6	-29.8	-12.6
	Waterways	3220	129	2810	428	177	4.6	27	51	0.53	-45.3	-32.7	-29.7	-12.6
	Waterways	3225	107	1770	290	134	4.2	22	43	0.51	-44.7	-32.3	-29.7	-12.4
	Waterways	3230	86	2240	296	123	5.3	20	39	0.51	-45.0	-32.3	-29.6	-12.7
	Waterways	3235	223	6770	722	227	7.1	32	55	0.58	-45.8	-32.3	-29.0	-13.5
	Waterways	3241	208	5910	724	236	6.2	31	51	0.61	-45.9	-32.5	-29.1	-13.4
	Waterways	3245	207	5740	746	257	5.7	36	60	0.60	-45.1	-32.0	-28.8	-13.1
	Waterways	3250	219	5640	763	276	5.4	41	67	0.61	-45.0	-32.0	-28.7	-13.0
	Waterways	3255	235	5710	771	276	5.5	41	66	0.62	-45.2	-32.0	-28.6	-13.2
	Waterways	32628	229	6040	806	290	5.5	43	69	0.62	-45.2	-32.0	-28.7	-13.2
	Waterways	3270	219	6110	813	292	5.5	44	70	0.63	-45.2	-32.3	-28.8	-12.9
	Waterways	3275	307	5390	722	266	5.5	42	68	0.63	-45.1	-31.8	-28.6	-13.3
	Waterways	3280	201	6380	855	313	5.5	48	78	0.62	-45.3	-31.7	-28.4	-13.6
	Waterways	3285	240	6300	835	303	5.6	47	76	0.62	-45.2	-31.8	-28.5	-13.4
	Waterways	3290	229	5860	777	284	5.5	45	72	0.62	-45.1	-31.8	-28.3	-13.3
	Waterways	3295	201	5690	757	277	5.5	44	71	0.62	-45.2	-31.8	-28.3	-13.4
	Waterways	3300	212	6930	848	293	6.1	45	72	0.63	-45.7	-31.8	-28.7	-13.9
	Swan Hills Member	3305	775	52400	5160	1140	8.3	113	182	0.62	-46.7	-31.1	-28.2	-15.3
	Swan Hills Member	3310	952	62400	6210	1410	8.2	143	236	0.61	-46.9	-31.2	-28.3	-15.7
	Swan Hills Member	3315	1009	68600	7600	1820	7.3	188	314	0.60	-46.3	-31.0	-28.1	-15.3
	Watt Mountain	3320	1119	72700	8070	1960	7.2	203	342	0.59	-46.0	-30.8	-28.1	-15.2
	Watt Mountain	3325	1048	69100	7910	1990	7.0	210	360	0.58	-45.9	-30.9	-28.2	-15.0
	Watt Mountain	3330	1037	68300	7930	2030	6.9	218	376	0.58	-45.9	-30.8	-28.1	-15.1
	Watt Mountain	3334	1087	68700	7960	2050	6.9	220	381	0.58	-45.8	-30.9	-28.0	-14.9

Appendix 2. $\delta^{13}C$ Methane versus gas wetness

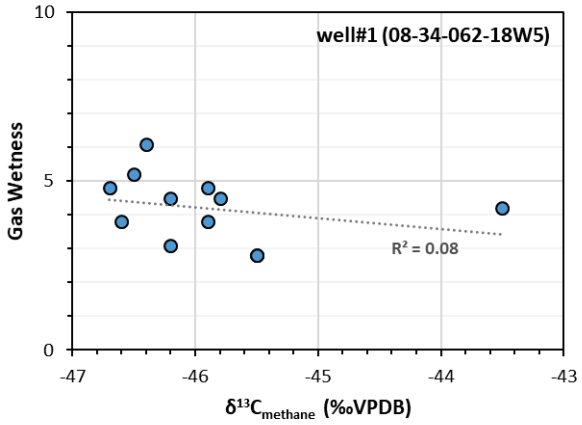

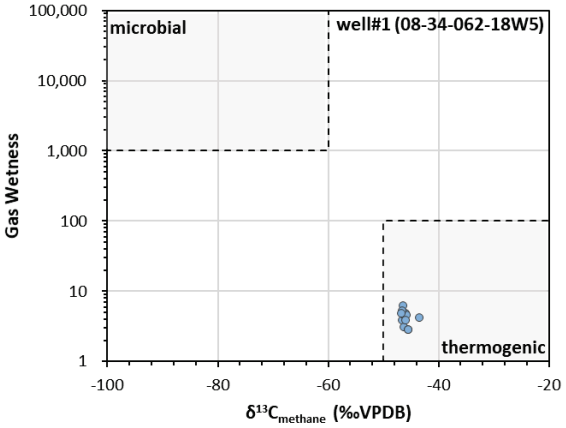

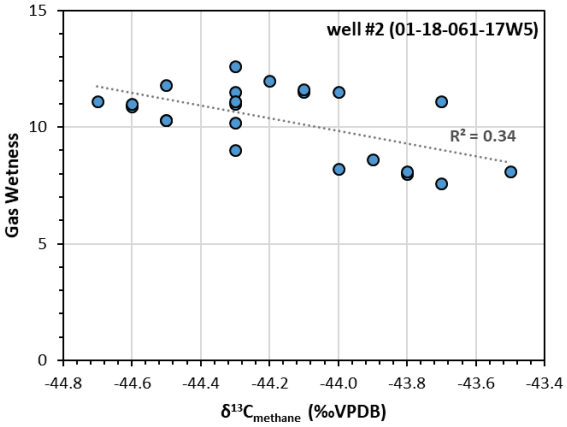

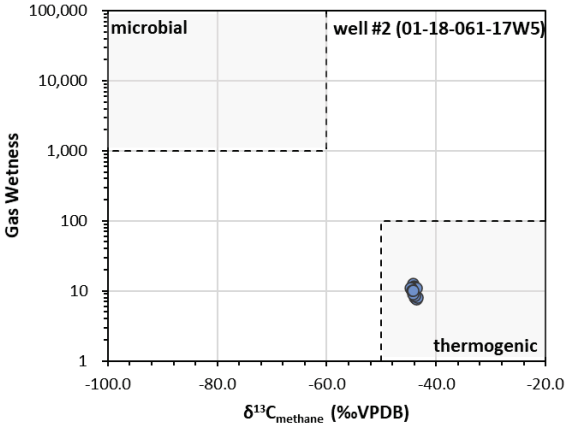

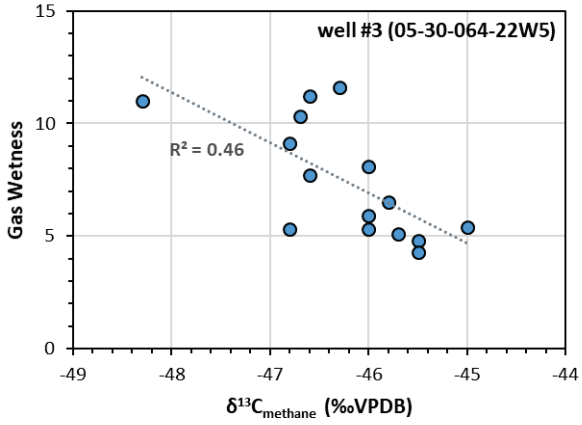

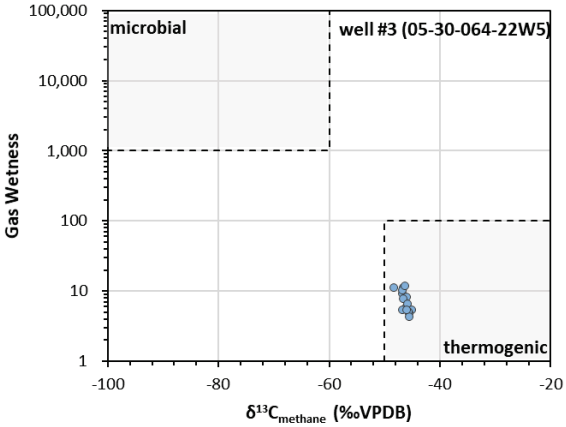

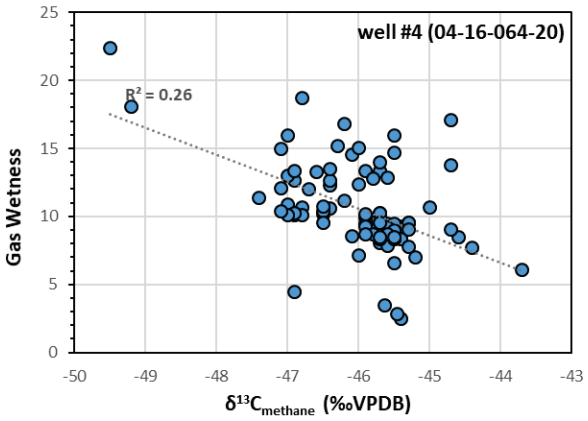
well #4 (04-16-064-20)
R² = 0.26
Gas Wetness
δ13Cmethane (‰VPDB)

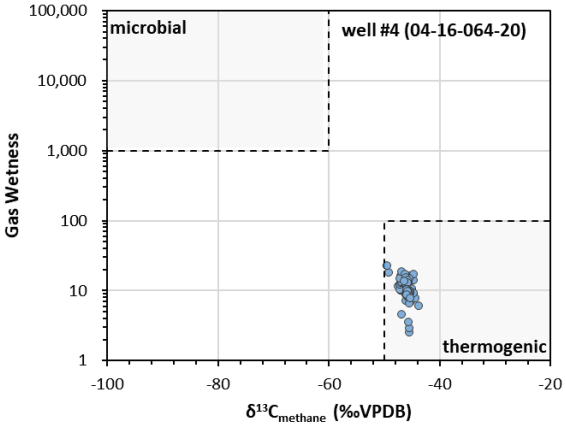
microbial
well #4 (04-16-064-20)
thermogenic
Gas Wetness
δ13Cmethane (‰VPDB)

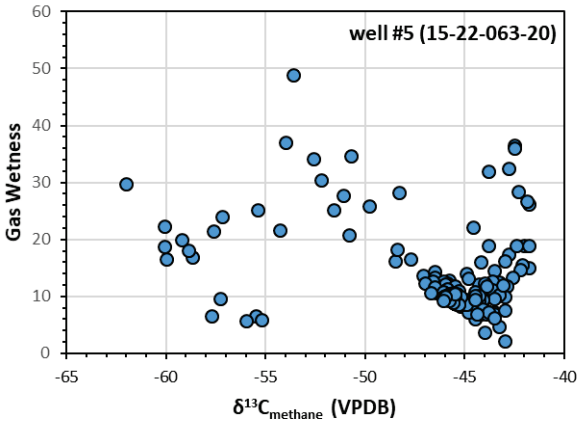
well #5 (15-22-063-20)
Gas Wetness
δ13Cmethane (VPDB)

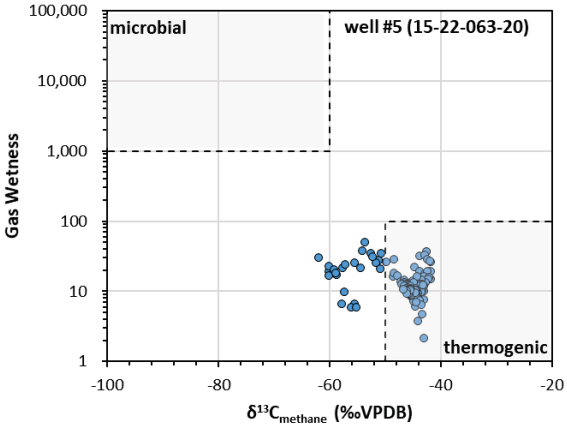
microbial
well #5 (15-22-063-20)
thermogenic
Gas Wetness
δ13Cmethane (‰VPDB)

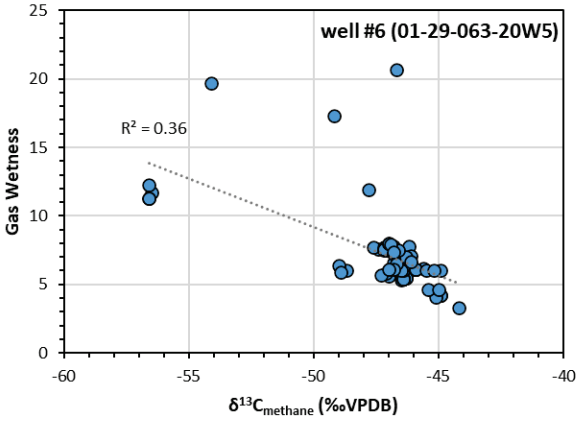
well #6 (01-29-063-20W5)
R² = 0.36
Gas Wetness
δ13Cmethane (‰VPDB)

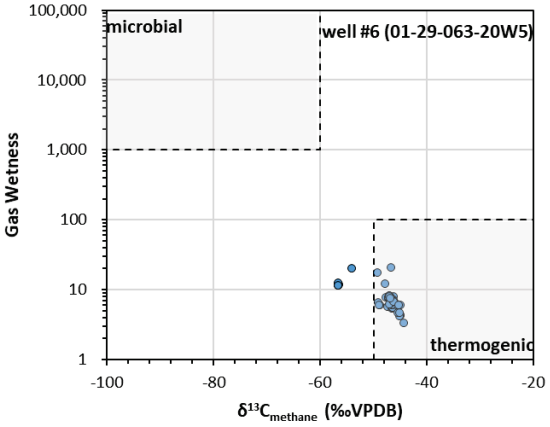
microbial
well #6 (01-29-063-20W5)
thermogenic
Gas Wetness
δ13Cmethane (‰VPDB)

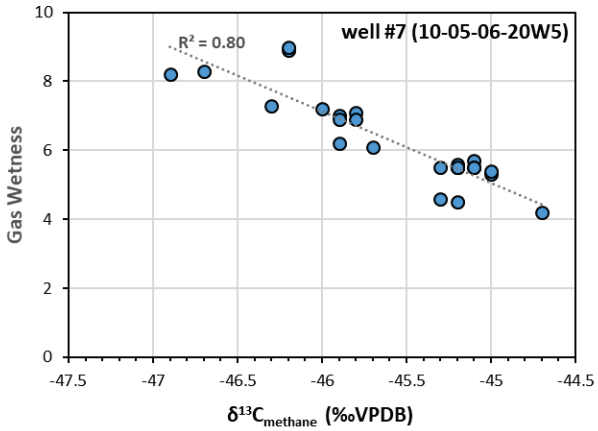
well #7 (10-05-06-20W5)
R² = 0.80
Gas Wetness
δ13Cmethane (‰VPDB)
10
8
6
4
2
0
-47.5
-47
-46.5
-46
-45.5
-45
-44.5

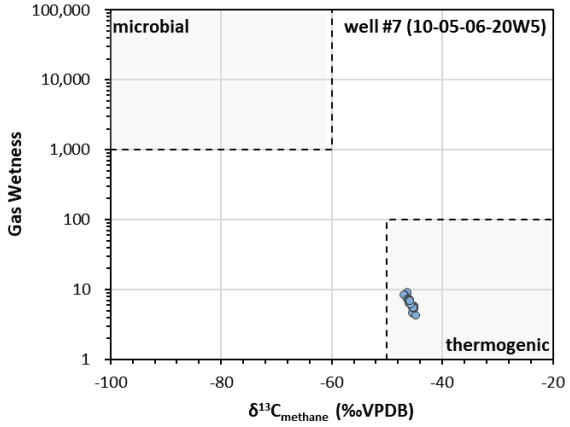
microbial
well #7 (10-05-06-20W5)
thermogenic
Gas Wetness
δ13Cmethane (‰VPDB)
100,000
10,000
1,000
100
10
1
-100
-80
-60
-40
-20

Appendix 3. Depth versus $\delta^{13}C$ Methane

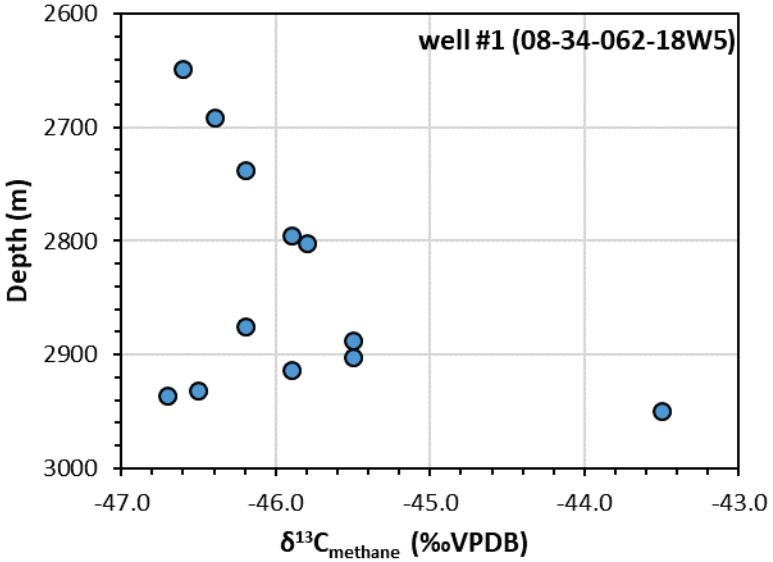

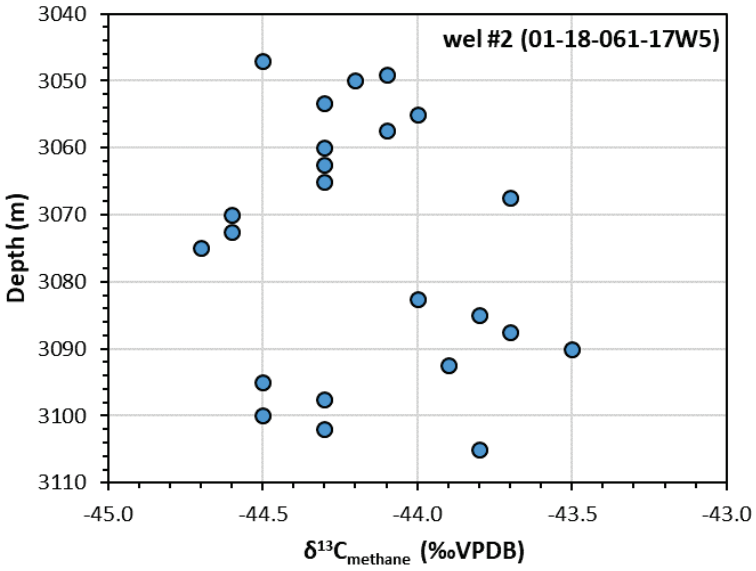

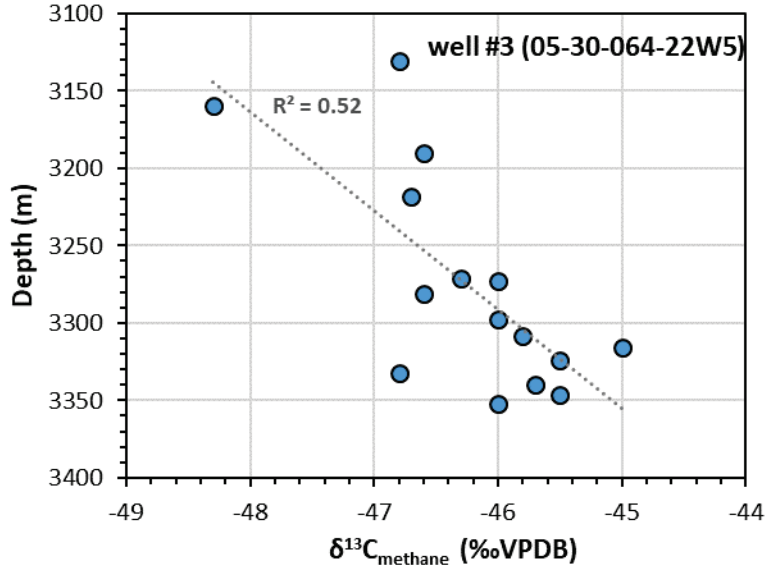
well #3 (05-30-064-22W5)
R² = 0.52
Depth (m)
3100
3150
3200
3250
3300
3350
3400
-49
-48
-47
-46
-45
-44
δ13Cmethane (‰VPDB)

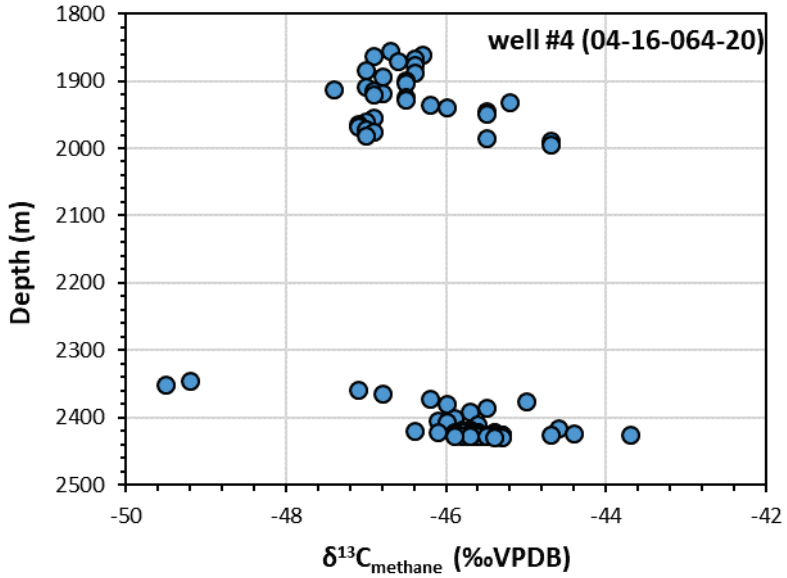
well #4 (04-16-064-20)
Depth (m)
1800
1900
2000
2100
2200
2300
2400
2500
-50
-48
-46
-44
-42
δ13Cmethane (‰VPDB)

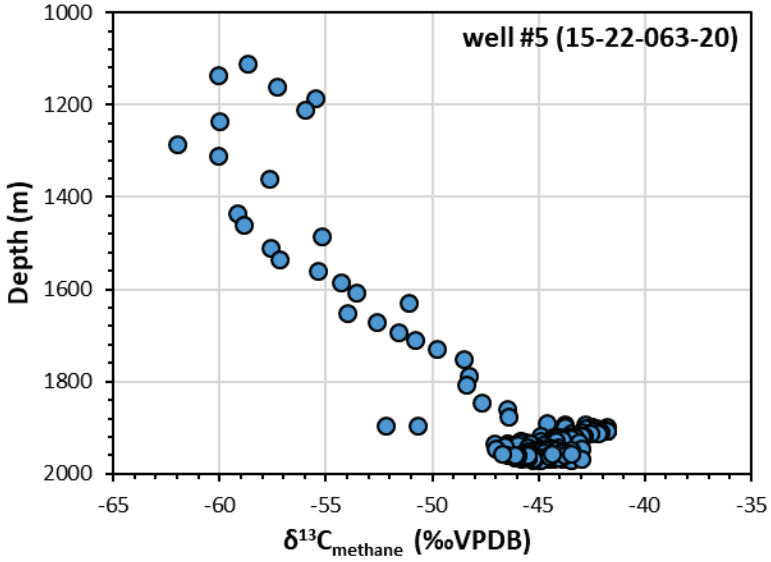
well #5 (15-22-063-20)
Depth (m)
1000
1200
1400
1600
1800
2000
-65
-60
-55
-50
-45
-40
-35
δ13Cmethane (‰VPDB)

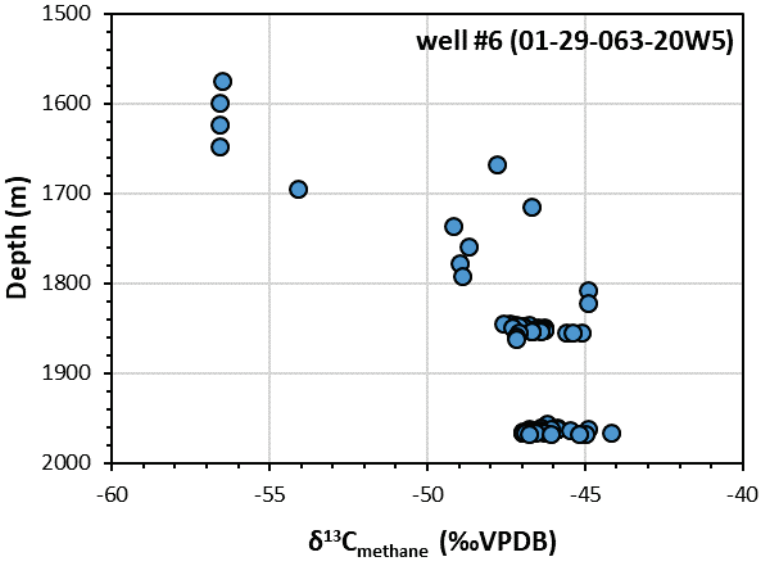
well #6 (01-29-063-20W5)
Depth (m)
1500
1600
1700
1800
1900
2000
-60
-55
-50
-45
-40
δ13Cmethane (‰VPDB)

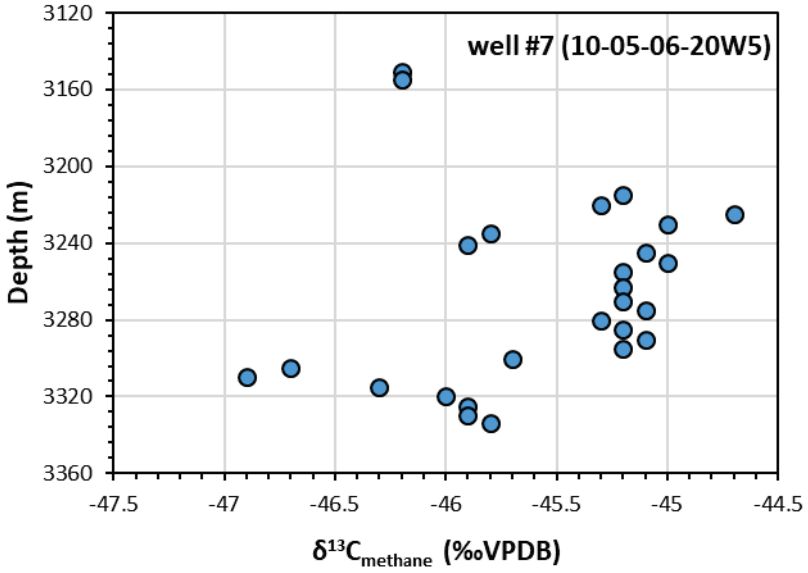
well #7 (10-05-06-20W5)
Depth (m)
3120
3160
3200
3240
3280
3320
3360
-47.5
-47
-46.5
-46
-45.5
-45
-44.5
δ13Cmethane (‰VPDB)

Appendix 4. Depth versus $\delta^{13}C$ Ethane

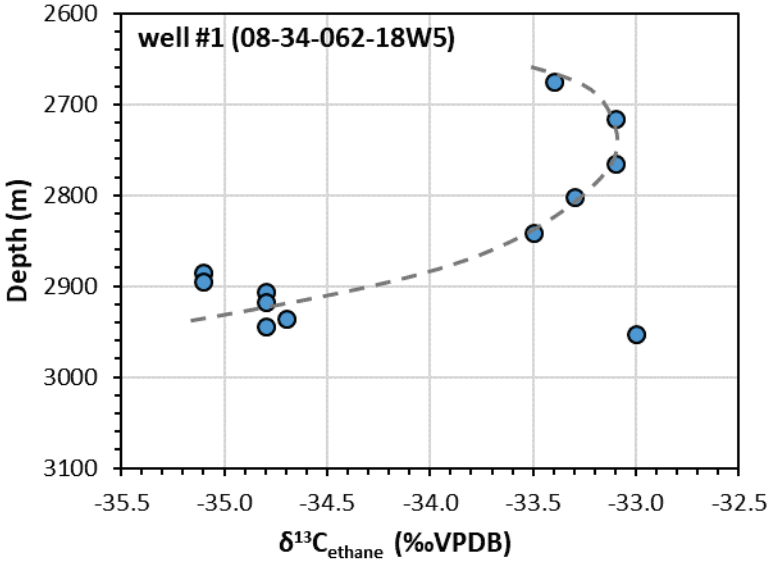

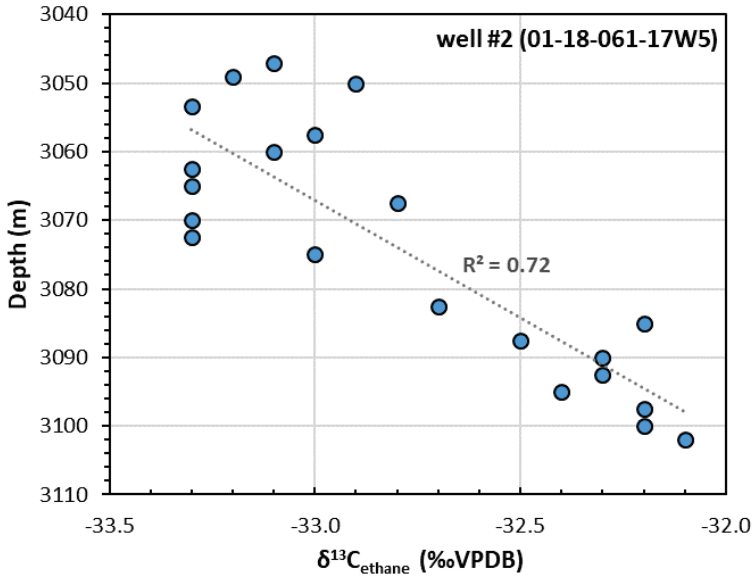

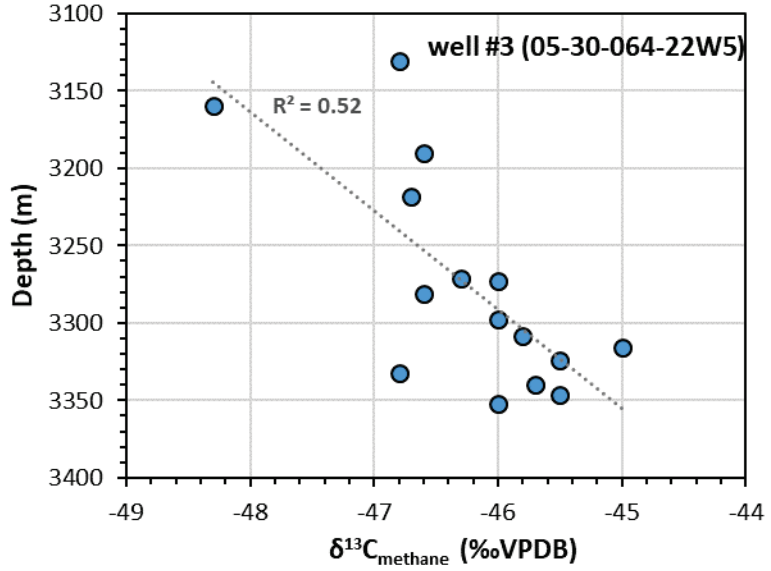
well #3 (05-30-064-22W5)
R² = 0.52
Depth (m)
3100
3150
3200
3250
3300
3350
3400
-49
-48
-47
-46
-45
-44
δ13Cmethane (‰VPDB)

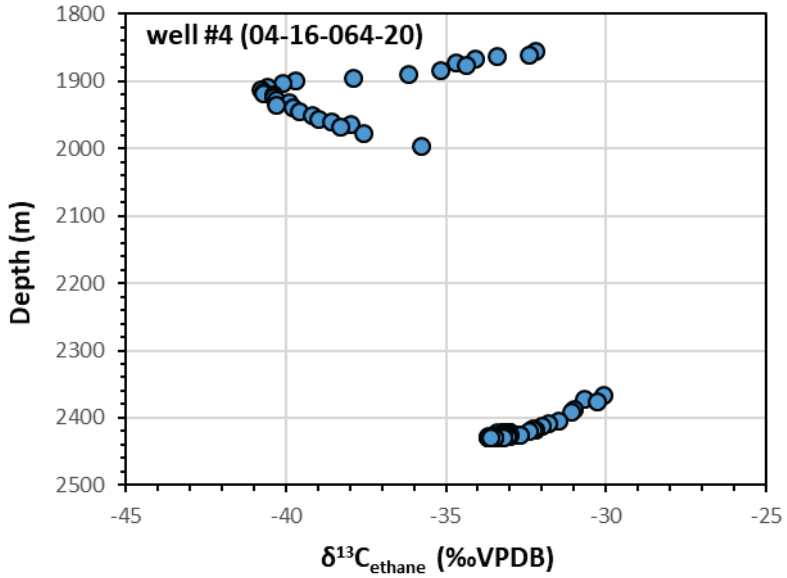
well #4 (04-16-064-20)
Depth (m)
1800
1900
2000
2100
2200
2300
2400
2500
-45
-40
-35
-30
-25
δ13Cethane (‰VPDB)

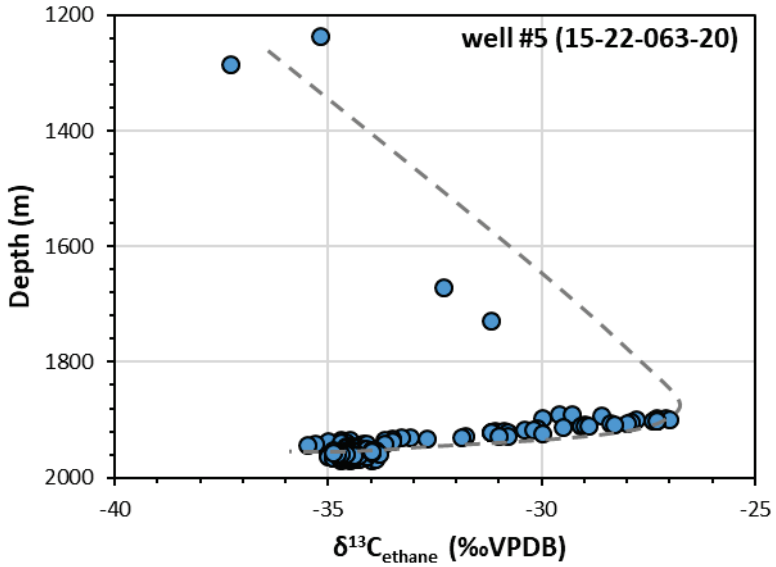
well #5 (15-22-063-20)
Depth (m)
1200
1400
1600
1800
2000
-40
-35
-30
-25
δ13Cethane (‰VPDB)

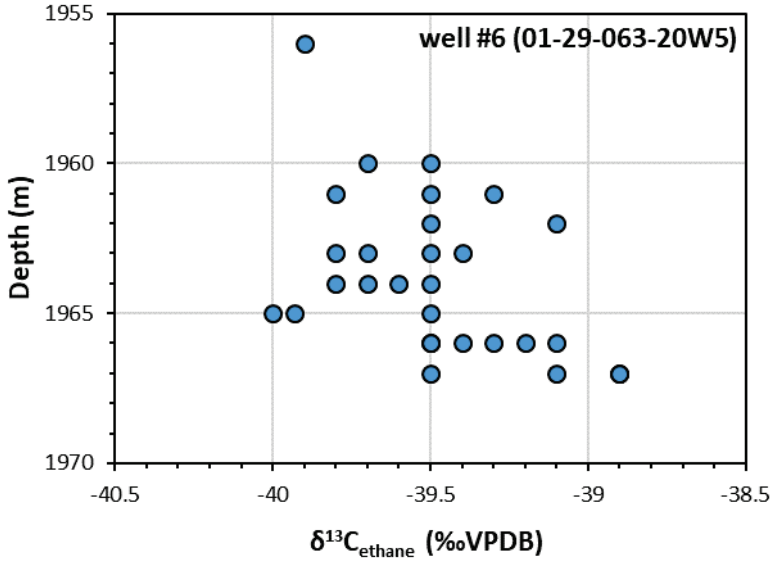
well #6 (01-29-063-20W5)
Depth (m)
1955
1960
1965
1970
-40.5
-40
-39.5
-39
-38.5
δ13Cethane (‰VPDB)

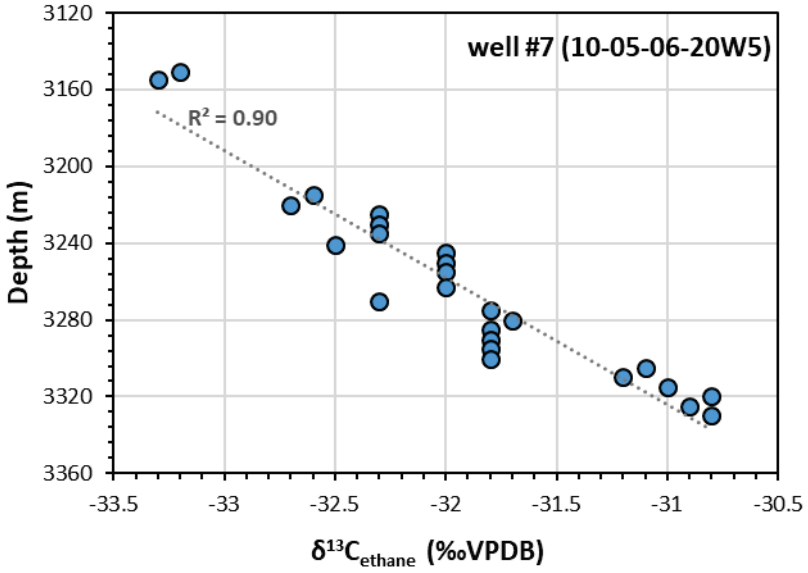
well #7 (10-05-06-20W5)
R² = 0.90
Depth (m)
3120
3160
3200
3240
3280
3320
3360
-33.5
-33
-32.5
-32
-31.5
-31
-30.5
δ13Cethane (‰VPDB)

Appendix 5. $\delta^{13}C$ Ethane versus $\delta^{13}C$ Propane

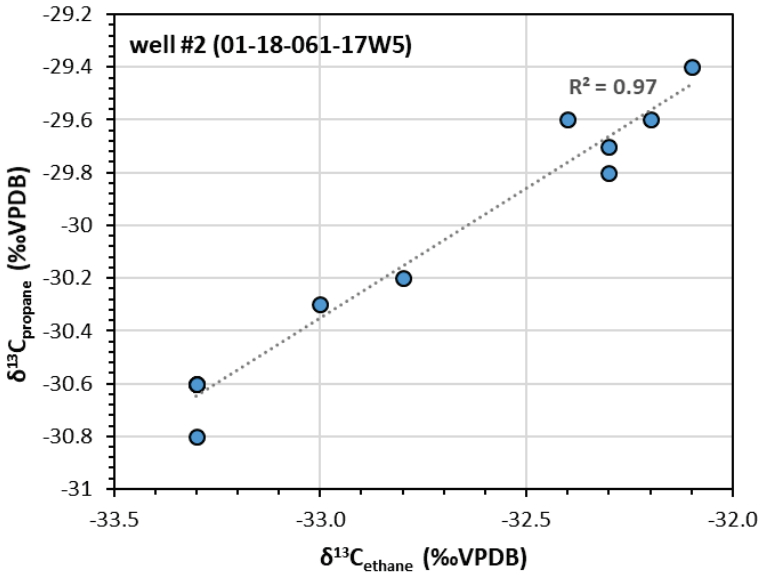

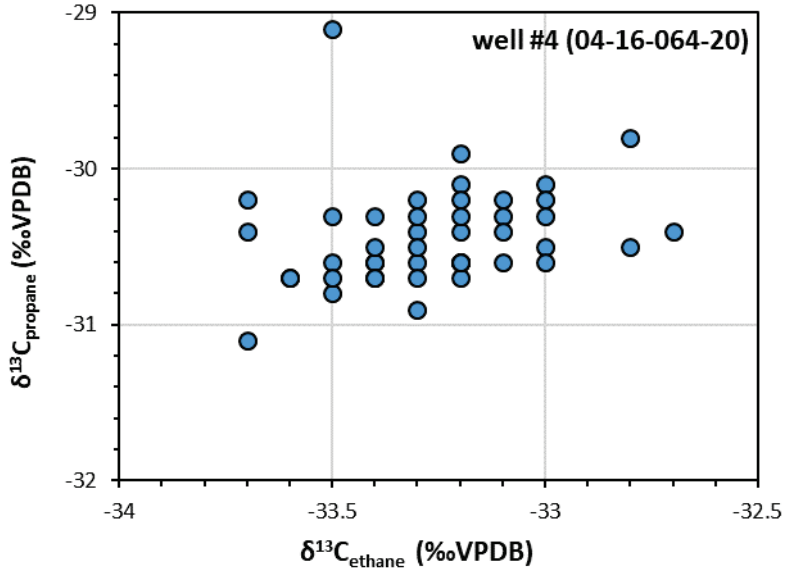

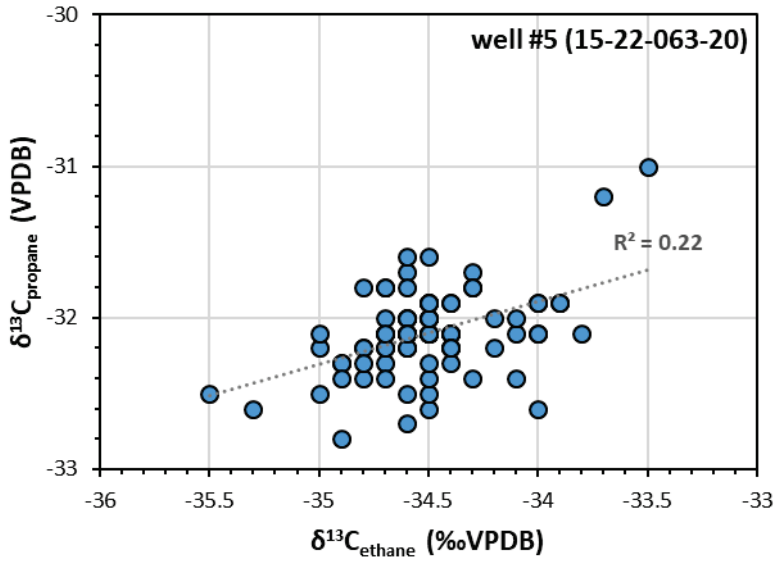
well #5 (15-22-063-20)
R² = 0.22
δ13Cpropane (VPDB)
δ13Cethane (‰VPDB)
-30
-31
-32
-33
-36
-35.5
-35
-34.5
-34
-33.5
-33

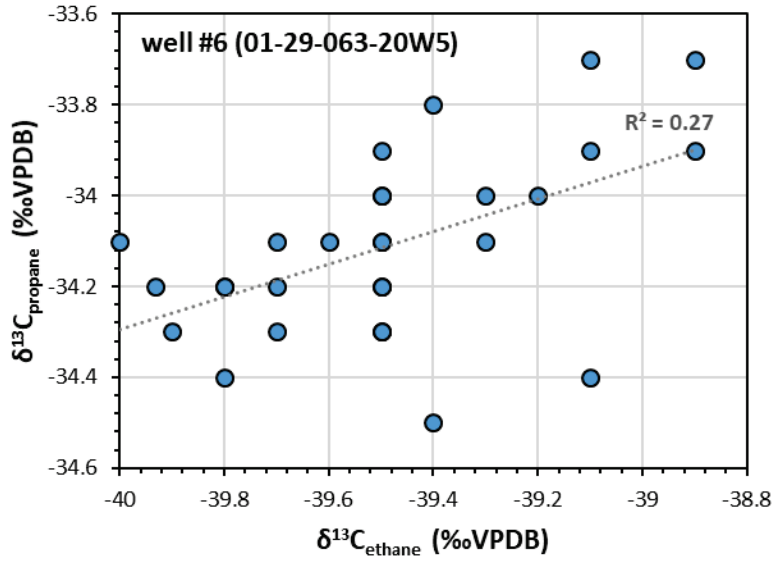
well #6 (01-29-063-20W5)
R² = 0.27
δ13Cpropane (‰VPDB)
δ13Cethane (‰VPDB)
-33.6
-33.8
-34
-34.2
-34.4
-34.6
-40
-39.8
-39.6
-39.4
-39.2
-39
-38.8

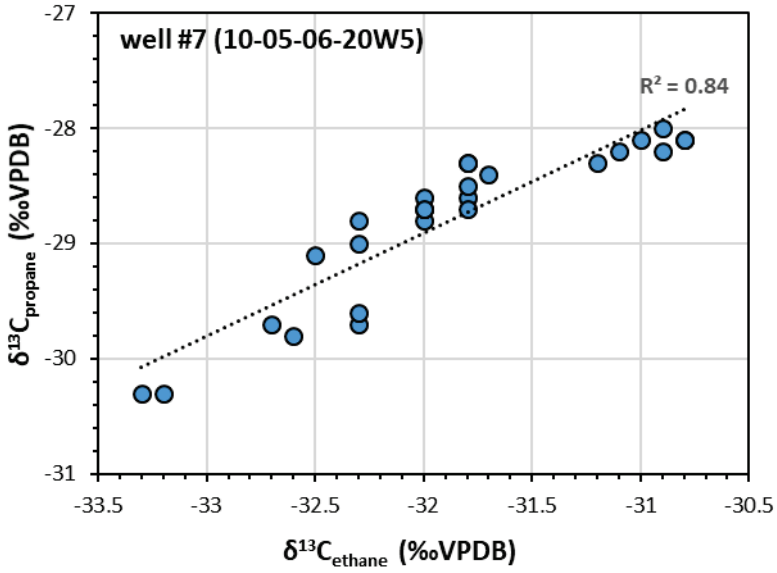
well #7 (10-05-06-20W5)
R² = 0.84
-27
-28
-29
-30
-31
-33.5
-33
-32.5
-32
-31.5
-31
-30.5
δ13Cpropane (‰VPDB)
δ13Cethane (‰VPDB)

Appendix 6. Depth versus iC4/nC4

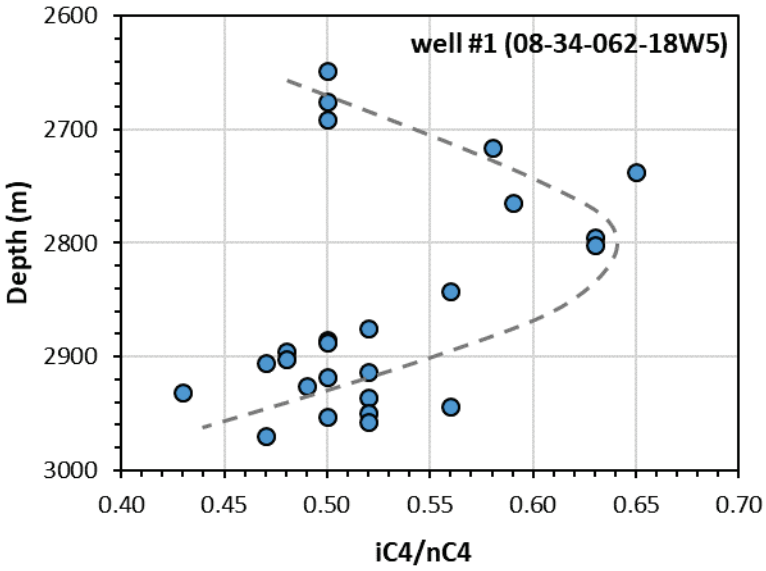

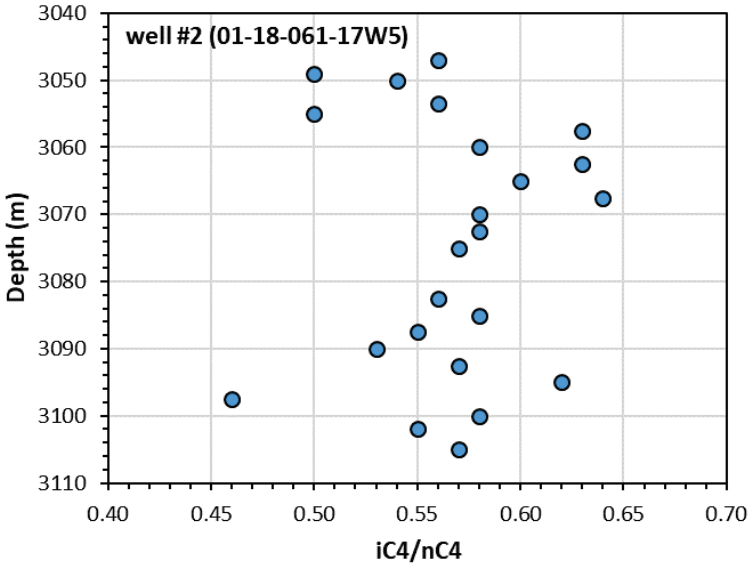

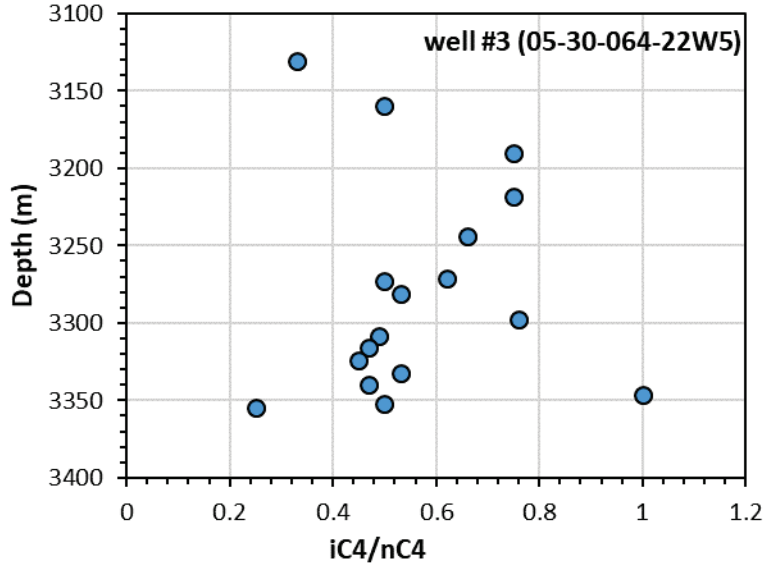
well #3 (05-30-064-22W5)
Depth (m)
3100
3150
3200
3250
3300
3350
3400
0
0.2
0.4
0.6
0.8
1
1.2
iC4/nC4

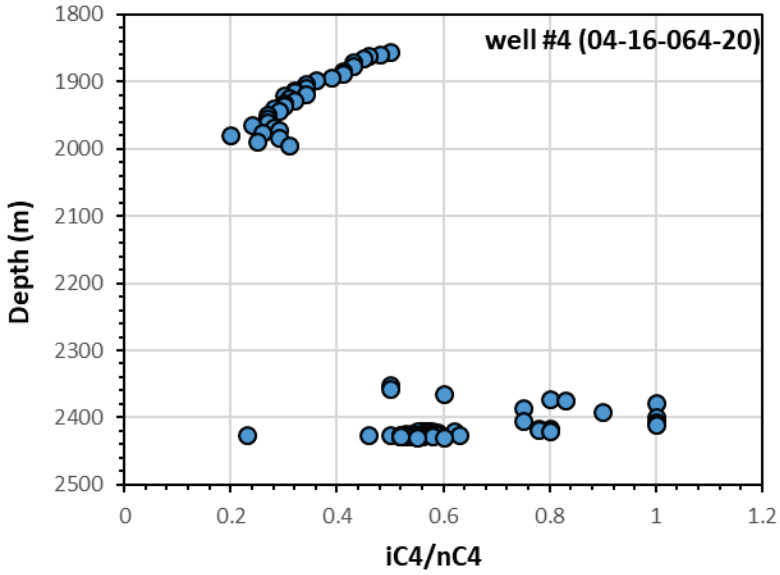
well #4 (04-16-064-20)
Depth (m)
1800
1900
2000
2100
2200
2300
2400
2500
0
0.2
0.4
0.6
0.8
1
1.2
iC4/nC4

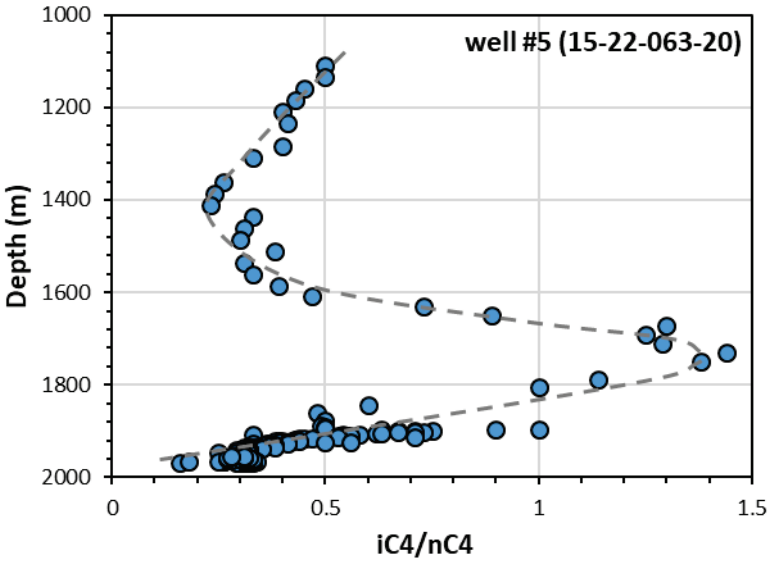
well #5 (15-22-063-20)
Depth (m)
1000
1200
1400
1600
1800
2000
0
0.5
1
1.5
iC4/nC4

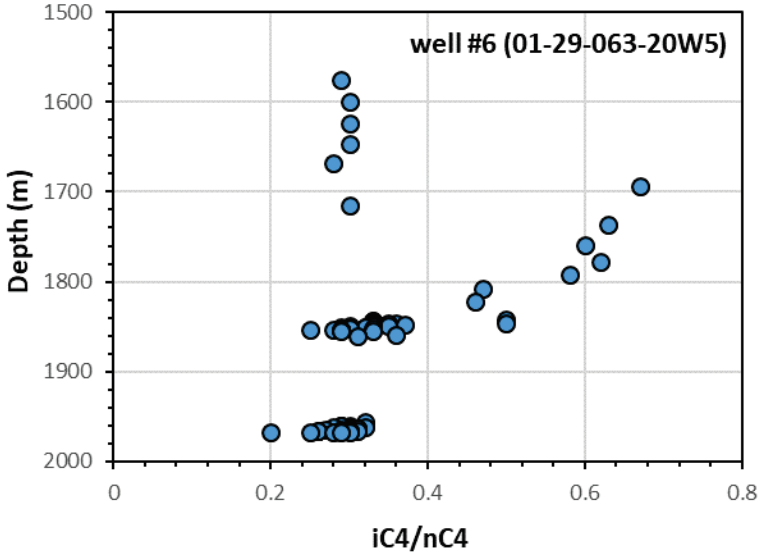
well #6 (01-29-063-20W5)
Depth (m)
1500
1600
1700
1800
1900
2000
0
0.2
0.4
0.6
0.8
iC4/nC4

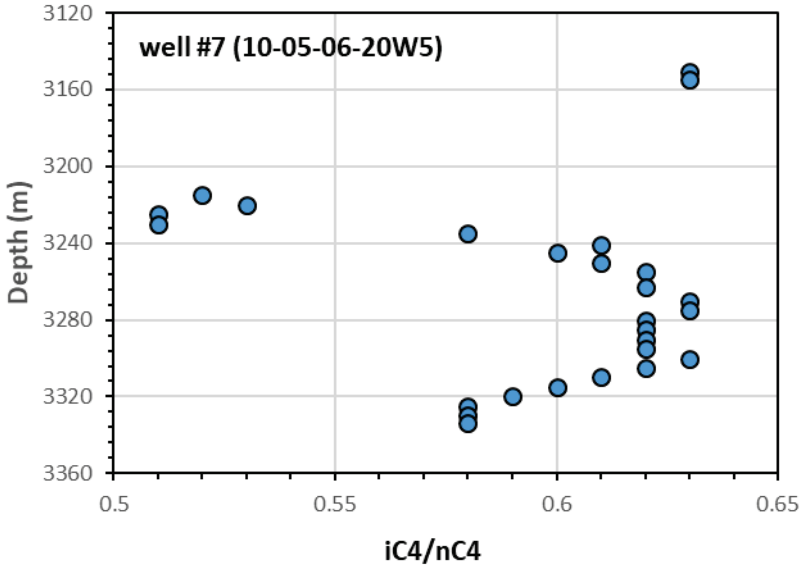
well #7 (10-05-06-20W5)
Depth (m)
3120
3160
3200
3240
3280
3320
3360
0.5
0.55
0.6
0.65
iC4/nC4

Appendix 7. $\delta^{13}C1 - \delta^{13}C2$ versus depth

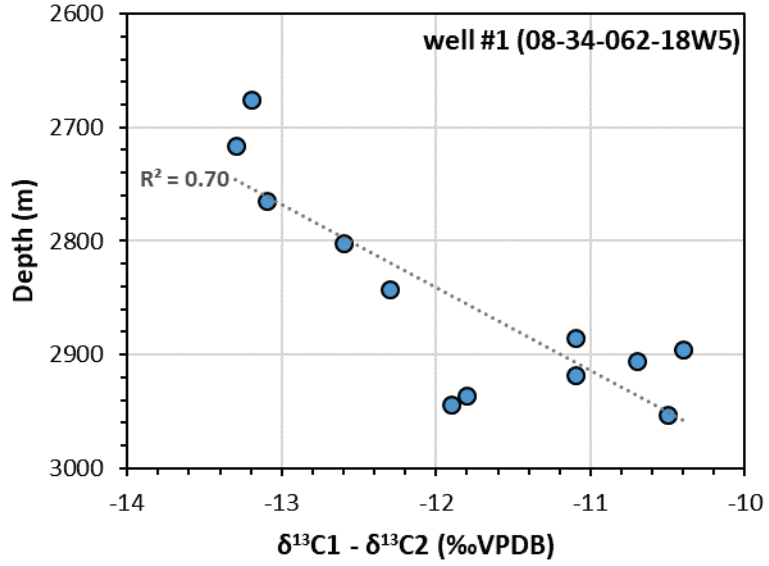

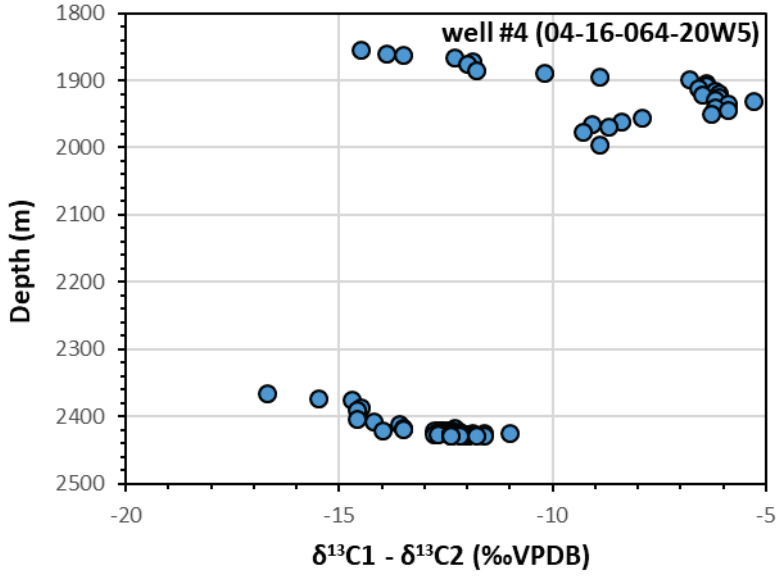

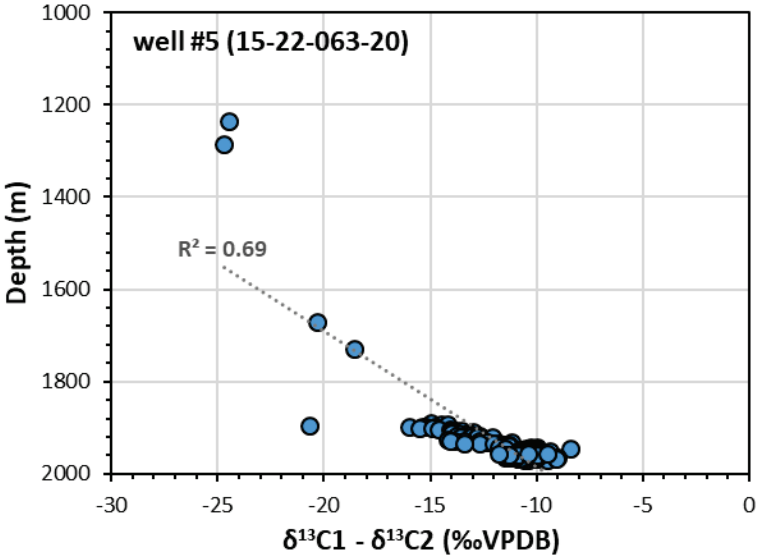
well #5 (15-22-063-20)
R² = 0.69
Depth (m)
1000
1200
1400
1600
1800
2000
-30
-25
-20
-15
-10
-5
0
δ13C1 - δ13C2 (‰VPDB)

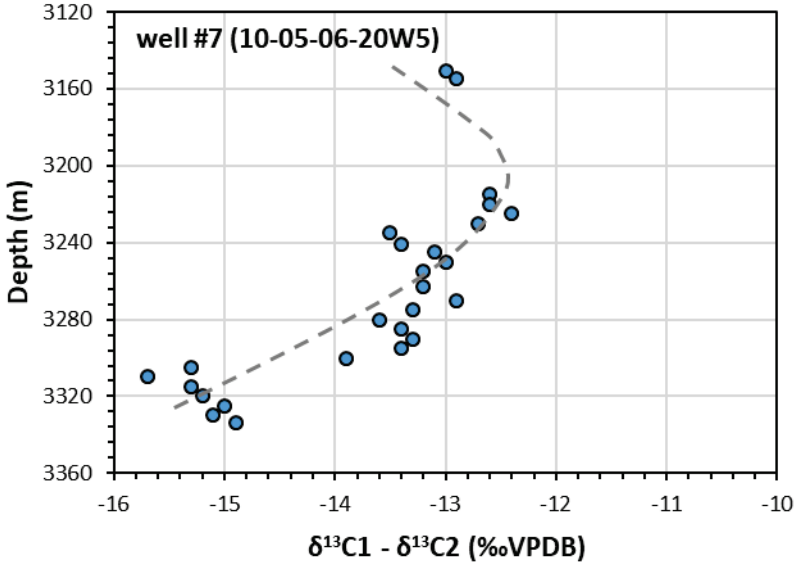
well #7 (10-05-06-20W5)
Depth (m)
3120
3160
3200
3240
3280
3320
3360
-16
-15
-14
-13
-12
-11
-10
δ13C1 - δ13C2 (‰VPDB)

Appendix 8. $\delta^{13}C$ Ethane versus gas wetness

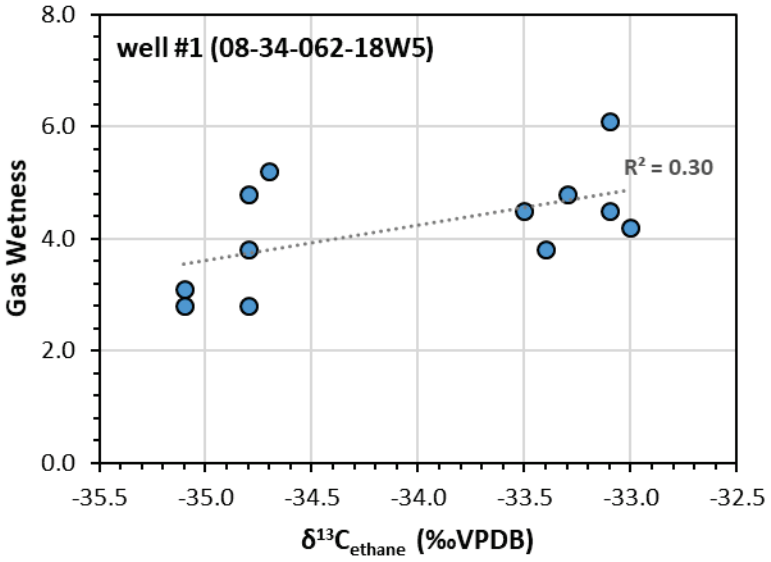

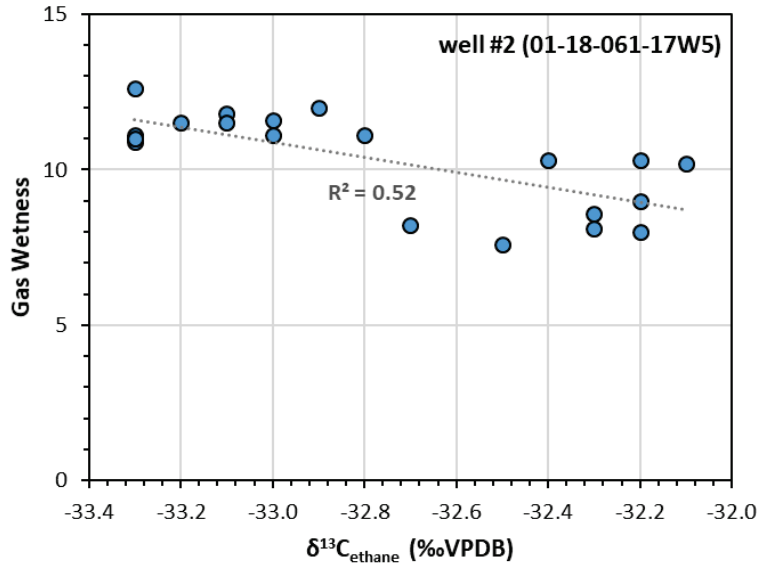

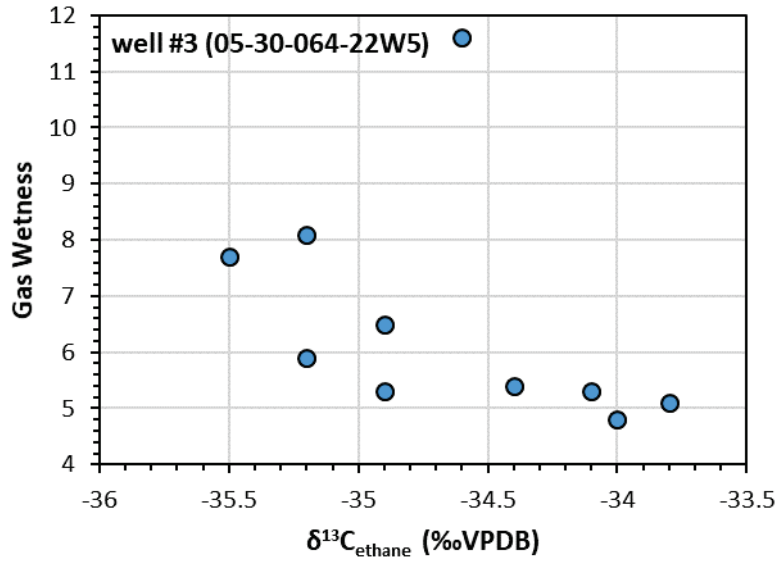
well #3 (05-30-064-22W5)
Gas Wetness
12
11
10
9
8
7
6
5
4
-36
-35.5
-35
-34.5
-34
-33.5
δ13Cethane (‰VPDB)

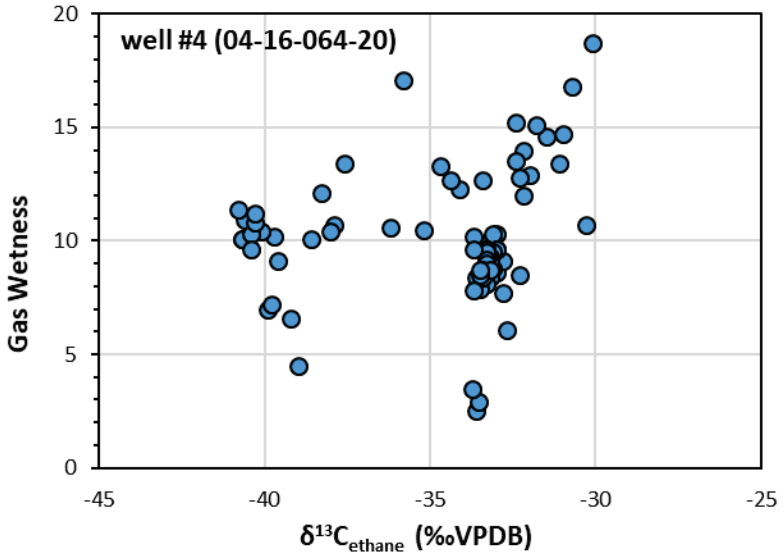
well #4 (04-16-064-20)
Gas Wetness
20
15
10
5
0
-45
-40
-35
-30
-25
δ13Cethane (‰VPDB)

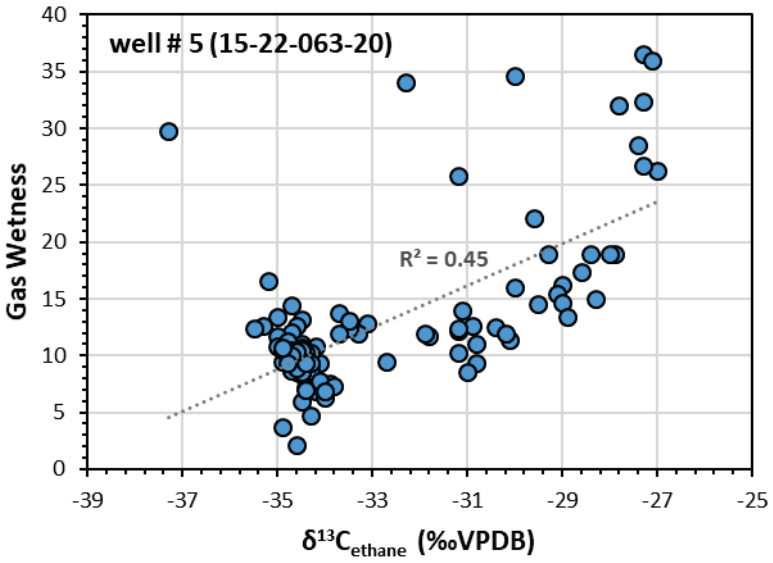
well # 5 (15-22-063-20)
Gas Wetness
R² = 0.45
δ13Cethane (‰VPDB)
40
35
30
25
20
15
10
5
0
-39
-37
-35
-33
-31
-29
-27
-25

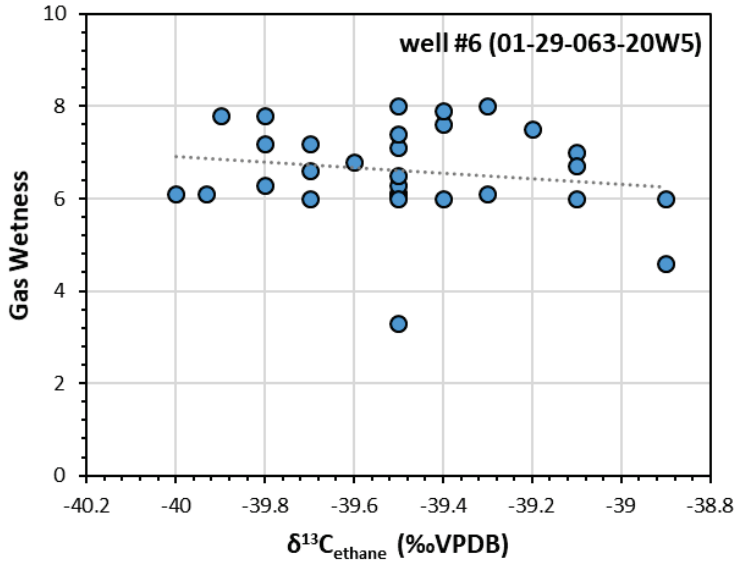
well #6 (01-29-063-20W5)
Gas Wetness
δ13Cethane (‰VPDB)
10
8
6
4
2
0
-40.2
-40
-39.8
-39.6
-39.4
-39.2
-39
-38.8

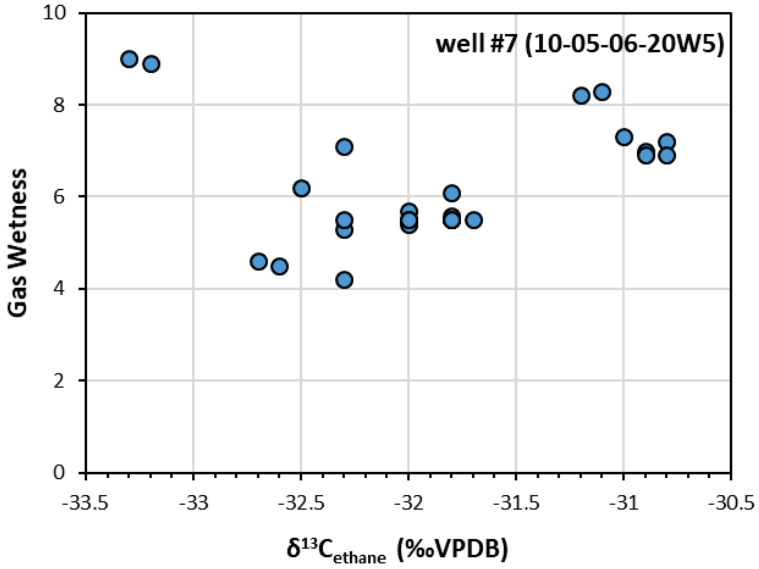
well #7 (10-05-06-20W5)
Gas Wetness
10
8
6
4
2
0
-33.5
-33
-32.5
-32
-31.5
-31
-30.5
δ13Cethane (‰VPDB)

Appendix 9. Butane ratio versus gas wetness

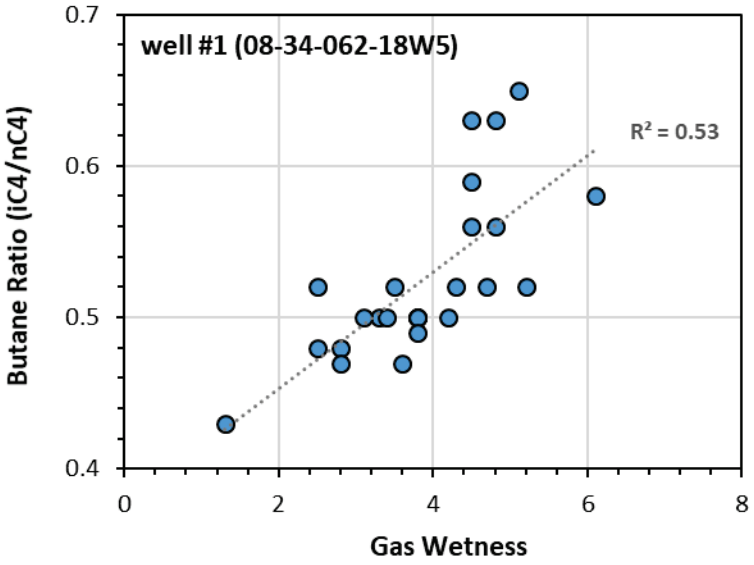

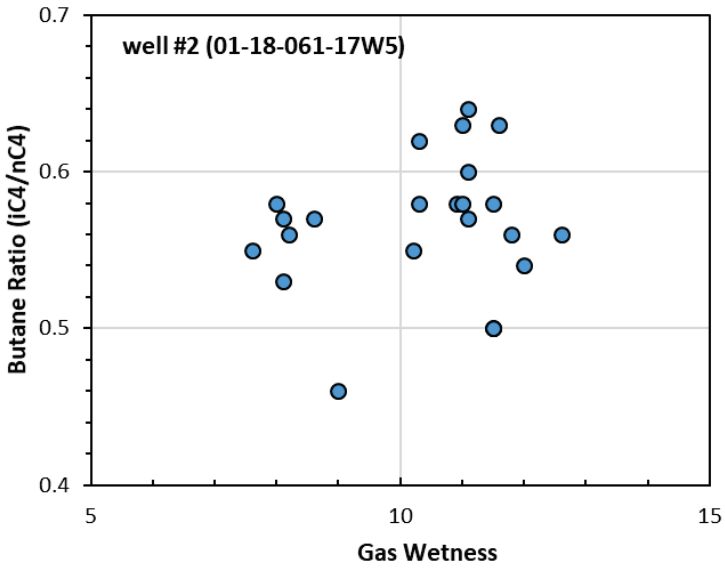

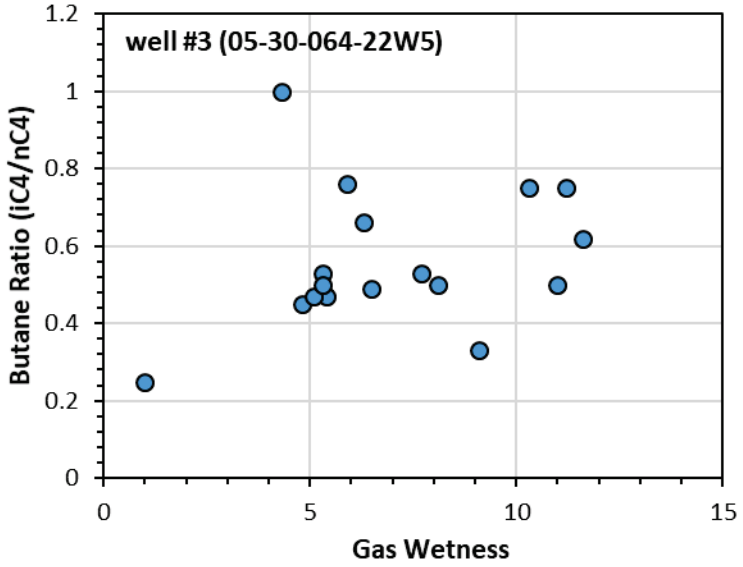
well #3 (05-30-064-22W5)
Butane Ratio (iC4/nC4)
Gas Wetness
0
0.2
0.4
0.6
0.8
1
1.2
0
5
10
15

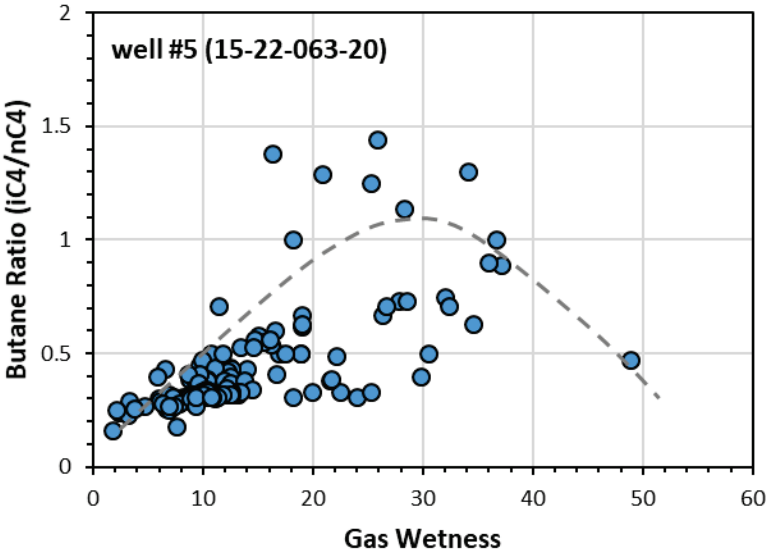
well #5 (15-22-063-20)
Butane Ratio (iC4/nC4)
Gas Wetness
0
0.5
1
1.5
2
0
10
20
30
40
50
60

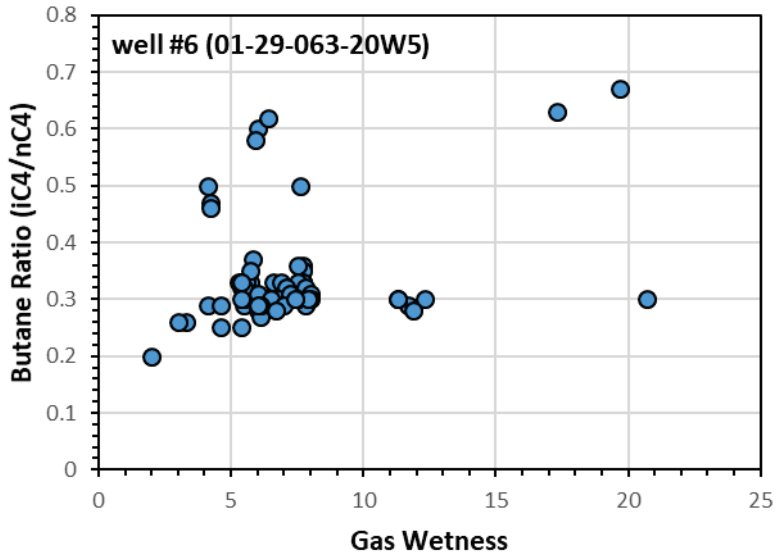
well #6 (01-29-063-20W5)
Butane Ratio (iC4/nC4)
Gas Wetness
0.8
0.7
0.6
0.5
0.4
0.3
0.2
0.1
0
0
5
10
15
20
25

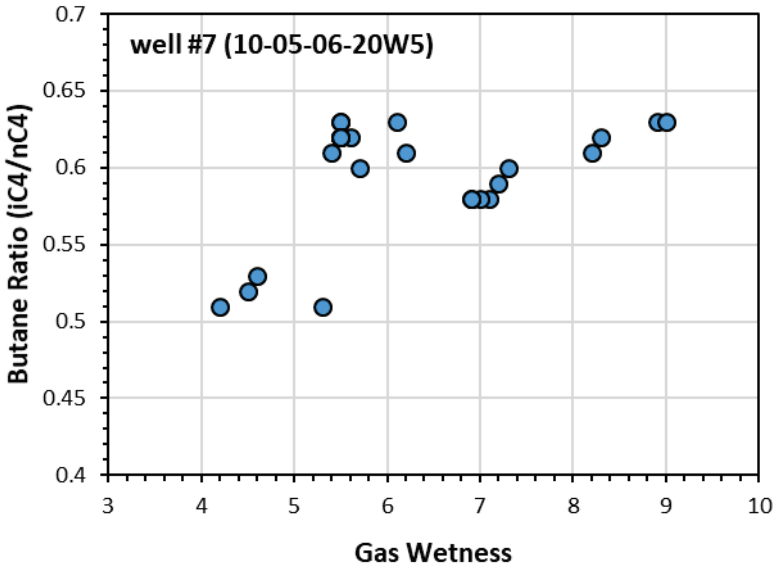
well #7 (10-05-06-20W5)
Butane Ratio (iC4/nC4)
Gas Wetness
0.7
0.65
0.6
0.55
0.5
0.45
0.4
3
4
5
6
7
8
9
10

Appendix 10. $\delta^{13}C1 - \delta^{13}C2$ versus gas wetness

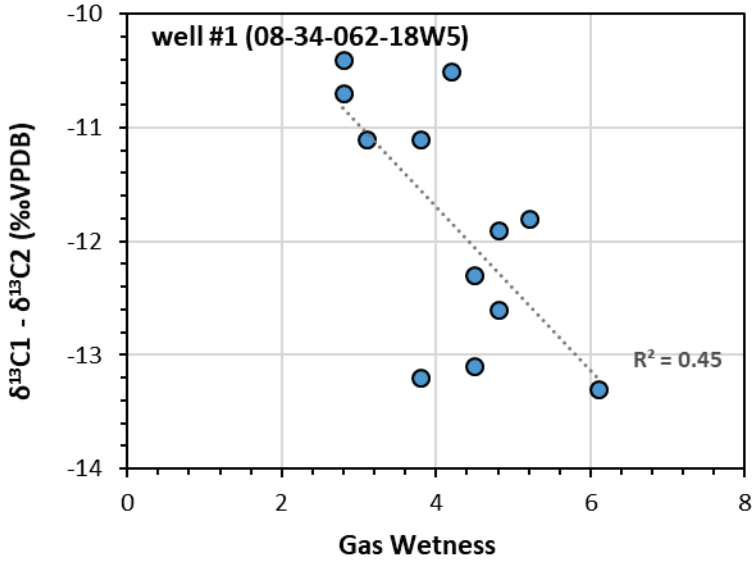

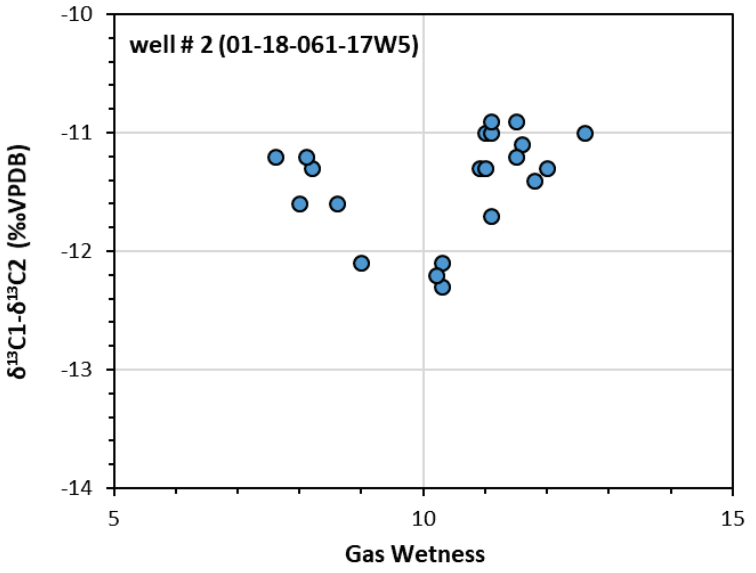

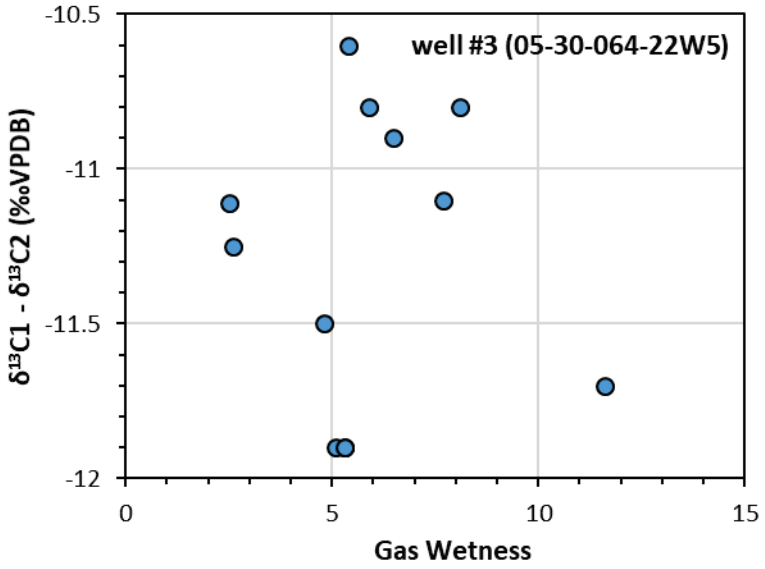
well #3 (05-30-064-22W5)
δ13C1 - δ13C2 (‰VPDB)
-10.5
-11
-11.5
-12
0
5
10
15
Gas Wetness

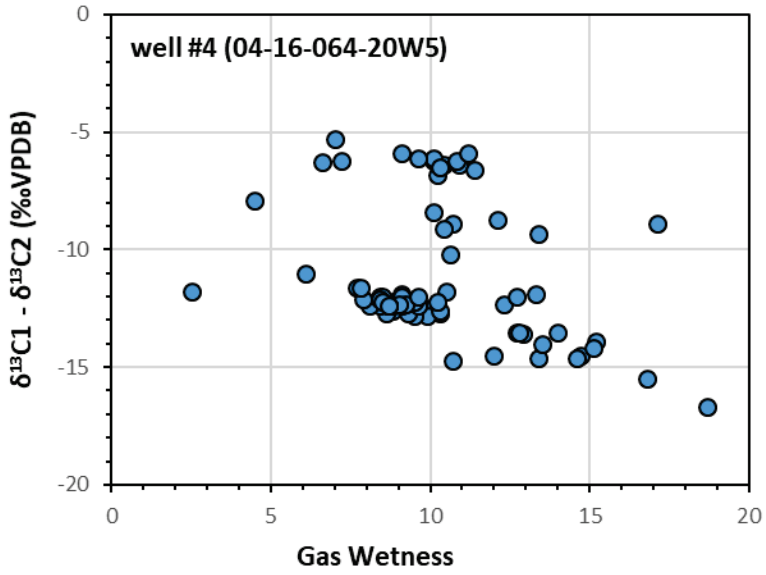
well #4 (04-16-064-20W5)
δ13C1 - δ13C2 (‰VPDB)
0
-5
-10
-15
-20
0
5
10
15
20
Gas Wetness

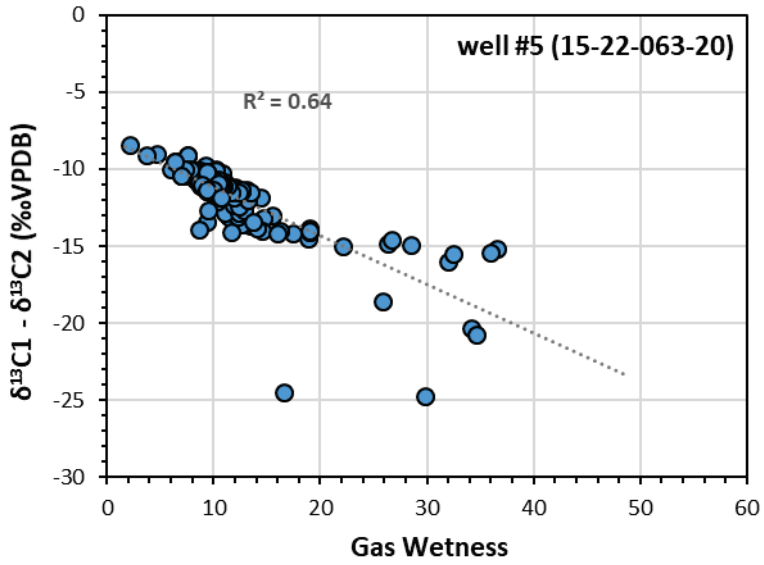
well #5 (15-22-063-20)
R² = 0.64
δ13C1 - δ13C2 (‰VPDB)
Gas Wetness
0
-5
-10
-15
-20
-25
-30
0
10
20
30
40
50
60

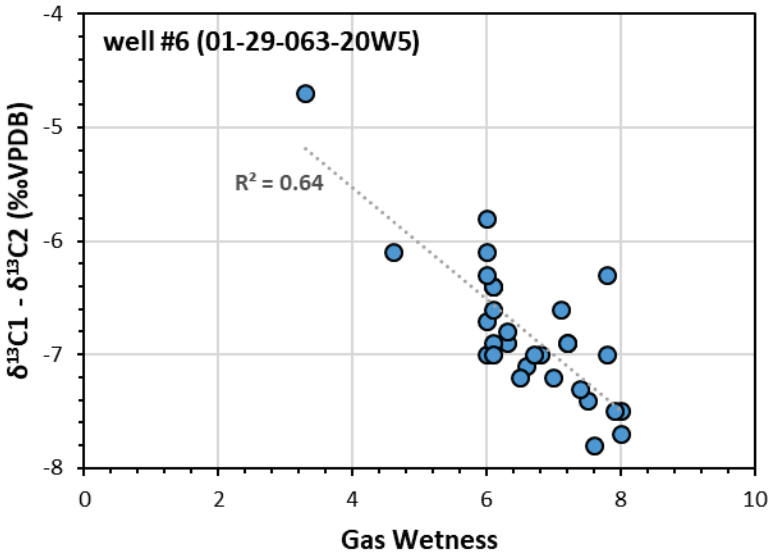
well #6 (01-29-063-20W5)
R² = 0.64
δ13C1 - δ13C2 (‰VPDB)
Gas Wetness
-4
-5
-6
-7
-8
0
2
4
6
8
10

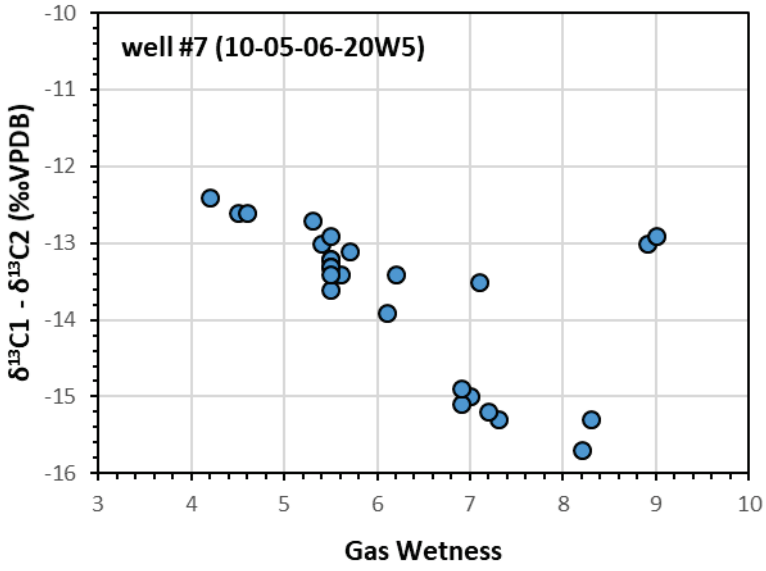
well #7 (10-05-06-20W5)
δ13C1 - δ13C2 (‰VPDB)
-10
-11
-12
-13
-14
-15
-16
3
4
5
6
7
8
9
10
Gas Wetness